The Dissertation Committee for Clinton Edward Leysath Certifies that this is the approved version of the following dissertation:

Structure and Engineering of Neutralizing Antibodies to Anthrax Toxin

Committee:

Brent L. Iverson, Co-Supervisor

George Georgiou, Co-Supervisor

Andrew D. Ellington

David W. Hoffman

Jon D. Robertus

Structure and Engineering of Neutralizing Antibodies to Anthrax Toxin

by

Clinton Edward Leysath, B.S.

Dissertation

Presented to the Faculty of the Graduate School of

The University of Texas at Austin

in Partial Fulfillment

of the Requirements

for the Degree of

Doctor of Philosophy

The University of Texas at Austin

December, 2008

Dedication

To Kat and my family

Structure and Engineering of Neutralizing Antibodies to Anthrax Toxin

Publication No._____

Clinton Edward Leysath, Ph.D.

The University of Texas at Austin, 2008

Co-Supervisors: Brent L. Iverson and George Georgiou

Recombinant antibodies have increased in prominence as therapeutics and diagnostic tools since their introduction to the market in the mid-1980's. They are used to treat diverse conditions from Crohn's disease to cancer. Since the Anthrax letter attacks of 2001, a great deal of work has been carried out to develop therapeutics to this disease, and antibodies that neutralize the toxic action of *Bacillus anthracis* are prominent among them.

This dissertation describes the elucidation of the structure of the 14B7 family of neutralizing antibodies directed at protective antigen (PA) of *B. anthracis* and the complex of PA domain 4 (PAD4) with an ultra-high affinity neutralizing antibody (M18), and then utilizes this information to aid in the engineering of the antibody to various ends. Chapter 2 presents the structure of the M18-PAD4 complex and of the 14B7 family of antibodies, which aids in the understanding of the affinity maturation process for this antibody family. Chapter 3 describes the affinity maturation of M18 to a PA variant by applying the knowledge gained from the complex structure. This previously intractable challenge was met by employing saturation mutagenesis in highly focused libraries to

M18 directed by the complex structure to the area of variation on PA. These results indicate that this could be a generalizable method for the engineering of M18 to natural and deliberate variation of PA. Chapter 4 reports work toward the development of a reversible, photoresponsive antibody using small molecule and polymer-protein conjugates. The results indicate that a probable site on M18 was located for placement of the polymer appendage, although further work is necessary to empirically refine the properties of the photoresponsive polymer. Chapter 5 presents an unrelated project, which was to confirm the existence of a proposed RNA thermosensor in the 5' untranslated region of LcrF from the pathogenic bacterium *Yersinia pestis*, the causative agent of plague.

Overall, these studies reveal the power of structure-based engineering in this antibody-antigen system. In addition, the structural elucidation of the M18-PAD4 complex and the 14B7 family of antibodies furthers our basic understanding of protein-protein interactions and the process of affinity maturation of antibodies.

Table of Contents

List of Tables

List of Figures

CHAPTER 1

Introduction and Background

1.1 ANTIBODY THERAPEUTICS

Antibodies have become an integral sector of the human therapeutics and diagnostics market. With therapies designed to treat maladies from Crohn's Disease to cancer, antibodies have become a mainstay in the physician's arsenal over the past twenty years. From the first United States Food and Drug Administration (FDA) approval in 1986, the use of antibodies has increased to become a multi-billion dollar industry. Currently, there are 26 antibodies licensed by the US FDA for use as therapeutics or imaging agents, and their application generated $31 billion in worldwide revenue for 2007 (Johnson 2008). In 2004, forecasters predicted that the 2008 therapeutic antibody market would generate $16.7 billion in revenue (Pavlou and Belsey 2005); however, the market outpaced these predictions and had already achieved $19 billion in revenue during 2006. With a current estimated annual growth rate of 16%, analysts forecast $56 billion in projected revenue for antibody therapeutics in 2012 (Johnson 2008). With the approval of antibodies by the FDA maintaining a constant trajectory over almost fifteen years, and with the existence of a healthy pipeline of antibody therapeutics under investigation currently, it appears that these forecasts should be met or exceeded as were previous predictions. Because the use of antibodies is a high-growth area in the therapeutic market, considerable research is being carried out with regard to targets, selection systems, expression systems, and scale-up.

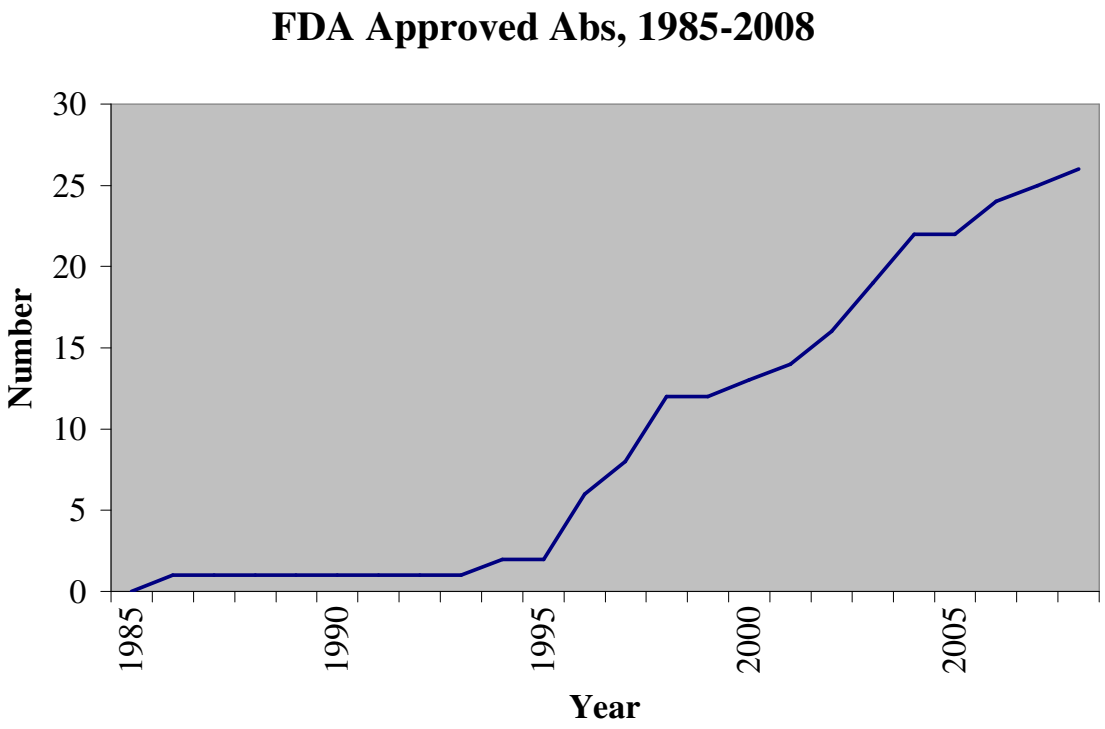

FIGURE 1.1. APPROVAL OF ANTIBODIES BY THE US FOOD AND DRUG ADMINISTRATION, 1985-2008.

1.2 ANTIBODIES

1.2.1 Antibodies—Immunity

Antibodies represent one of the main lines of natural defense against disease and infection. Antibodies recognize intruders as non-self and trigger an immune response. Evolutionary ancestors to antibodies exist even in sharks.

In our immune system, we have several different versions of immunoglobulins (Ig): IgA, IgD, IgG, IgE, and IgM. IgA is the major antibody utilized in mucosal immunity, which exists primarily in the dimeric state. IgD is a monomeric antibody that

is displayed on the surface of B cells. IgG is the primary form of secreted antibody in the immune system. It is monomeric, and is able to cross the placenta to provide immunity to a gestating fetus before it has developed an immune system of its own. IgE is another monomeric form of antibody that is implicated in allergy and the fighting of gut parasites and protozoans. Finally, IgM is the largest antibody, at 900 kD. It exists primarily as a pentamer, and is the first antibody expressed by mature B cells. Because of its 10 binding sites, with two per monomer, it has very high avidity that makes up for generally lower binding site affinities.

These antibodies are all expressed from B cells, which use recombination of a set of V, D, and J genes to create diversity that can recognize antigens of foreign organisms (Market and Papavasiliou 2003). Early in the development of B cells, each individual cell recombines these genes to create unique variable regions for the heavy and light chains of the immunoglobulin that it is to express. If this B cell recognizes its antigen specifically and becomes co-stimulated by helper T cells, it will migrate to the peripheral lymph glands and become a centroblast B cell, and begin the process of creating a high affinity, soluble IgG (Li *et al.* 2004).

At this point, two processes occur that lead to soluble expression of high affinity IgG: somatic hypermutation and antibody class switching. As stimulated B cells divide, they increase the mutation rate in the variable regions of their immunoglobulins which leads to affinity maturation of the immunoglobulin and the production of better binders (Li *et al.* 2004) in a stochastic process. Class switching is a recombination process in which the constant regions of the antibody are switched, allowing any of the different forms of immunoglobulins previously mentioned to be expressed (Stavnezer and Amemiya 2004). As most of the antibodies presented in the body are in the IgG form, class switching to this constant region is common for high affinity antibodies.

1.2.2 Antibodies—Structure

The basic form of an antibody is represented as the familiar "Y" format, consisting of two heavy chains and two light chains which pair as a "dimer of heterodimers." That is, one light chain pairs with a heavy chain to make a binding unit, and two of these heterodimers pair to form the full immunoglobulin. Both heavy and light chains have constant and variable regions; light chains are composed of a variable (V_L) and constant region (C_L), and heavy chains are composed of a variable (V_H) and three constant regions (C_{H1}, C_{H2}, and C_{H3}). Variable and light chains are held together by a disulfide bond formed between C_L and C_{H1} regions, and the constant regions of each side of the "Y" are held together by disulfide bonds formed between interstitial "hinge" regions intervening between C_{H1} and C_{H2} domains. V_H and V_L interact to form the minimal binding unit of an antibody, interfacing to create the binding surface that contacts antigen; this is also known as the variable fragment or Fv. Various forms of truncation and addition of linker regions can be utilized to aid in cloning, expression, and stability of these antibody fragments. The most common antibody fragments utilized are Fab, scFv, and scAb fragments. A Fab fragment is composed of the full light chain (V_L and C_L) interacting with the V_H and C_{H1} regions of the heavy chain. scFv fragments are composed only of the V_L and V_H regions, connected with a flexible linker in between; this single gene can be constructed in either V_L-linker-V_H or V_H-linker-V_L orientations. A common flexible linker sequence is twenty amino acids composed of four repeats of GGGGS (four glycines followed by a single serine). The scFv is often used because it represents the minimal binding unit of an antibody that is expressed in a single polypeptide chain. The final antibody fragment defined here is the scAb, which is an scFv with a C_L domain fused to the *C*-terminus. This format is used at times to increase

expression of an antibody fragment, as fusion to the C_L domain has been implicated in increased soluble expression (Hayhurst 2000); additionally, this format can be useful when screening by ELISA, as it adds another domain that can be easily targeted for detection with commercially available antibodies.

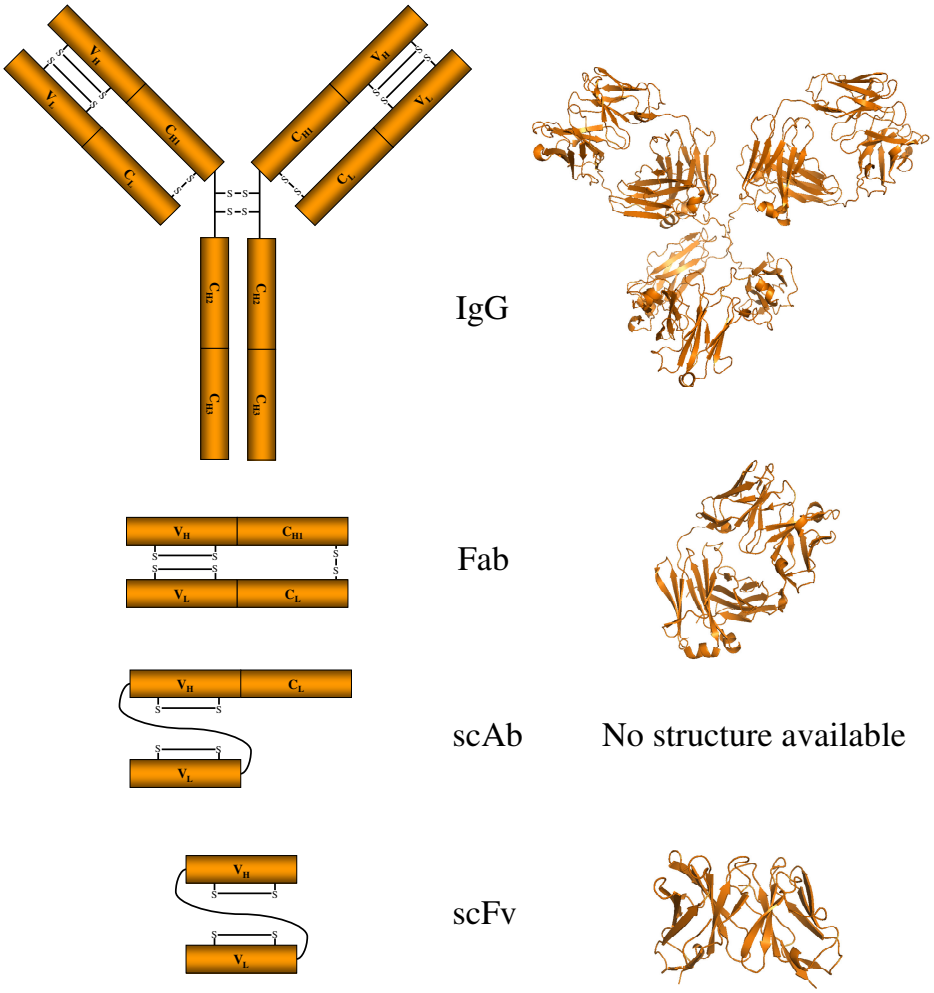

Figure 1.2. Schematic representations and crystal structures of several antibody fragments.

1.2.3 Antibodies—Function

The binding unit of an antibody that recognizes an antigen is contained within the variable regions; the surface of interaction is generally composed of the complementarity determining regions (CDRs) with framework regions (FRs) located in between. There are 3 CDRs and 4 FRs in each variable chain (heavy and light), yielding a total of 6 CDRs that contain the binding site; generally, all six CDRs make contact with their protein antigen (Sheriff *et al.* 1987; Padlan *et al.* 1989; Huang *et al.* 1998; Mylvaganam *et al.* 1998; Prasad *et al.* 1998; Li *et al.* 2000; Niemi *et al.* 2007), and they typically target a discontinuous epitope (Padlan *et al.* 1989; Fischmann *et al.* 1991; Tulip *et al.* 1992; Su *et al.* 2007). For protein antigens, the surface of interaction is primarily flat and rectangular (Amit *et al.* 1986; Sheriff *et al.* 1987), though exceptions have been observed (Bossart-Whitaker *et al.* 1995); hapten binders typically have a trough into which the small molecule is accommodated. Solvation of the complex interface can be sparse to extensive (Braden *et al.* 1994; Cohen *et al.* 1996), and solvent molecules, typically water, can intercede to create stable hydrogen bond bridges that may aid in the binding interaction (Braden *et al.* 1995; Li *et al.* 2000).

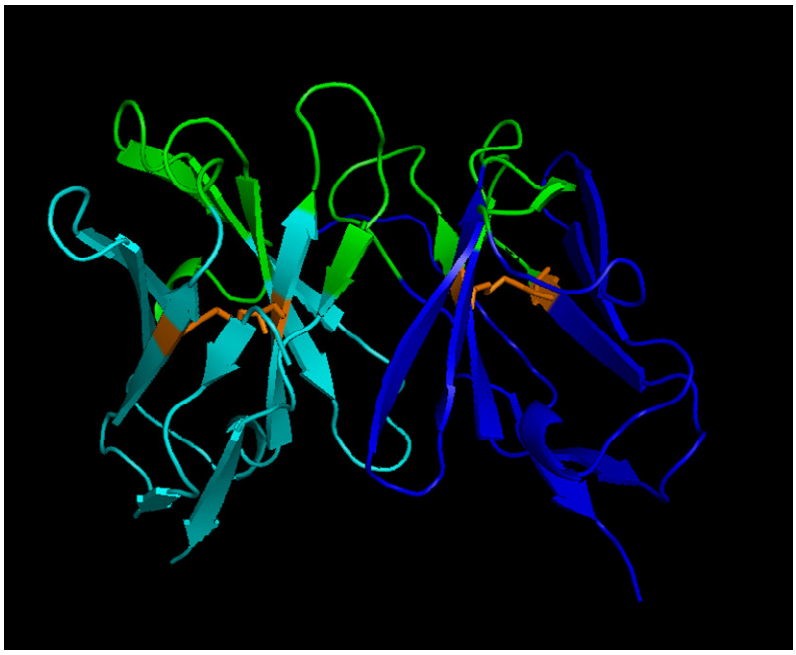

Figure 1.3. scFv structure. VH is light blue, VL is dark blue, CDR's are green, disulfide bonds are orange.

X-ray crystallographic structures of a series of affinity matured anti-lysozyme antibodies in complex with their antigen revealed that the two main driving forces for antibody affinity were shape complementarity and the ability to bury apolar surfaces. Energetics of the interaction appeared to be dominated by a core hydrophobic interaction that was encircled by other interactions (Li *et al.* 2003). These studies revealed that affinity maturation appeared to occur when more hydrophobic interactions were created peripheral to this core interaction by rearrangements of amino acid residues. Apart from the portions of antibody responsible for creating and supporting the antigen binding site, the C_{H2} and C_{H3} regions are the domains of the antibody that are responsible for interacting with the immune system to initiate effector functions, such as complement activation or phagocytosis.

1.3 ANTIBODY ENGINEERING

The term antibody engineering refers to the laboratory process by which an antibody is given beneficial characteristics. This process can utilize rational design or directed evolution, and is often used when referring to affinity maturation, or the engineering of antibodies to bind with higher affinity to their cognate antigen. However, antibody engineering also describes proesses such as engineering hyperstable frameworks (Proba *et al.* 1998), antibodies that can function in a reducing environment, called intrabodies (Messer and McLear 2006; Williams and Zhu 2006; Cardinale and Biocca 2008; Lo *et al.* 2008), or the altering of constant regions to perform specific effector functions. Recent advances have been made in the use of computational approaches to aid in the design of antigen binding sites (Barderas *et al.* 2008). However, a great deal of antibody engineering involves the directed evolution of antibody fragments by introducing diversity to the antibody gene and then screening that library for enhanced characteristics. To that end, there are a number of protein display systems that have been developed for this purpose. These differ by the organisms that they utilize, but the common, and most important, feature of each is that they allow the linking of the genotype (DNA encoding the antibody fragment gene) to the phenotype (protein form of the antibody fragment).

1.3.1 Phage Display

The most commonly utilized display system for engineering of proteins has been phage display. Roughly 300 publications a year are produced featuring this technique (Gai and Wittrup 2007). With antibody engineering, the most common usage is to display the scFv antibody fragment on the surface of a filamentous phage, like fd or M13, through fusion with one of the viral coat proteins (Gao *et al.* 1999). A fusion protein

with gene III is the most widespread (Barbas *et al.* 1991), as it has fewer limitations as compared to other coat proteins, though other protein fusions have been used (Gao *et al.* 2002). When the phage library is constructed, the phage particles exhibit scFv proteins decorated on the exterior, while the DNA encoding the scFv gene is located inside.

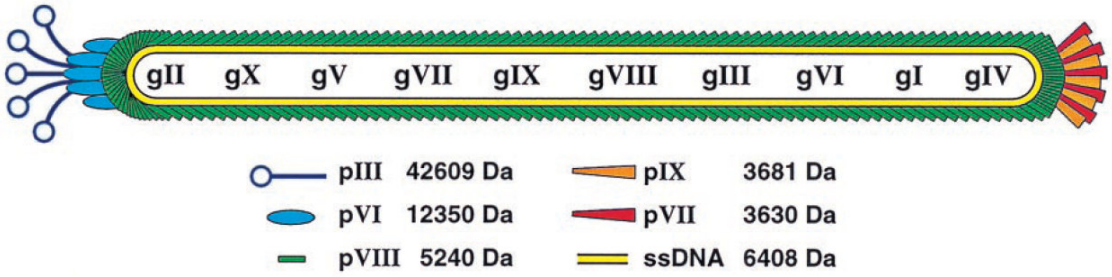

Figure 1.4. Schematic representation of the structure of the filamentous phage fd (Gao *et al.* 1999).

The phage library is exposed to antigen that is tethered either to beads or a solid surface, allowed to bind, washed to remove nonspecific binding phage, eluted, and then the library is used to infect bacteria in order to repropagate the selected phage. This process is called panning, and successive rounds of increasing stringency can be utilized to select for tighter binding clones. Because the phage particle contains approximately 5 copies of gene III, scFv fusions can be displayed multiple times which leads to avidity effects rather than solely affinity as the primary selection parameter. The panning procedures have been improved upon to help eliminate avidity issues during selection (Hoogenboom 2002). Regardless of its potential limitations, phage display has resulted in the isolation of numerous antibodies in the twenty years since its introduction.

1.3.2 Yeast Surface Display

Another competing technology that has been adopted as a mainstream display system is yeast display. In this technique, a library of protein variants is expressed as a fusion protein with a membrane protein of the yeast cell. A common format for this is a *C*-terminal fusion with the yeast agglutinin protein Aga2p (Wittrup 2001; Gai and Wittrup 2007). Because yeast is a single celled eukaryote, it can apply post-translational modifications and quality control for folding of proteins in the golgi and endoplasmic reticulum; this allows for mostly correctly folded protein to be displayed for selection purposes (Shusta *et al.* 1998; Boder *et al.* 2000). When a yeast-displayed library of antibody fragment variants is incubated with fluorescently-labeled antigen, the library can then be screened using high-throughput methods like Fluorescence Activated Cell Sorting (FACS) to obtain an enriched population that can be regrown, relabeled, and resorted until sufficient enrichment is observed. This technique has been increasing in popularity since its introduction slightly over ten years ago, and the number of publications utilizing yeast display is currently experiencing exponential growth (Gai and Wittrup 2007).

1.3.3 Gram Positive Surface Display

With only a single membrane, one might think that gram positive bacteria would be an ideal candidate for display systems. Surface display of proteins on gram positive bacteria for the purpose of directed evolution has been largely overlooked however, primarily due to the low transformation efficiency of most gram positive strains. However, recent studies have shown that affinity proteins, "affibodies," that are derived from a staphylococcal protein A domain with a variant binding region can be selected to bind to Tumor Necrosis Factor alpha (TNFα) from a large library of greater than 10^6

clones while displayed on the surface of *Staphylococcus carnosus*. Proteins with apparent affinities of 95 pM to 2.2 nM were selected (Kronqvist *et al.* 2008). While this is not selection based upon a traditional antibody framework, scFvs have been expressed successfully on the surface of gram positive bacteria previously (Gunneriusson *et al.* 1996), so presumably scFv screening can be carried out in a similar fashion.

1.3.4 Gram Negative Display Systems

Because of its use as the workhorse of molecular biology, the gram negative bacterium *Escherichia coli* is an excellent platform for use as a display system for directed evolution experiments. With numerous facile cloning systems, highly efficient transformation efficiencies, and an oxidizing periplasmic space to aid in the proper folding of proteins containing disulfide bonds, this widely used bacterium is an ideal candidate for protein display, and great effort has been spent to develop it as a successful approach.

1.3.4.1 Lpp-OmpA Surface Display

One of the first bacterial display technologies that would go on to provide a successful platform for antibody fragment directed evolution was the Lpp-OmpA display system. Our laboratory created a fusion system that could display an active, soluble protein, β-lactamase, on the outside of the outer membrane of *E. coli* (Francisco *et al.* 1992). It utilized a construct that carried the signal sequence and first nine amino acids of Braun's lipoprotein (Lpp), residues 46-159 of outer membrane protein A (OmpA), followed by the β-lactamase protein. The Lpp domain was responsible for anchoring the fusion protein to the inside of the outer membrane of *E. coli*, and the OmpA fragment

was five of the eight membrane spanning domains, which left the soluble, periplasmic protein β-lactamase exposed extracellularly and active.

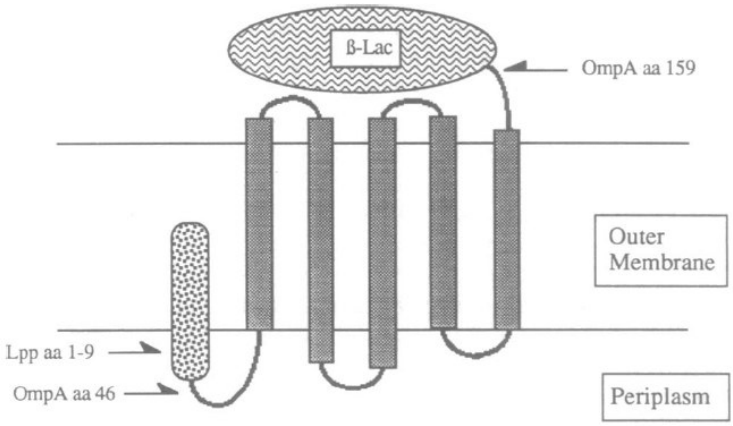

FIGURE 1.5. SCHEMATIC REPRESENTATION OF THE ORIGINAL LPP-OMPA-β-LACTAMASE SURFACE DISPLAY SYSTEM (Francisco *et al.* 1992).

Later, the Lpp-OmpA system was used to display an scFv on the surface of *E. coli* and showed enrichment by FACS of cells expressing the scFv versus control cells by a factor of greater than 100,000 using two rounds of sorting (Francisco *et al.* 1993). This system was subsequently used to select for an enhanced binding antibody fragment to the hapten digoxin. In this study, Patrick Daugherty in our laboratory was able to select an antibody fragment from a library of variants that bound with three-fold better affinity than the wild type scFv 26-10 (Daugherty *et al.* 1998). Although this system was successful in its selection for hapten binders, the presence of lipopolysaccharides (LPS) and other moieties on the outer membrane interfered with protein-protein interactions and limited the size of antigens that could be used in this selection system (Chen and Georgiou 2002). For this reason, attempts to create alternative display systems were undertaken.

1.3.4.2 Periplasmic Expression with Cytometric Screening

In an effort to circumvent challenges associated with Lpp-OmpA display, a "displayless" system was developed. Periplasmic Expression with Cytometric Screening (PECS) utilized soluble expression of scFvs into the periplasm with a pelB leader sequence coupled with treatment of the cells to allow diffusion into the periplasm of fluorescently labeled antigen up to approximately 10 kDa in size while still maintaining the viability of those cells (Chen *et al.* 2001). Another strength of this system was that no cloning manipulations were required for soluble expression of scFv after isolation of improved variants. However, while diffusion of proteins up to 10 kDa in size was permitted, screening against larger proteins was still not feasible because the outer membrane was acting as a semi-permeable dialysis membrane; treatment to enlarge the pores to allow larger antigens access would permit scFv to escape as well. Therefore, further effort was commenced to create a display system that could allow screening against proteins of great size.

1.3.4.3 Anchored Periplasmic Expression

The next evolution in gram negative display and selection technology was reported by Barrett Harvey in our laboratory in 2004. First, an *N*-terminal sequence of six amino acids from the native lipoprotein A (NlpA) was placed on the scFv to direct lipidation and subsequent display on the periplasmic side of the inner membrane. This was followed by disruption of the outer membrane using Lysozyme and EDTA in Tris-Sucrose buffer to create so-called spheroplasts, allowing very large proteins that were fluorescently labeled access to the scFvs displayed on the inner membrane. Sorting of

these samples of spheroplasts followed by recovery of the scFv genes by PCR meant that the viability of cells after labeling and sorting was no longer a determinant for recovery of successful binders. Repeated rounds of cloning, sorting, and recovery PCR could be carried out to provide desired enrichment of the library. By removing the outer membrane and the LPS associated with it, much larger protein antigens (with molecular weight >240 kDa) were able to freely associate with displayed scFv. Additionally, screening within the periplasmic space resulted in increased protein levels when the isolated variants were placed in vectors utilizing pelB leader sequences for soluble periplasmic expression. This system produced a scFv variant that bound to protective antigen (PA) of *Bacillus anthracis* at 35 pM, a greater than 200-fold enhancement of affinity from the parental scFv (Harvey *et al.* 2004). In addition to affinity maturation, this technology has also been used to produce a two-hybrid system(Jeong *et al.* 2007), selection of intrabodies in a reducing periplasmic space (Seo *et al.* in press), and isolation of novel scFvs from a mouse-derived immune library (VanBlarcom and Georgiou, unpublished results).

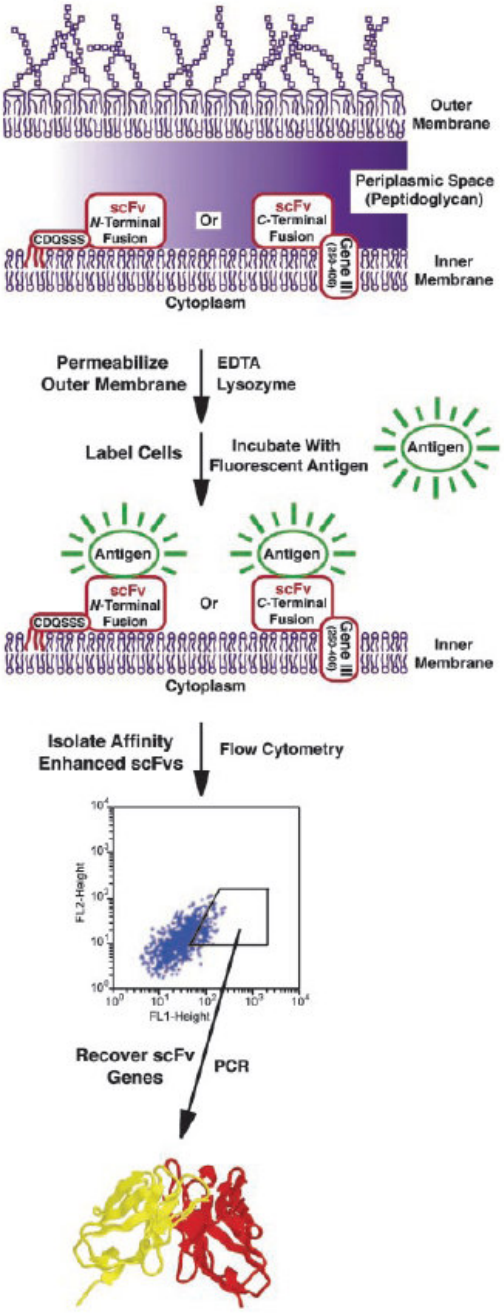

FIGURE 1.6. SCHEMATIC REPRESENTATION OF APEX PROTOCOL (Harvey *et al.* 2004).

1.3.4.4 Full IgG Display and Screening

Another advance in screening technologies is the use of full IgG in a screening system. All previous antibody display and screening technologies discussed have employed antibody fragments. However, it is not clear that an antibody variant selected in the screening format as a fragment will translate to a highly expressing, well folded full IgG. The screening system developed by Yariv Mazor in our laboratory utilizes full IgG expression and assembly in the periplasmic space of *E. coli* with the display system inspired by inner membrane anchoring similar to APEx. IgG expression was elicited from a dicistronic operon under the control of an inducible promoter, while the anchoring protein, a fusion of the NlpA anchoring sequence and the IgG binding ZZ domain, were expressed from a different inducible promoter. The ZZ domain is a dimeric analog of *Staphylococcus aureus* Protein A (Nilsson *et al.* 1987). In this system, the NlpA-ZZ fusion protein is anchored into the periplasmic side of the inner membrane and captures correctly assembled IgG. Lysozyme-EDTA treatment removes the outer membrane, and the spheroplasts are incubated with fluorescently labeled antigen and subjected to FACS. PCR recovery of the IgG variable genes is carried out, and the cycle of screening is continued until sufficient enrichment is observed. The vector housing the desired IgG gene can be utilized for soluble expression in *E. coli* simply by not inducing the NlpA-ZZ fusion construct. This display system was utilized to recover several IgG binders to PA of *B. anthracis* from a murine immune library extracted from an immunized mouse (Mazor *et al.* 2007).

1.4 DIVERSITY

Regardless of the display system used for screening, some method of creating genetic diversity must be used to allow high affinity antibody fragments to be isolated.

Extremely large naïve libraries mimicking the diversity of the natural immune system have been created and utilized with phage display to produce antibodies against many antigens (De Lorenzo *et al.* 2002). Another method is to create a biased immune library by immunizing an animal with the antigen of choice, then isolating lymphocytes and harnessing the diversity of antibodies produced during the animal's immune response (Hayhurst *et al.* 2003). These systems are both useful for isolating novel binders to a given antigen as an initial step in antibody engineering. However, once an initial antibody has been isolated, new methods for introducing diversity are needed to continue progress toward engineering ultra-high affinity antibodies.

1.4.1 Error-Prone PCR

One of the most common methods for introducing diversity into gene sequences is error-prone PCR. Because of the ubiquity of PCR in molecular biology and the ease with which it is carried out, it has become quite commonplace to use for the creation of libraries. Error-prone PCR takes advantage of conditions that lead to a relatively high error rate of *Taq* polymerase. Several groups have published studies that have systematically looked at various conditions to reduce the apparent bias of polymerases to make certain base misincorporations while increasing the overall mutation rate (Cadwell and Joyce 1992; 1994; Fromant *et al.* 1995). The most common method is to manipulate dNTP concentrations and supplement $MgCl_2$ with $MnCl_2$ to increase the promiscuity of *Taq* polymerase. This methodology will introduce mutations within the bounds of the two primers used for PCR, so very wide regions can be covered, up to an entire gene. However, the ability to sample sequence space across large regions is tempered by the likelihood that complete accessibility to all other 19 amino acids is not probable from a given codon. Because error rates associated with these libraries are generally in the 1-2%

range, the chance of having two or three base changes side by side in a give codon are prohibitively small, thus protein space is not sampled completely at individual codons. In cases where smaller regions of a protein would benefit from being sampled more exhaustively in protein space, another method is needed to introduce diversity.

1.4.2 Saturation Mutagenesis

A complementary method to error-prone PCR, saturation mutagenesis, has the ability to introduce complete diversity at a given codon (Arkin and Youvan, 1992). PCR is utilized to introduce primers that contain degenerate codons, most commonly NNK or NNS (N=A, G, C, or T; K=G or T; S=C or G), at specified locations within a gene (Varadarajan *et al.* 2008). Generally, overlap PCR is used because it allows multiple locations to be randomized simultaneously. While sampling of sequence space is complete for each randomized codon, the number of codons that can be completely randomized should be limited to four or five for a given library if the complete sequence space is to be covered. For example, a library of five NNS codons already contains a diversity at the DNA level of more than $3x10^7$ possible variants, which can be difficult to cover using standard molecular biological techniques. Other studies have recommended different degenerate codons for use, such as NDT (D=A, G, or T;(Reetz *et al.* 2008). Although it does not cover all 20 amino acids in its diversity, the utility of such a codon is that it contains twelve codons that each code for a different amino acid. Protein engineering studies based upon libraries utilizing the NDT codon allowed the isolation of a significantly higher number of positive variants from a given library when compared to a similar NNS library. While this degenerate codon will certainly allow more residues to be covered in sequence space with a library of equivalent size, coverage of the complete repertoire of amino acids may be preferable in many cases.

1.5 CRYSTALLOGRAPHY

To aid in the placement of diversity for the creation of more effective libraries, fundamental characterization of the system can provide a starting point by identifying key features of the protein in question. In systems where antibody fragments interact with protein antigens, X-ray crystallography is the primary method used to reveal exacting, highly accurate detail within these complexes. While the process yields structural data when finished, it begins with the expression and purification of the proteins of interest.

1.5.1 Expression and Purification of Antibody Fragments

For our purposes, protocols for expression and purification of antibody fragments have become quite refined. The use of gene construction *via* PCR allows facile construction of an antibody fragment, and there are numerous vectors for cytoplasmic or periplasmic expression. Expression in the periplasm is preferred, as removal of the outer membrane followed by immobilized metal affinity chromatography (IMAC) reproducibly yields highly active, relatively pure protein.

If extremely high purity is needed, then isolation of protein by IMAC often requires additional purification. Chromatographic systems utilizing Fast Performance Liquid Chromatography (FPLC) are among the most powerful methods of separation. Size exclusion chromatography (SEC) or ion exchange chromatography (IEC) can provide a platform for separation of protein in this setting. IEC is useful when the isoelectric point (pI) of the protein of interest is separated from the pI's of contaminant proteins by one pH unit or more. IEC can be employed by utilizing a column with either an anionic or cationic matrix that will nonspecifically bind protein based on electrostatic

attraction. The mixed protein sample can be bound to the appropriate column matrix by injection into the column, and protein can be eluted selectively as a salt gradient is applied to the column.

If the properties of proteins in the milieu preclude use of IEC, then SEC can usually be employed. This methodology employs a column packed with very small beads that have pores of a defined size. Proteins injected into this column and subjected to a constant flow rate will separate based upon size because of the ability of smaller proteins to reside in the pores for greater amounts of time. Thus, larger proteins elute first, followed by smaller proteins. In general, protein obtained by IMAC can be purified to very high purity using SEC.

1.5.2 Crystallographic Screening

Once pure protein has been acquired, it is necessary to ascertain what conditions are favorable for crystallization of the protein of interest. The first consideration is the method of crystallization that will be used. Two of the most commonly used methodologies are vapor diffusion (by hanging or sitting drop) and microbatch. In typical vapor diffusion screening, a large volume (400-600 μL) of a solution of buffer, salts, and/or precipitant is sealed into a closed well with a drop (typically 1-2 μL) of a 1:1 mixture of concentrated protein with the screening solution sitting on a pedestal (sitting drop) or suspended from a slide cover (hanging drop). As time passes, water evaporates and diffuses out of the drop and into the air and reservoir well solution until the concentration of salt or precipitant comes to equilibrium between the reservoir well and the drop; this causes concentration of the protein in the drop, and if supersaturation occurs in a solution that is amenable to ordered formation of a reproducible lattice, then crystal growth occurs (McPherson 1999).

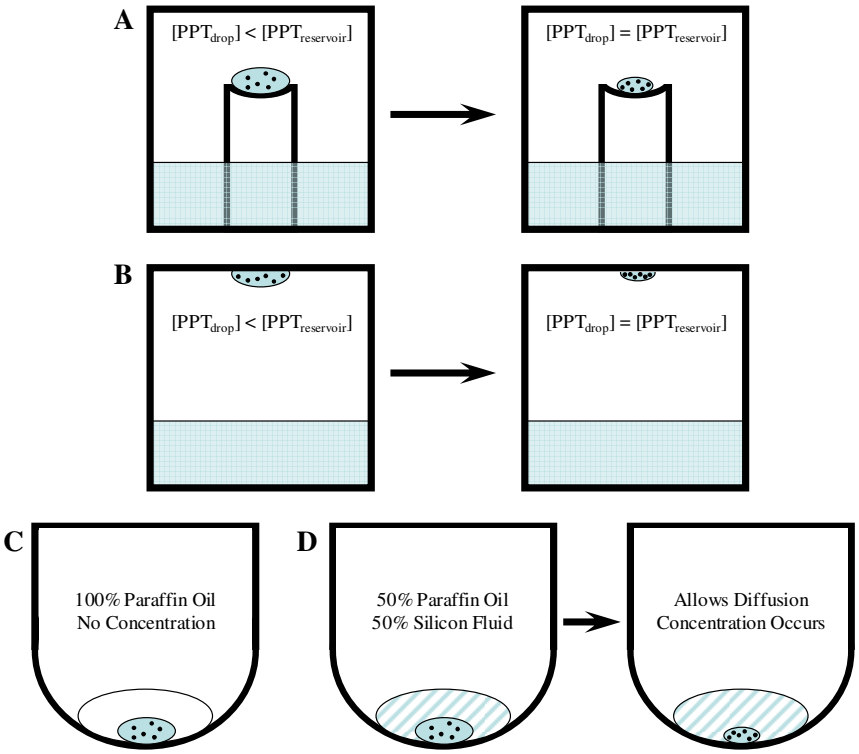

FIGURE 1.7. DIFFERENT METHODOLOGIES FOR CRYSTAL SCREENING. (A) Sitting drop vapor diffusion, (B) Hanging drop vapor diffusion, (C) Microbatch, (D) Microbatch diffusion. Adapted from (McPherson 1999).

Microbatch is another very simple method of screening for crystallization conditions. In this system, a small drop of concentrated protein solution is mixed in a well with another small drop of the screening solution consisting of buffer, salts, and/or precipitant under a large volume of paraffin oil (D'Arcy *et al.* 2004). The paraffin oil provides a seal to prevent evaporation of liquid from the drop, so crystallization occurs if supersaturation occurs when the small drops mix. A variation of this technique, known as microbatch diffusion, has been developed which is a fusion of the concepts of

microbatch and vapor diffusion (D'Arcy *et al.* 2003). In this methodology, a screen is set up as for microbatch, except that a 1:1 mixture of paraffin oil and silicon fluid is used. The silicon fluid allows the diffusion and subsequent evaporation of water away from the drop, thus providing simultaneous concentration of the protein and precipitant that can lead to crystal formation.

1.5.3 Crystal Screens

Once a screening format is chosen, then the conditions to test during screening must be considered. Conditions among those known to affect crystallization are pH, precipitant, temperature, and additives. There are, of course, a great many other factors, but it is generally inconvenient to begin screening beyond these initial variables (Kundrot 2004). As it is, one could create many more conditions with only these four variables than is feasible to cover in a screen for crystallization of a protein. Because of this, much effort has been devoted to determining the most efficient set of experiments to discover crystallization conditions for a given protein. While diffraction quality crystals might be formed from the initial screen, its true importance lies in uncovering those small regions in "condition space" where crystal growth is likely; more refined screens can be constructed around conditions of initial success to enhance quality of crystals.

A variety of initial screens have been developed using different designs for the mixing of reagents such as random screens (Shieh *et al.* 1995), grid screens (McPherson 1989), incomplete factorial screens (Carter and Carter 1979), footprint screens (Stura *et al.* 1992), and sparse matrix screens (Jancarik and Kim 1991). These screens generally are using reagents that had success inducing crystallization of previous proteins, so the selection of these reagents is based upon their historical effectiveness, not their actual efficiency of stimulating crystal growth. While there exists an assortment of initial

screens, studies indicate that an average lower limit of success is 2%, or 1 crystal observed in 50 screened conditions (Segelke 2001). In this case, the probability of observing at least one "hit" in screening when using three commercially available screens of 96 conditions each is 99.7% ($P = 1 - 0.98^{288}$). Even assuming a much more pessimistic success rate of 0.2%, or 1 "hit" in 500 conditions, the probability is still 43.8% ($P = 1 - 0.998^{288}$). Therefore, the most important factor in discovering crystallization conditions is the number of different conditions attempted (Kundrot 2004). To amplify this point, a high throughput crystallization facility that utilizes a 1,536 condition screen reported that although most proteins deliver 50 or more "hits," there have been several cases where only one condition in 1,536 produced a protein crystal (Luft *et al.* 2003).

1.5.4 "Throughput" in Crystallographic Screening

Because increasing the number of conditions screened increases the chances of success, consideration of the level of throughput for a crystallographic endeavor is warranted. Traditionally, screening was carried out in low-throughput fashion, as every event in the process of crystal screening was performed by hand. While low-throughput methodology has certainly been successful historically, the use of robotics to automate certain aspects of the screening process has aided in the efficiency of man hours spent searching for "hits." High-throughput screening utilizes automation at every point in the process: dispensing of crystal trays, visualization scoring, creating refined screens, and screen mixing. These systems are typically made up of several robots and are extremely costly, making them available only to those facilities that are intensely dedicated to producing great numbers of crystal structures (Kundrot 2004). Between these two extremes, medium-throughput screening generally employs some degree of automation in conjunction with some manual work. Typically, setup of protein screening plates is

automated by a single instrument, while scoring of conditions for crystal growth, and designing and preparing fine screens are done by hand. This level of automation is quickly being adopted as the standard by crystallography labs far and wide, as robotics can prepare in minutes what takes hours for an experienced technician to prepare by hand.

Another benefit of automation in the setup of crystal screening trays is miniaturization. When preparing trays by hand, it is typical to prepare 2 µL drops (1 µL of a 10 mg/mL protein solution added to 1 µL of screen) because manual micro-pipettors are not very precise below 1 µL. However, with robotics that can reliably deliver 100 nL (0.1 µL), utilizing 0.2 µL drops for screening becomes feasible. This results in the ability to cover 10-fold more conditions using the same amount of protein. For costly, difficult to purify, or poorly expressing proteins, this reduction in the requirement of sample can be the difference between initiating screening or abandoning the effort altogether.

A number of systems are available for these purposes, and they vary by their functionalities. Most systems are capable of preparing either vapor diffusion or microbatch screens. Commercially available instruments currently include the Art Robbins Instruments Phoenix, the Matrix-Drop Maker Hybrid™ from Emerald Biosystems, the Genomic Solutions® Honeybee, the Oryx line of robots from Douglas Instruments, and the Fluidigm Topaz®.

1.6 ANTHRAX

Bacillus anthracis, a gram positive, sporulating bacterium, is the causative agent of the zoonotic disease anthrax. Three forms of the disease occur in humans, cutaneous, gastrointestinal, and inhalational. Cutaneous anthrax is the most common form, and is rarely fatal. Gastrointestinal and inhalational anthrax are far less common and far more

fatal. Because of this fatality combined with the fact that anthrax spores are resistant to a wide variety of environmental conditions, it has long been feared as an agent of biowarfare. There is evidence of nations cultivating *B. anthracis* for use as an offensive weapon, and the Anthrax letter attacks of 2001 revealed the significant terror incited by even a relatively small scale attack.

Anthrax virulence is mediated through two independent mechanisms, its poly-gamma-D-glutamic acid capsule, and soluble, excreted binary toxin. Three proteins are involved in the toxic action, protective antigen (PA), lethal factor (LF), and edema factor (EF). PA is an 83 kDa protein that binds with high affinity to the mammalian cellular receptors ATR/TEM8 (Bradley *et al.* 2001) and CMG2 (Scobie *et al.* 2003; Scobie and Young 2005). Cleavage by furin protease to a 63 kDa form and heptamerization leads to the binding of LF or EF (Young and Collier 2007). Clathrin-mediated endocytosis of the PA/LF/EF complex provides the route of entry, which followed by acidification of the resulting endosome that, in turn, elicits a conformational change in heptameric PA. The result is that a pore is formed by PA that delivers LF and EF into the host cell cytoplasm to carry out their functions. EF is an adenylate cyclase, and LF is a protease that inactivates mitogen activated protein kinase kinases (MAPKKs) and thus interferes in their signaling pathways.

PA is a protein 735 amino acids in length that is composed of four domains, 1-4 from the *N*- to *C*-terminus (Petosa *et al.* 1997). Domain 1 is 258 residues long and contains the site of furin cleavage at amino acid 167. Domain 2, which is 238 residues in length, is responsible for pore formation and also makes partial contact with the cellular receptor when PA initially binds to ATR or CMG2 (Santelli *et al.* 2004). Domain 3 is a 109 amino acid region that is thought to be responsible for heptamerization of PA_{63} (Mogridge *et al.* 2001). Domain 4 is the *C*-terminal 139 amino acids of PA, and it is

responsible for a majority of binding to CMG2 or ATR (Singh *et al.* 1991; Santelli *et al.* 2004).

There are numerous examples of antibodies that have been generated to various epitopes of the toxin components that have neutralizing effects (Little *et al.* 1988; Little *et al.* 1997; Cirino *et al.* 1999; Maynard *et al.* 2002; Wild *et al.* 2003; Brossier *et al.* 2004; Harvey *et al.* 2004; Karginov *et al.* 2004; Sawada-Hirai *et al.* 2004; Wang *et al.* 2004; Cui *et al.* 2005; Huber *et al.* 2005; Hull *et al.* 2005; Laffly *et al.* 2005; Mohamed *et al.* 2005; Subramanian *et al.* 2005; Chen *et al.* 2006; Gubbins *et al.* 2006; Paddle *et al.* 2006; Rivera *et al.* 2006; Vitale *et al.* 2006; Albrecht *et al.* 2007; Kelly *et al.* 2007; Pelat *et al.* 2007; Staats *et al.* 2007; Steiniger *et al.* 2007; Zhou *et al.* 2008), and several of these are in clinical trials. In fact, one has even been utilized to treat inhalational anthrax in humans (Walsh *et al.* 2007). Many of these antibodies elicit their neutralizing action by preventing PA from interacting with the mammalian cellular receptors. It is clear that in order to effectively prevent intoxication *in vivo*, the affinity of the antibody for PA must be stronger that the affinity of PA for its cellular receptors (Maynard *et al.* 2002). One of the first well-characterized antibodies that was shown to target PA while interrupting interaction with its cellular receptors was 14B7 (Little *et al.* 1988). Phage display and Anchored Periplasmic Expression (APEx) were utilized to produce the high affinity 14B7 variants called 1H (Maynard *et al.* 2002) and M18 (Harvey *et al.* 2004) respectively. These antibodies have been shown to be protective in various assays (Maynard *et al.* 2002; Mabry *et al.* 2005). Affinities for the 14B7 family of antibodies are as follows: 4nM (14B7), to 250pM (1H) and 35pM (M18).

Previous work has revealed the structures of monomeric and heptameric PA (Petosa *et al.* 1997), LF (Pannifer *et al.* 2001), as well as the interaction of PA with

CMG2 (Santelli *et al.* 2004). These structures, in combination with other molecular studies have augmented our knowledge of the intoxication processes of *B. anthracis*.

Alanine scanning studies have initiated our understanding of the interactions that PA has with the 14B7 family of neutralizing antibodies. The alanine scanning indicated that 14B7 and the cellular receptors had overlapping, but non-identical, epitopes on PA. Consequently, PA variants that retained near-wild type toxicity while abrogating 14B7 binding were found (Rosovitz *et al.* 2003). These variants, chiefly L685A and Y688A, revealed potential circumventions to successful therapy in the event of malicious intent to alter the toxin.

1.7 PROJECT BIOSHIELD

After the Anthrax letter attacks of 2001, a great deal of research was conducted to discover novel inhibitors of anthrax toxin. Additionally, congress authorized the creation of Project Bioshield in 2004. This initiative was initially placed under the purview of the Department of Health and Human Services. Its scope was to accelerate research and development of countermeasures to chemical, biological, radiological, and nuclear (CBRN) threats, as well as to acquire therapeutics for these contingencies for addition to the Strategic National Stockpile (SNS). This legislation allocated up to $5.6 billion over ten years for this endeavor. Contracts have been awarded for anthrax vaccine, anthrax therapeutics, botulinum antitoxin, smallpox vaccine, and agents to treat nuclear and radiological side effects (Russell 2007).

1.8 PROJECT AIMS

The focus of this research is to uncover the structure of the interaction of PA with a member of the 14B7 neutralizing antibody family, and to use that information to allow engineering of the antibody family for various applications.

Chapter 2 focuses on the X-ray crystallographic studies that reveal the structure of the antibodies in the 14B7 family as well as the complex of the ultra-high affinity variant M18 with PA domain 4. This work exposes the mechanism of interaction of this neutralizing antibody family with the anthrax toxin, and it increases understanding of the basis of affinity maturation in this system.

Chapter 3 utilizes this information to create libraries with highly focused diversity to engineer a member of the 14B7 antibody family to achieve better binding to the Y688A variant of PA, a previously intractable problem for *in vitro* evolution. This appears to represent a generalizable solution to the engineering of the 14B7 family of antibodies for altered forms of the toxin.

Chapter 4 focuses on the effort to create a photoresponsive antibody. Using the M18—PA interaction as a model system, this endeavor works through two platforms for affecting antibody affinity using an appendage that is reversibly responsive to light.

Chapter 5 describes an unrelated project, which was to confirm the existence of a proposed RNA thermosensor in the 5' untranslated region of LcrF from the pathogenic bacterium *Yersinia pestis*, the causative agent of plague.

1.9 REFERENCES

Albrecht, M.T., Li, H., Williamson, E.D., LeButt, C.S., Flick-Smith, H.C., Quinn, C.P., Westra, H., Galloway, D., Mateczun, A., Goldman, S.*, et al.* 2007. Human monoclonal antibodies against anthrax lethal factor and protective antigen act independently to protect against Bacillus anthracis infection and enhance endogenous immunity to anthrax. *Infect Immun* **75:** 5425-5433.

Amit, A.G., Mariuzza, R.A., Phillips, S.E., and Poljak, R.J. 1986. Three-dimensional structure of an antigen-antibody complex at 2.8 A resolution. *Science* **233:** 747-753.

Arkin, A.P., and Youvan, D.C. 1992. Optimizing nucleotide mixtures to encode specific subsets of amino acids for semi-random mutagenesis. *Biotechnology (N Y)* **10:** 297-300.

Barbas, C.F., 3rd, Kang, A.S., Lerner, R.A., and Benkovic, S.J. 1991. Assembly of combinatorial antibody libraries on phage surfaces: the gene III site. *Proc Natl Acad Sci U S A* **88:** 7978-7982.

Barderas, R., Desmet, J., Timmerman, P., Meloen, R., and Casal, J.I. 2008. Affinity maturation of antibodies assisted by in silico modeling. *Proc Natl Acad Sci U S A* **105:** 9029-9034.

Boder, E.T., Midelfort, K.S., and Wittrup, K.D. 2000. Directed evolution of antibody fragments with monovalent femtomolar antigen-binding affinity. *Proc Natl Acad Sci U S A* **97:** 10701-10705.

Bossart-Whitaker, P., Chang, C.Y., Novotny, J., Benjamin, D.C., and Sheriff, S. 1995. The crystal structure of the antibody N10-staphylococcal nuclease complex at 2.9 A resolution. *J Mol Biol* **253:** 559-575.

Braden, B.C., Fields, B.A., and Poljak, R.J. 1995. Conservation of water molecules in an antibody-antigen interaction. *J Mol Recognit* **8:** 317-325.

Braden, B.C., Souchon, H., Eisele, J.L., Bentley, G.A., Bhat, T.N., Navaza, J., and Poljak, R.J. 1994. Three-dimensional structures of the free and the antigen-complexed Fab from monoclonal anti-lysozyme antibody D44.1. *J Mol Biol* **243:** 767-781.

Bradley, K.A., Mogridge, J., Mourez, M., Collier, R.J., and Young, J.A. 2001. Identification of the cellular receptor for anthrax toxin. *Nature* **414:** 225-229.

Brossier, F., Levy, M., Landier, A., Lafaye, P., and Mock, M. 2004. Functional analysis of Bacillus anthracis protective antigen by using neutralizing monoclonal antibodies. *Infect Immun* **72:** 6313-6317.

Cadwell, R.C., and Joyce, G.F. 1992. Randomization of genes by PCR mutagenesis. *PCR Methods Appl* **2:** 28-33.

Cadwell, R.C., and Joyce, G.F. 1994. Mutagenic PCR. *PCR Methods Appl* **3:** S136-140.

Cardinale, A., and Biocca, S. 2008. Combating protein misfolding and aggregation by intracellular antibodies. *Curr Mol Med* **8:** 2-11.

Carter, C.W., Jr., and Carter, C.W. 1979. Protein crystallization using incomplete factorial experiments. *J Biol Chem* **254:** 12219-12223.

Chen, G., Hayhurst, A., Thomas, J.G., Harvey, B.R., Iverson, B.L., and Georgiou, G. 2001. Isolation of high-affinity ligand-binding proteins by periplasmic expression with cytometric screening (PECS). *Nat Biotechnol* **19:** 537-542.

Chen, W., and Georgiou, G. 2002. Cell-Surface display of heterologous proteins: From high-throughput screening to environmental applications. *Biotechnol Bioeng* **79:** 496-503.

Chen, Z., Moayeri, M., Zhou, Y.H., Leppla, S., Emerson, S., Sebrell, A., Yu, F., Svitel, J., Schuck, P., St Claire, M.*, et al.* 2006. Efficient neutralization of anthrax toxin by chimpanzee monoclonal antibodies against protective antigen. *J Infect Dis* **193:** 625-633.

Cirino, N.M., Sblattero, D., Allen, D., Peterson, S.R., Marks, J.D., Jackson, P.J., Bradbury, A., and Lehnert, B.E. 1999. Disruption of anthrax toxin binding with the use of human antibodies and competitive inhibitors. *Infect Immun* **67:** 2957-2963.

Cohen, G.H., Sheriff, S., and Davies, D.R. 1996. Refined structure of the monoclonal antibody HyHEL-5 with its antigen hen egg-white lysozyme. *Acta Crystallogr D Biol Crystallogr* **52:** 315-326.

Cui, X., Li, Y., Moayeri, M., Choi, G.H., Subramanian, G.M., Li, X., Haley, M., Fitz, Y., Feng, J., Banks, S.M.*, et al.* 2005. Late treatment with a protective antigen-directed monoclonal antibody improves hemodynamic function and survival in a lethal toxin-infused rat model of anthrax sepsis. *J Infect Dis* **191:** 422-434.

D'Arcy, A., Mac Sweeney, A., Stihle, M., and Haber, A. 2003. The advantages of using a modified microbatch method for rapid screening of protein crystallization conditions. *Acta Crystallogr D Biol Crystallogr* **59:** 396-399.

D'Arcy, A., Sweeney, A.M., and Haber, A. 2004. Practical aspects of using the microbatch method in screening conditions for protein crystallization. *Methods* **34:** 323-328.

Daugherty, P.S., Chen, G., Olsen, M.J., Iverson, B.L., and Georgiou, G. 1998. Antibody affinity maturation using bacterial surface display. *Protein Eng* **11:** 825-832.

De Lorenzo, C., Palmer, D.B., Piccoli, R., Ritter, M.A., and D'Alessio, G. 2002. A new human antitumor immunoreagent specific for ErbB2. *Clin Cancer Res* **8:** 1710-1719.

Fischmann, T.O., Bentley, G.A., Bhat, T.N., Boulot, G., Mariuzza, R.A., Phillips, S.E., Tello, D., and Poljak, R.J. 1991. Crystallographic refinement of the three-dimensional structure of the FabD1.3-lysozyme complex at 2.5-A resolution. *J Biol Chem* **266:** 12915-12920.

Francisco, J.A., Campbell, R., Iverson, B.L., and Georgiou, G. 1993. Production and fluorescence-activated cell sorting of Escherichia coli expressing a functional antibody fragment on the external surface. *Proc Natl Acad Sci U S A* **90:** 10444-10448.

Francisco, J.A., Earhart, C.F., and Georgiou, G. 1992. Transport and anchoring of beta-lactamase to the external surface of Escherichia coli. *Proc Natl Acad Sci U S A* **89:** 2713-2717.

Fromant, M., Blanquet, S., and Plateau, P. 1995. Direct random mutagenesis of gene-sized DNA fragments using polymerase chain reaction. *Anal Biochem* **224:** 347-353.

Gai, S.A., and Wittrup, K.D. 2007. Yeast surface display for protein engineering and characterization. *Curr Opin Struct Biol* **17:** 467-473.

Gao, C., Mao, S., Kaufmann, G., Wirsching, P., Lerner, R.A., and Janda, K.D. 2002. A method for the generation of combinatorial antibody libraries using pIX phage display. *Proc Natl Acad Sci U S A* **99:** 12612-12616.

Gao, C., Mao, S., Lo, C.H., Wirsching, P., Lerner, R.A., and Janda, K.D. 1999. Making artificial antibodies: a format for phage display of combinatorial heterodimeric arrays. *Proc Natl Acad Sci U S A* **96:** 6025-6030.

Gubbins, M.J., Berry, J.D., Corbett, C.R., Mogridge, J., Yuan, X.Y., Schmidt, L., Nicolas, B., Kabani, A., and Tsang, R.S. 2006. Production and characterization of neutralizing monoclonal antibodies that recognize an epitope in domain 2 of Bacillus anthracis protective antigen. *FEMS Immunol Med Microbiol* **47:** 436-443.

Gunneriusson, E., Samuelson, P., Uhlen, M., Nygren, P.A., and Stahl, S. 1996. Surface display of a functional single-chain Fv antibody on staphylococci. *J Bacteriol* **178:** 1341-1346.

Harvey, B.R., Georgiou, G., Hayhurst, A., Jeong, K.J., Iverson, B.L., and Rogers, G.K. 2004. Anchored periplasmic expression, a versatile technology for the isolation of high-affinity antibodies from Escherichia coli-expressed libraries. *Proceedings of the National Academy of Sciences* **101:** 9193-9198.

Hayhurst, A. 2000. Improved expression characteristics of single-chain Fv fragments when fused downstream of the Escherichia coli maltose-binding protein or upstream of a single immunoglobulin-constant domain. *Protein Expr Purif* **18:** 1-10.

Hayhurst, A., Happe, S., Mabry, R., Koch, Z., Iverson, B.L., and Georgiou, G. 2003. Isolation and expression of recombinant antibody fragments to the biological warfare pathogen Brucella melitensis. *J Immunol Methods* **276:** 185-196.

Hoogenboom, H.R. 2002. Overview of antibody phage-display technology and its applications. *Methods Mol Biol* **178:** 1-37.

Huang, M., Syed, R., Stura, E.A., Stone, M.J., Stefanko, R.S., Ruf, W., Edgington, T.S., and Wilson, I.A. 1998. The mechanism of an inhibitory antibody on TF-initiated blood coagulation revealed by the crystal structures of human tissue factor, Fab 5G9 and TF.G9 complex. *J Mol Biol* **275:** 873-894.

Huber, M., Vor Dem Esche, U., Grunow, R., and Bessler, W.G. 2005. Generation of mouse polyclonal and human monoclonal antibodies against Bacillus anthracis toxin. *Drugs Exp Clin Res* **31:** 35-43.

Hull, A.K., Criscuolo, C.J., Mett, V., Groen, H., Steeman, W., Westra, H., Chapman, G., Legutki, B., Baillie, L., and Yusibov, V. 2005. Human-derived, plant-produced monoclonal antibody for the treatment of anthrax. *Vaccine* **23:** 2082-2086.

Jancarik, J., and Kim, S.H. 1991. Sparse matrix sampling: a screening method for crystallization of proteins. *Journal of Applied Crystallography* **24:** 409-411.

Jeong, K.J., Seo, M.J., Iverson, B.L., and Georgiou, G. 2007. APEx 2-hybrid, a quantitative protein-protein interaction assay for antibody discovery and engineering. *Proceedings of the National Academy of Sciences* **104:** 8247-8252.

Jiang, L., Althoff, E.A., Clemente, F.R., Doyle, L., Rothlisberger, D., Zanghellini, A., Gallaher, J.L., Betker, J.L., Tanaka, F., Barbas, C.F., 3rd*, et al.* 2008. De novo computational design of retro-aldol enzymes. *Science* **319:** 1387-1391.

Johnson, K. 2008. Monoclonal therapeutics and companion diagnostic products, pp. 133. BCC Research, Wellesley, MA.

Karginov, V.A., Robinson, T.M., Riemenschneider, J., Golding, B., Kennedy, M., Shiloach, J., and Alibek, K. 2004. Treatment of anthrax infection with combination of ciprofloxacin and antibodies to protective antigen of Bacillus anthracis. *FEMS Immunol Med Microbiol* **40:** 71-74.

Kelly, C.D., O'Loughlin, C., Gelder, F.B., Peterson, J.W., Sower, L.E., and Cirino, N.M. 2007. Rapid generation of an anthrax immunotherapeutic from goats using a novel non-toxic muramyl dipeptide adjuvant. *J Immune Based Ther Vaccines* **5:** 11.

Kronqvist, N., Lofblom, J., Jonsson, A., Wernerus, H., and Stahl, S. 2008. A novel affinity protein selection system based on staphylococcal cell surface display and flow cytometry. *Protein Eng Des Sel* **21:** 247-255.

Kundrot, C.E. 2004. Which strategy for a protein crystallization project? *Cell Mol Life Sci* **61:** 525-536.

Laffly, E., Danjou, L., Condemine, F., Vidal, D., Drouet, E., Lefranc, M.P., Bottex, C., and Thullier, P. 2005. Selection of a macaque Fab with framework regions like those in humans, high affinity, and ability to neutralize the protective antigen (PA) of Bacillus anthracis by binding to the segment of PA between residues 686 and 694. *Antimicrob Agents Chemother* **49:** 3414-3420.

Li, Y., Li, H., Smith-Gill, S.J., and Mariuzza, R.A. 2000. Three-dimensional structures of the free and antigen-bound Fab from monoclonal antilysozyme antibody HyHEL-63. *Biochemistry* **39:** 6296-6309.

Li, Y., Li, H., Yang, F., Smith-Gill, S.J., and Mariuzza, R.A. 2003. X-ray snapshots of the maturation of an antibody response to a protein antigen. *Nat Struct Biol* **10:** 482-488.

Li, Z., Woo, C.J., Iglesias-Ussel, M.D., Ronai, D., and Scharff, M.D. 2004. The generation of antibody diversity through somatic hypermutation and class switch recombination. *Genes Dev* **18:** 1-11.

Little, S.F., Ivins, B.E., Fellows, P.F., and Friedlander, A.M. 1997. Passive protection by polyclonal antibodies against Bacillus anthracis infection in guinea pigs. *Infect Immun* **65:** 5171-5175.

Little, S.F., Leppla, S.H., and Cora, E. 1988. Production and characterization of monoclonal antibodies to the protective antigen component of Bacillus anthracis toxin. *Infect Immun* **56:** 1807-1813.

Lo, A.S., Zhu, Q., and Marasco, W.A. 2008. Intracellular antibodies (intrabodies) and their therapeutic potential. *Handb Exp Pharmacol***:** 343-373.

Luft, J.R., Collins, R.J., Fehrman, N.A., Lauricella, A.M., Veatch, C.K., and DeTitta, G.T. 2003. A deliberate approach to screening for initial crystallization conditions of biological macromolecules. *J Struct Biol* **142:** 170-179.

Mabry, R., Rani, M., Geiger, R., Hubbard, G.B., Carrion, R., Jr., Brasky, K., Patterson, J.L., Georgiou, G., and Iverson, B.L. 2005. Passive protection against anthrax by using a high-affinity antitoxin antibody fragment lacking an Fc region. *Infect Immun* **73:** 8362-8368.

Market, E., and Papavasiliou, F.N. 2003. V(D)J recombination and the evolution of the adaptive immune system. *PLoS Biol* **1:** E16.

Maynard, J.A., Maassen, C.B., Leppla, S.H., Brasky, K., Patterson, J.L., Iverson, B.L., and Georgiou, G. 2002. Protection against anthrax toxin by recombinant antibody fragments correlates with antigen affinity. *Nat Biotechnol* **20:** 597-601.

Mazor, Y., Blarcom, T.V., Mabry, R., Iverson, B.L., and Georgiou, G. 2007. Isolation of engineered, full-length antibodies from libraries expressed in Escherichia coli. *Nat Biotech* **25:** 563.

McPherson, A. 1989. *Preparation and analysis of protein crystals*. Krieger Publishing Company, Malabar, FL, pp. 384.

McPherson, A. 1999. *Crystallization of biological macromolecules*, 1st ed. Cold Spring Harbor Laboratory Press, Woodbury, NY, pp. 586.

Messer, A., and McLear, J. 2006. The therapeutic potential of intrabodies in neurologic disorders: focus on Huntington and Parkinson diseases. *BioDrugs* **20:** 327-333.

Mogridge, J., Mourez, M., and Collier, R.J. 2001. Involvement of domain 3 in oligomerization by the protective antigen moiety of anthrax toxin. *J Bacteriol* **183:** 2111-2116.

Mohamed, N., Clagett, M., Li, J., Jones, S., Pincus, S., D'Alia, G., Nardone, L., Babin, M., Spitalny, G., and Casey, L. 2005. A high-affinity monoclonal antibody to anthrax protective antigen passively protects rabbits before and after aerosolized Bacillus anthracis spore challenge. *Infect Immun* **73:** 795-802.

Mylvaganam, S.E., Paterson, Y., and Getzoff, E.D. 1998. Structural basis for the binding of an anti-cytochrome c antibody to its antigen: crystal structures of FabE8-cytochrome c complex to 1.8 A resolution and FabE8 to 2.26 A resolution. *J Mol Biol* **281:** 301-322.

Niemi, M., Jylha, S., Laukkanen, M.L., Soderlund, H., Makinen-Kiljunen, S., Kallio, J.M., Hakulinen, N., Haahtela, T., Takkinen, K., and Rouvinen, J. 2007. Molecular interactions between a recombinant IgE antibody and the beta-lactoglobulin allergen. *Structure* **15:** 1413-1421.

Nilsson, B., Moks, T., Jansson, B., Abrahmsen, L., Elmblad, A., Holmgren, E., Henrichson, C., Jones, T.A., and Uhlen, M. 1987. A synthetic IgG-binding domain based on staphylococcal protein A. *Protein Eng* **1:** 107-113.

Paddle, B.M., Wong, V.K., and Muller, B.D. 2006. The cytotoxic effect of anthrax lethal toxin on human lung cells in vitro and the protective action of bovine antibodies to PA and LF. *J Appl Toxicol* **26:** 162-168.

Padlan, E.A., Silverton, E.W., Sheriff, S., Cohen, G.H., Smith-Gill, S.J., and Davies, D.R. 1989. Structure of an antibody-antigen complex: crystal structure of the HyHEL-10 Fab-lysozyme complex. *Proc Natl Acad Sci U S A* **86:** 5938-5942.

Pannifer, A.D., Wong, T.Y., Schwarzenbacher, R., Renatus, M., Petosa, C., Bienkowska, J., Lacy, D.B., Collier, R.J., Park, S., Leppla, S.H.*, et al.* 2001. Crystal structure of the anthrax lethal factor. *Nature* **414:** 229-233.

Pavlou, A.K., and Belsey, M.J. 2005. The therapeutic antibodies market to 2008. *Eur J Pharm Biopharm* **59:** 389-396.

Pelat, T., Hust, M., Laffly, E., Condemine, F., Bottex, C., Vidal, D., Lefranc, M.P., Dubel, S., and Thullier, P. 2007. High-affinity, human antibody-like antibody fragment (single-chain variable fragment) neutralizing the lethal factor (LF) of Bacillus anthracis by inhibiting protective antigen-LF complex formation. *Antimicrob Agents Chemother* **51:** 2758-2764.

Petosa, C., Collier, R.J., Klimpel, K.R., Leppla, S.H., and Liddington, R.C. 1997. Crystal structure of the anthrax toxin protective antigen. *Nature* **385:** 833-838.

Prasad, L., Waygood, E.B., Lee, J.S., and Delbaere, L.T. 1998. The 2.5 A resolution structure of the jel42 Fab fragment/HPr complex. *J Mol Biol* **280:** 829-845.

Proba, K., Worn, A., Honegger, A., and Pluckthun, A. 1998. Antibody scFv fragments without disulfide bonds made by molecular evolution. *J Mol Biol* **275:** 245-253.

Reetz, M.T., Kahakeaw, D., and Lohmer, R. 2008. Addressing the numbers problem in directed evolution. *Chembiochem* **9:** 1797-1804.

Rivera, J., Nakouzi, A., Abboud, N., Revskaya, E., Goldman, D., Collier, R.J., Dadachova, E., and Casadevall, A. 2006. A monoclonal antibody to Bacillus anthracis protective antigen defines a neutralizing epitope in domain 1. *Infect Immun* **74:** 4149-4156.

Rosovitz, M.J., Schuck, P., Varughese, M., Chopra, A.P., Mehra, V., Singh, Y., McGinnis, L.M., and Leppla, S.H. 2003. Alanine-scanning mutations in domain 4 of anthrax toxin protective antigen reveal residues important for binding to the cellular receptor and to a neutralizing monoclonal antibody. *J Biol Chem* **278:** 30936-30944.

Rothlisberger, D., Khersonsky, O., Wollacott, A.M., Jiang, L., DeChancie, J., Betker, J., Gallaher, J.L., Althoff, E.A., Zanghellini, A., Dym, O*., et al.* 2008. Kemp elimination catalysts by computational enzyme design. *Nature* **453:** 190-195.

Russell, P.K. 2007. Project BioShield: what it is, why it is needed, and its accomplishments so far. *Clin Infect Dis* **45 Suppl 1:** S68-72.

Santelli, E., Bankston, L.A., Leppla, S.H., and Liddington, R.C. 2004. Crystal structure of a complex between anthrax toxin and its host cell receptor. *Nature* **430:** 905-908.

Sawada-Hirai, R., Jiang, I., Wang, F., Sun, S.M., Nedellec, R., Ruther, P., Alvarez, A., Millis, D., Morrow, P.R., and Kang, A.S. 2004. Human anti-anthrax protective antigen neutralizing monoclonal antibodies derived from donors vaccinated with anthrax vaccine adsorbed. *J Immune Based Ther Vaccines* **2:** 5.

Scobie, H.M., Rainey, G.J., Bradley, K.A., and Young, J.A. 2003. Human capillary morphogenesis protein 2 functions as an anthrax toxin receptor. *Proc Natl Acad Sci U S A* **100:** 5170-5174.

Scobie, H.M., and Young, J.A. 2005. Interactions between anthrax toxin receptors and protective antigen. *Curr Opin Microbiol* **8:** 106-112.

Segelke, B.W. 2001. Efficiency analysis of sampling protocols used in protein crystallization screening. *Journal of Crystal Growth* **232:** 553-362.

Sheriff, S., Silverton, E.W., Padlan, E.A., Cohen, G.H., Smith-Gill, S.J., Finzel, B.C., and Davies, D.R. 1987. Three-dimensional structure of an antibody-antigen complex. *Proc Natl Acad Sci U S A* **84:** 8075-8079.

Shieh, H.S., Stallings, W.C., Stevens, A.M., and Stegeman, R.A. 1995. Using sampling techniques in protein crystallization. *Acta Crystallogr D Biol Crystallogr* **51:** 305-310.

Shusta, E.V., Raines, R.T., Pluckthun, A., and Wittrup, K.D. 1998. Increasing the secretory capacity of Saccharomyces cerevisiae for production of single-chain antibody fragments. *Nat Biotechnol* **16:** 773-777.

Singh, Y., Klimpel, K.R., Quinn, C.P., Chaudhary, V.K., and Leppla, S.H. 1991. The carboxyl-terminal end of protective antigen is required for receptor binding and anthrax toxin activity. *J Biol Chem* **266:** 15493-15497.

Staats, H.F., Alam, S.M., Scearce, R.M., Kirwan, S.M., Zhang, J.X., Gwinn, W.M., and Haynes, B.F. 2007. In vitro and in vivo characterization of anthrax anti-protective antigen and anti-lethal factor monoclonal antibodies after passive transfer in a mouse lethal toxin challenge model to define correlates of immunity. *Infect Immun* **75:** 5443-5452.

Stavnezer, J., and Amemiya, C.T. 2004. Evolution of isotype switching. *Semin Immunol* **16:** 257-275.

Steiniger, S.C., Altobell, L.J., 3rd, Zhou, B., and Janda, K.D. 2007. Selection of human antibodies against cell surface-associated oligomeric anthrax protective antigen. *Mol Immunol* **44:** 2749-2755.

Stura, E.A., Nemerow, G.R., and Wilson, I.A. 1992. Strategies in the crystallization of glycoproteins and protein complexes. *Journal of Crystal Growth* **122:** 273-285.

Su, H.P., Golden, J.W., Gittis, A.G., Hooper, J.W., and Garboczi, D.N. 2007. Structural basis for the binding of the neutralizing antibody, 7D11, to the poxvirus L1 protein. *Virology* **368:** 331-341.

Subramanian, G.M., Cronin, P.W., Poley, G., Weinstein, A., Stoughton, S.M., Zhong, J., Ou, Y., Zmuda, J.F., Osborn, B.L., and Freimuth, W.W. 2005. A phase 1 study of PAmAb, a fully human monoclonal antibody against Bacillus anthracis protective antigen, in healthy volunteers. *Clin Infect Dis* **41:** 12-20.

Tulip, W.R., Varghese, J.N., Laver, W.G., Webster, R.G., and Colman, P.M. 1992. Refined crystal structure of the influenza virus N9 neuraminidase-NC41 Fab complex. *J Mol Biol* **227:** 122-148.

Varadarajan, N., Rodriguez, S., Hwang, B.Y., Georgiou, G., and Iverson, B.L. 2008. Highly active and selective endopeptidases with programmed substrate specificities. *Nat Chem Biol* **4:** 290-294.

Vitale, L., Blanset, D., Lowy, I., O'Neill, T., Goldstein, J., Little, S.F., Andrews, G.P., Dorough, G., Taylor, R.K., and Keler, T. 2006. Prophylaxis and therapy of

inhalational anthrax by a novel monoclonal antibody to protective antigen that mimics vaccine-induced immunity. *Infect Immun* **74:** 5840-5847.

Walsh, J.J., Pesik, N., Quinn, C.P., Urdaneta, V., Dykewicz, C.A., Boyer, A.E., Guarner, J., Wilkins, P., Norville, K.J., Barr, J.R., *et al.* 2007. A case of naturally acquired inhalation anthrax: clinical care and analyses of anti-protective antigen immunoglobulin G and lethal factor. *Clin Infect Dis* **44:** 968-971.

Wang, F., Ruther, P., Jiang, I., Sawada-Hirai, R., Sun, S.M., Nedellec, R., Morrow, P.R., and Kang, A.S. 2004. Human monoclonal antibodies that neutralize anthrax toxin by inhibiting heptamer assembly. *Hum Antibodies* **13:** 105-110.

Wild, M.A., Xin, H., Maruyama, T., Nolan, M.J., Calveley, P.M., Malone, J.D., Wallace, M.R., and Bowdish, K.S. 2003. Human antibodies from immunized donors are protective against anthrax toxin in vivo. *Nat Biotechnol* **21:** 1305-1306.

Williams, B.R., and Zhu, Z. 2006. Intrabody-based approaches to cancer therapy: status and prospects. *Curr Med Chem* **13:** 1473-1480.

Wittrup, K.D. 2001. Protein engineering by cell-surface display. *Curr Opin Biotechnol* **12:** 395-399.

Young, J.A., and Collier, R.J. 2007. Anthrax toxin: receptor binding, internalization, pore formation, and translocation. *Annu Rev Biochem* **76:** 243-265.

Zhou, B., Carney, C., and Janda, K.D. 2008. Selection and characterization of human antibodies neutralizing Bacillus anthracis toxin. *Bioorg Med Chem* **16:** 1903-1913.

CHAPTER 2

Crystal Structure of the Engineered Neutralizing Antibody M18 Complexed to the Anthrax Protective Antigen (PA)

This chapter is a manuscript that has been submitted for publication. Jennifer A. Maynard prepared 14B7 protein and crystallized 14B7*. Clinton E. Leysath prepared all other proteins and crystallized 1H, M18, and the M18-PAD4 complex; he was also responsible for solving the structure of 1H, carrying out the kinetic studies, and co-authoring of the manuscript. Arthur F. Monzingo was responsible for solving the structures of 14B7*, M18, and the M18-PAD4 complex; he also created the figures and co-authored the manuscript. Jon D. Robertus, Brent L. Iverson, and George Georgiou were all responsible for co-authoring of the manuscript.*

2.1 INTRODUCTION

Anthrax remains a significant threat as a biological weapon due in large part to its ease of both large-scale manufacture and weaponization in the spore state. Following spore inhalation, anthrax is lethal in humans due to the combined actions of secreted toxins (Moayeri and Leppla 2004; Young and Collier 2007). An effective countermeasure strategy requires an effective anti-toxin therapy (Little *et al.* 1988; Cirino *et al.* 1999; Sellman *et al.* 2001; Maynard *et al.* 2002; Wild *et al.* 2003; Brossier *et al.* 2004; Harvey *et al.* 2004; Sawada-Hirai *et al.* 2004; Turk *et al.* 2004; Shoop *et al.* 2005; Subramanian *et al.* 2005; Chen *et al.* 2006; Jiao *et al.* 2006; Rivera *et al.* 2006; Albrecht *et al.* 2007; Pelat *et al.* 2007; Steiniger *et al.* 2007) to be used in combination with antibiotics, or as a stand alone treatment of an antibiotic resistant strain of anthrax (Mohamed *et al.* 2005).

We, and others, have been developing a combination prophylactic-post exposure therapeutic for anthrax based on an engineered antibody against the anthrax protective antigen (PA) toxin (Little *et al.* 1988; Little *et al.* 1997; Cirino *et al.* 1999; Maynard *et al.* 2002; Wild *et al.* 2003; Brossier *et al.* 2004; Harvey *et al.* 2004; Karginov *et al.* 2004; Sawada-Hirai *et al.* 2004; Cui *et al.* 2005; Mohamed *et al.* 2005; Subramanian *et al.* 2005; Chen *et al.* 2006; Rivera *et al.* 2006; Vitale *et al.* 2006; Albrecht *et al.* 2007; Kelly *et al.* 2007; Pelat *et al.* 2007; Steiniger *et al.* 2007). Briefly, the PA toxin facilitates host cellular targeting and transport of the lethal factor (LF) and edema factor (EF) into the cytoplasm. LF is a protease that targets mitogen-activated protein kinase kinases (MAPKKs). EF is an adenylate cyclase. The presence of cytoplasmic LF and EF trigger a series of biochemical events that lead to anthrax symptoms and eventually to death (Moayeri and Leppla 2004; Young and Collier 2007).

The intoxication process is initiated when monomeric PA83 is processed by host proteases to form the PA63 fragment, which binds as a heptamer with high affinity to the TEM8 and CMG2 cellular receptors on host cells such as macrophages. High affinity antibodies that block the PA-receptor interaction are effective post-exposure treatments for anthrax in animal models (Little *et al.* 1997; Karginov *et al.* 2004; Cui *et al.* 2005; Vitale *et al.* 2006; Kelly *et al.* 2007). In addition, the same anti-PA antibodies can serve as prophylactics to prevent infection from spore inhalation, although the mechanism of prophylaxis is not well understood (Kobiler *et al.* 2002; Cote *et al.* 2005; Mabry *et al.* 2005; Mohamed *et al.* 2005; Peterson *et al.* 2006).

The 14B7 murine monoclonal antibody (KD = 4.3 nM), originally developed at USAMRIID (Little *et al.* 1988), was shown to delay time-to-death following exposure to anthrax spores in a guinea pig model (Little *et al.* 1997). 14B7 is known to recognize the receptor-binding region of PA and thereby block PA-host cell interactions (Rosovitz *et*

al. 2003). Originally, we used phage display to isolate an affinity enhanced version of 14B7 called 1H, exhibiting a KD of 250 pM (Maynard *et al.* 2002). 1H was shown to prevent PA-LF induced death in a rat model and in whole IgG format it is currently in clinical development. The approximately 20-fold affinity enhancement of 1H compared to 14B7 is achieved with two mutations, Q55L and S56P, in CDR L2. Subsequently, we used our bacterial display/FACS technology, referred to as APEx, to engineer an even higher affinity variant of 14B7 called M18 (Harvey *et al.* 2004). M18 has 10 mutations (light chain I21V, L46F, S56P, S76N, Q78L, and L94P; heavy chain S30N, T58S, K65E, and T69I) and exhibits a KD = 35 pM. We sought to use crystallographic studies to 1) reveal the structural details of the interactions between the 14B7 family of antibodies with PA and 2) to help elucidate how the mutations in 1H and M18 serve to enhance overall antibody affinity.

Crystallographic studies of antibody fragments in complex with a protein antigen have been ongoing for more than 25 years. A large number of these studies have been carried out on lysozyme variants and their antibodies, utilizing the propensity of lysozyme to crystallize to enable recovery of crystals of the complex (Amit *et al.* 1986; Padlan *et al.* 1989; Braden *et al.* 1994; Braden *et al.* 1995; Davies and Cohen 1996; Li *et al.* 2003). Other studies have targeted antibodies in complex with influenza neuraminidase (Colman *et al.* 1987), cytochrome C (Mylvaganam *et al.* 1998), tissue factor (Huang *et al.* 1998), outer surface proteins of Borrelia bergdorferi (Li *et al.* 1997), staphylococcal nuclease (Bossart-Whitaker *et al.* 1995), vascular endothelial growth factor (Muller *et al.* 1998), GP120 of HIV (Zhou *et al.* 2007), a phosphocarrier protein of E. coli (Prasad *et al.* 1998), a myelin oligodendrocyte glycoprotein (Breithaupt *et al.* 2003), the epidermal growth factor receptor (EGFR) family (Cho *et al.* 2003; Li *et al.* 2005), the CD3 epsilon gamma heterodimer (Kjer-Nielsen *et al.* 2004), the T-cell

costimulatory protein CD28 (Evans *et al.* 2005), the severe acute respiratory syndrome (SARS) coronavirus receptor binding domain (RBD) (Prabakaran *et al.* 2006), the poxvirus L1 protein (Su *et al.* 2007), the malaria apical membrane antigen 1 (AMA1) (Igonet *et al.* 2007), allergens (Li *et al.* 2008), human prostate-specific antigen (PSA) (Menez *et al.* 2008), dengue viral envelope glycoprotein (Lok *et al.* 2008), the membrane-type serine protease 1 (Farady *et al.* 2008), Ebola glycoprotein (Lee *et al.* 2008), idiotype-anti-idiotype interactions (Fields *et al.* 1995), and autoimmune disease interactions of antibodies to other antibodies (Corper *et al.* 1997).

Generally, antibodies to protein antigens target a discontinuous epitope on the antigen (Padlan *et al.* 1989). It is also common for all 6 complementarity-determining regions (CDRs) of the antibody to interact with the antigen (Padlan *et al.* 1989; Huang *et al.* 1998; Mylvaganam *et al.* 1998; Prasad *et al.* 1998), and on occasion, framework residues make contact as well (Padlan *et al.* 1989). The interaction surface is generally a flat, rectangular area (Amit *et al.* 1986), though there are exceptions (Bossart-Whitaker *et al.* 1995). Shape complementarity along the interaction surface appears to be important (Muller *et al.* 1998; Mylvaganam *et al.* 1998; Li *et al.* 2003) and a nonpolar "hotspot" is generally found to be an energetically important part of the complex. The degree of solvation at the interface can vary (Braden *et al.* 1994), and bound water molecules may add hydrogen bond interactions (Braden *et al.* 1995). However, there are also occasions where there are voids that remain unsolvated (Braden *et al.* 1994). A study of the affinity maturation of antibodies to lysozyme revealed that improved shape complementarity and burial of nonpolar surface at the expense of polar surface were generally correlated with increased affinity (Li *et al.* 2003). In addition, structural studies with small molecule haptens have indicated that affinity maturation via somatic mutation might involve

freezing out complementary conformations of CDR loops, involving mutations in residues that can be up to 15 Å away (Wedemayer *et al.* 1997).

Here we report the crystal structure of M18 in complex with domain 4 of PA and the crystal structures of high affinity antibodies 14B7, 1H, and M18. The M18-PA complex offers a detailed explanation for the neutralizing activity of the 14B7 family of antibodies, and also provides some insight into the affinity enhancements seen with engineered versions of 14B7. In the future, the M18-PA complex structure will serve as a useful reference to target specific regions of 14B7 family antibodies to make even higher affinity variants, and for mutagenesis in the event a non-neutralizing variant of PA is encountered through either deliberate or natural variation.

2.2 MATERIALS AND METHODS

2.2.1 Protein purification

M18, 1H, and 14B7* scFv's were cloned into the periplasmic expression vector pAK400. Protein was prepared as described previously (Hayhurst *et al.* 2003). See Figure 2.1 for their sequences, as well as that of the parent monoclonal antibody 14B7. Briefly, a pelB leader sequence was utilized to express protein into the periplasm of E. coli strain Jude-1, and osmotic shock followed by immobilized metal affinity chromatography was used for initial purification. Size exclusion chromatography (AKTA FPLC and Superdex 200 column, GE Healthcare) allowed isolation of monomeric scFv. Monomeric scFv was then digested overnight at 4ºC with Carboxypeptidase A (Calbiochem, San Diego, CA, 1:100 mass ratio, protease:scFv). A second round of FPLC was followed by concentration to 10 mg/ml (Amicon Ultra 15, 10000 MWCO) into 1xHBS-EP (10 mM Hepes, pH 7.4, 150 mM NaCl, 3 mM EDTA,

0.005% Polysorbate-20). Full-length Anthrax Protective Antigen (PA83) was purchased from List Biological Labs (Campbell, CA), resuspended at 1 mg/ml, and subjected to size exclusion FPLC. Protein was concentrated to 10 mg/ml into 1xHBS-EP.

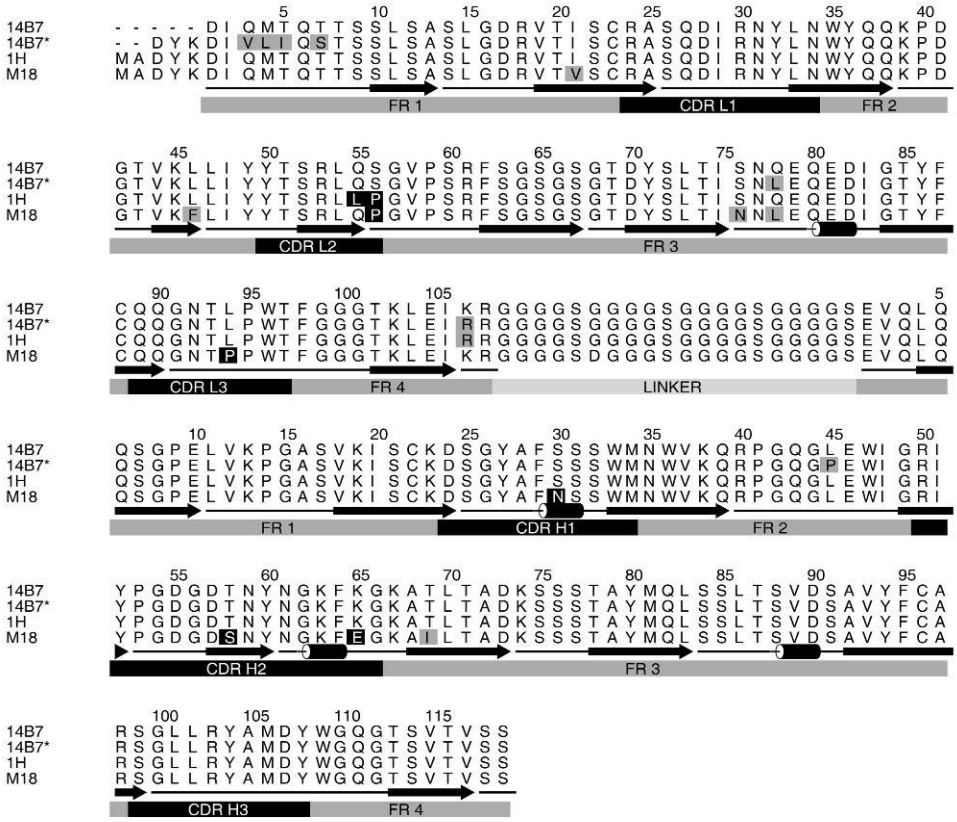

FIGURE 2.1 - SEQUENCE ALIGNMENT OF SCFV 14B7, 14B7*, 1H, AND M18. In these scFv constructs, the light chain precedes the heavy chain in the sequence, linked by a glycine-rich linker region. Framework and complementarity-determining regions are indicated as well as secondary structure. Differences from the 14B7 sequence in the framework regions are highlighted in gray; differences in the CDRs are highlighted in black. This figure was made using ALSCRIPT.

2.2.2 Site-directed mutagenesis and kinetic studies

Mutant scFv's 14B7-L46F and M18-F46L were constructed using the QuikChange protocol (Stratagene, La Jolla, CA). After protein expression, kinetic studies were carried out using a Biacore 3000 (Biacore, Inc., Piscataway, NJ). Briefly, amine coupling chemistry was used to immobilize 750 RU of either PA83 or BSA (control) to a CM5 chip. Samples were injected for 60 seconds at 100 µl/min in 1 x HBS-EP and allowed to dissociate for 15 minutes at the same flow rate. Regeneration of the flow cells was accomplished using a 30 second injection of 4 M $MgCl_2$ at 100 µl/min.

2.2.3 Crystallization and data collection

The 14B7* scFv protein was crystallized at room temperature in sitting drops from mixtures containing a one-to-one ratio of antibody solution (15 mg/mL) and reservoir solution [20% (w/v) PEG 4000, 0.1 HEPES, pH 7.5, 10% iso-propanol]. The higher affinity variants 1H and M18 were crystallized under the same conditions at 4°C. Prior to data collection, crystals were transferred to a cryoprotectant solution (the reservoir solution containing 25% glycerol) for 1-5 seconds. The 14B7* crystal was flash-frozen directly in the cold nitrogen stream on the goniostat. The 1H and M18 crystals, mounted in a cryoloop (Hampton Research, Laguna Niguel, CA), was frozen by dipping in liquid nitrogen and placed in the cold stream on the goniostat.

A mixture of PA83 and M18 with a 1:1.1 molar ratio was used to screen for crystallization conditions by the sitting drop method. Eleven months after the crystallization conditions were set up, a crystal was found in a condition at 4ºC with the reservoir solution 10% PEG 20,000, 0.05 M Tris-HCl, pH 7.5. Prior to data collection, crystals were transferred to a cryoprotectant solution (6% PEG 20,000, 0.05 M Tris-HCl,

pH 7.5, 25% glycerol) for 1-5 seconds. The complex crystal, mounted in a cryoloop, was frozen by dipping in liquid nitrogen and placed in the cold stream on the goniostat.

X-ray diffraction data from the 14B7* crystal were collected at 100 K on beamline 8.2.1 of the Advanced Light Source (Lawrence Berkeley National Laboratory). Diffraction data of the 1H, M18, and complex crystals were collected at 100 K on an RAXIS IV++ image plate detector (Rigaku, The Woodlands, TX) with X-rays generated by a Rigaku RU-H3R rotating anode generator operated at 50 mV, 100 mA. Diffraction images were processed and data reduced using HKL2000 (Otwinowski and Minor 1997).

2.2.4 Molecular replacement for the scFv's

The structure of the 14B7* scFv was solved by molecular replacement using the light chain of blood group A Fv (PDB accession code 1JV5) (Thomas *et al.* 2002) and the heavy chain of Fab17-IA (accession code 1FOR) (Liu *et al.* 1994) as search models; the structures were aligned with the EPMR (Evolutionary Protein Molecular Replacement) program (Kissinger *et al.* 2001). An initial chain tracing was generated from the molecular replacement solution using ARP/wARP (Perrakis *et al.* 1997). The structures of the 1H and M18 scFv's were solved by molecular replacement using the 14B7* structure as the search model with the program MOLREP (Vagin and Teplyakov 1997).

2.2.5 Molecular replacement for the Complex

Crystal cell parameters of the complex crystal suggested that the asymmetric unit might contain two PA83-M18 complexes. Molecular replacement searches using several programs and with various search models, including PA83 (PDB accession code 1ACC; Petosa *et al.* 1997), PA63, 14B7*, and individual PA domains, failed to find a solution.

Finally, a search using the program PHASER (McCoy 2007) with the single chain antibody 14B7* as a model gave a result that had a rotation function Z-score of 5.7 and a translation function Z-score of 5.9; the program authors have stated that scores of this magnitude may indicate a correct solution. Subsequent searches with 14B7* found solutions for three additional molecules, with increasingly improved Z-scores. Following that, solutions for the positions of four copies of PA domain 4 (PAD4) were determined. Examination of the packing of the four M18 scFv and four PAD4 molecules in the asymmetric unit showed that there were four essentially identical M18 scFv-PAD4 heterodimers; this initial model had an R-factor of 32.6% suggesting that this was the correct molecular replacement solution.

2.2.6 Structure determination and analysis

Model building was carried out using O (Jones *et al.* 1991). Refinement of models was performed with the Crystallography and NMR System (CNS) (Version 1.1)(Brunger *et al.* 1998). The structures of the scFv's were refined using the slow-cooling protocol. For the 3.8 Å resolution complex structure, atomic positions were restrained by non-crystallographic symmetry and refined using conjugate gradient minimization. Temperature factors for each residue in the complex were also refined. There were several rounds of refinement followed by manual rebuilding of the model. To facilitate manual rebuilding, a difference map and a $2F_o$-F_c map, SIGMAA-weighted to eliminate bias from the model (Read 1986), were prepared. 5% of the diffraction data were set aside throughout refinement for cross-validation (Brunger 1993). Computations and model building were carried out on Silicon Graphics Indy (Mountain View, CA), Gateway SB Select (Poway, CA), and HP Pavilion a1610n (Hewlett-Packard Co., Palo Alto, CA) computers.

Superpositions of protein molecules were done with O. Model pictures were made using MOLSCRIPT, BOBSCRIPT, Raster3D, and PYMOL (DeLano Scientific, San Carlos, CA).

2.3 RESULTS AND DISCUSSION

2.3.1 X-ray structure determination

The 14B7* scFv crystallized in space group $P4_12_12$ with cell constants a = b = 80.18, c = 67.83 Å and with one molecule per asymmetric unit, giving a V_m of 2.3 $Å^3$ / dalton. The structure was solved by molecular replacement using the κ chain of the blood group A Fv (PDB accession code 1JV5) (Thomas *et al.* 2002) and the heavy chain of Fab17-IA (PDB code 1FOR) (Liu *et al.* 1994) as search models for the light and heavy chains, respectively. Of known antibody structures, these two showed the highest sequence homology with 14B7*. The final refined structure consists of residues 1-107 of the light chain and 4-118 of the heavy chain; it has an $R_{working}$ of 21.7% and an R_{free} of 23.6%, at a resolution of 1.3 Å. The 20 residue linker between the *C*-terminus of the light chain and the *N*-terminus of the heavy chain is not visible in electron density maps nor were residues 1- 3 and the *C*-terminal residue (119) of the heavy chain. We assume the missing residues are all disordered. The refined model includes 265 solvent molecules. A representative section of electron density is shown in Figure 2.2a.

A Ramachandran plot shows 92.5% of residues in the most favorable region and 7.0% in additional allowed space. Light chain Thr 51, located on the CDR L2 loop, is found in an energetically disfavored conformation, stabilized by hydrogen bonds with neighboring residues. This residue is also in this same disallowed conformation in both variants 1H and M18, as well as M18 in complex with PAD4.

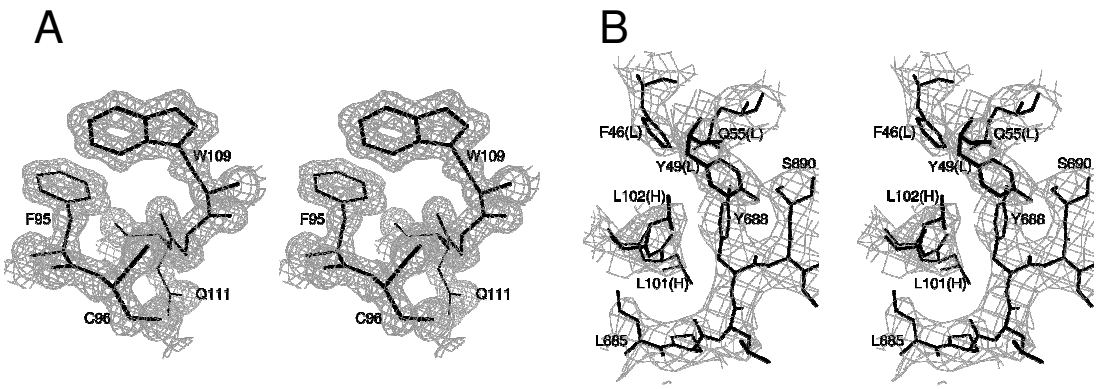

FIGURE 2.2 - ELECTRON DENSITY FROM A SIGMAA-WEIGHTED (READ 1986) 2FO-FC MAP, CALCULATED WITH PHASES FROM THE FINAL REFINED MODEL. These stereo maps are contoured at 1.0 . (a) 14B7*; (b) from the PAD4-M18 interface region around residue Y688 of PAD4.

Crystals of the high affinity variant 1H, crystallized under the same conditions as 14B7* but at 4°C, grew in the same crystal form as 14B7* but diffracted to only 2.8 Å. The structure was solved by molecular replacement using the 14B7* structure as the search model. The final refined structure consists of residues 1-108 of the light chain and 3-119 of the heavy chain and has an $R_{working}$ of 21.7% and an R_{free} of 25.6%. In addition, there is clear electron density for one leader residue preceding the N-terminus of the light chain, and this residue is included in the final model. As with 14B7*, the 20 residue linker between the light and heavy chains was not visible in electron density maps. A Ramachandran plot shows 88.4% of residues in the most favorable region and 11.1% in additional allowed space. The refined model includes 16 solvent molecules.

Crystals of the ultrahigh affinity variant M18 scFv were grown under the same conditions as 1H and diffracted to 2.0 Å. Unlike 14B7* and 1H, the M18 scFv crystallized in space group P1 with cell constants a = 36.07, b = 54.21, c = 61.95 Å, =

71.8°, □ = 75.6°,and □ = 71.3° and with two molecules per asymmetric unit, giving a Vm of 2.2 Å^3 / dalton. The structure was solved by molecular replacement using the 14B7* structure as the search model. The final refined structure consists of residues of 1-108 of the light chain and 2-119 of the heavy chain and has an $R_{working}$ of 19.4% and an R_{free} of 22.9%. In addition, there is density for two leader residues preceding the N-terminus of the light chain. As with 14B7* and 1H, the 20 residue linker between the light and heavy chains was not visible in electron density maps. A Ramachandran plot shows 88.2% of residues in the most favorable region and 11.3% in additional allowed. The refined model includes 291 solvent molecules.

The complex of M18 and the Anthrax Protective Antigen domain 4 (PAD4) crystallized in space group $P2_1$ with cell constants a = 48.94, b = 299.72, c = 68.95, and □ = 94.5º. Four antigen-scFv complexes were found in the asymmetric unit, giving a V_m of 3.1 Å^3 / dalton. The crystal diffracted to only 3.8 Å, but four-fold non-crystallographic restraints permitted the refinement of individual atomic positions and of group temperature factors for each residue. The final refined structure has an $R_{working}$ of 23.2% and an R_{free} of 27.6%. Figure 2.2b shows electron density from a $2F_o$-F_c map at the interface between PA domain 4 and both the H and L chains of M18. Crystallographic data for the three scFv structures and the PAD4-M18 complex are shown in Table 2.1.

Table 2.1. Crystallographic Data

	14B7*	1H	M18	PAD4-M18
Space group	$P4_12_12$	$P4_12_12$	P1	$P2_1$
Cell constants	a=b=80.18, c=67.83 Å	a=b=79.94, c=68.17 Å	a=36.07, b=54.21, c=61.95 Å α=71.8°, β=75.6°, γ=71.3°	a=48.94, b=299.72, c=68.95, β=94.5°
# of molecules per asymmetric unit	1	1	2	4
Resolution (Å)	20.-1.3 (1.35-1.3)	20.-2.8 (2.9-2.8)	20.-2.0 (2.08-2.0)	20.-3.8 (3.94-3.8)
R_{merge} (%)	7.9 (46.6)	16.0 (39.0)	4.0 (10.7)	12.0 (28.3)
$<I/\sigma_I>$	9.4 (4.5)	13.7 (5.2)	26.4 (7.4)	6.1 (3.7)
Completeness (%)	99.1 (100.)	99.9 (99.3)	94.8 (92.4)	96.0 (91.6)
Unique reflections	54,301	5839	26,245	18,357
Redundancy	12.8	8.2	2.0	2.6
# of residues	222	226	455	1485
# of protein atoms	1704	1724	3521	11,546
# of solvent atoms	265	16	291	
$R_{working}$	0.216	0.217	0.194	0.232
R_{free}	0.236	0.256	0.229	0.276
rms deviation from ideality bonds (Å) angles (º)	0.004 1.419	0.008 2.195	0.006 1.370	0.010 1.45

Values in parentheses correspond to highest resolution shell

As mentioned above, the asymmetric unit of the complex contains four PAD4-M18 heterodimers. In particular, each heterodimer is related to a second heterodimer by a non-crystallographic two-fold rotation with the dimer interface of this greater dimer involving principally □-strands of the light chain 62-67 and 70-74. The two greater dimer

particles in the asymmetric unit are, in turn, related by a rotation of 178° about an axis that is around 91° from the greater dimerization axis. Contact between the greater dimer particles of the asymmetric unit involves a single PAD4 monomer in each.

The four M18 molecules within the asymmetric unit are virtually identical. As was observed in the structures of unbound 14B7*, 1H, and M18, electron density is observed for residues of the light chain and heavy chain but not for the 20 amino acids linking the C-terminus of the light chain to the N-terminus of the heavy chain in the scFv. In two of the M18 monomers, residues 1-119 of the heavy chain are observed while only heavy chain residues 2-119 can be seen in the other two monomers.

The four PAD4 molecules within the asymmetric unit are also virtually identical with the largest differences seen in the N-terminal loop, residues 592-605. This loop extends away from the rest of the molecule, and as a result, the crystal packing environment differs for each PAD4 monomer in the asymmetric unit producing subtle conformational differences. There is also some variation in the PAD4 sequence length observed. For three of the PAD4 monomers, density for residues 592-735 is observed, but for the fourth monomer, only residues 593-735 are seen.

2.3.2 Comparison of the scFv structures

The structures of the 14B7* scFv and the engineered variants 1H and M18 all show the expected typical immunoglobulin fold presenting a large binding surface formed by the CDRs. The folds of the three scFv antibodies are virtually identical. The rms distance between equivalent C positions of 14B7* and 1H is 0.24 Å, and similarly, the rmsd between C's 14B7* and M18 is 0.54 Å. The only significant difference occurs in the CDR H3 loop of M18 with a C rmsd of 2.0 Å.

However in the PAD4-M18 complex, the H3 loop assumes a conformation more like that of 14B7* and 1H. In the 14B7* and 1H scFv crystals, the H3 loop packing involves hydrophobic contacts between heavy chain L101 and L102 interacting between two adjacent molecules related by crystallographic symmetry. This differs from the packing in the P1 crystal of M18 scFv, where L101 makes hydrophobic contacts with heavy chain W33 and Y52, as well as light chain T93 and a leader Lys in an adjacent molecule. L102 is contacted by light chain P95 and heavy chain F47 in an adjacent molecule. Although the difference in H3 conformation appears to be due to crystal packing forces, it does demonstrate the flexibility of the H3 loop. A superposition of the Cα traces of the 14B7*, 1H, and M18 scFv's, along with that of M18 from the antibody-antigen complex Cα traces is shown in Figure 2.3.

Analysis of the temperature factors associated with the CDR H3 relative to the temperature factors of the remaining heavy chain reveals an increase that is statistically significant for CDR H3 in 1H and M18 (Table 2.2). This implies that there is increased flexibility in the CDR H3 loop compared to other regions in the scFv molecule.

Table 2.2. B-factor analysis of 14B7, 1H, and M18.

		Mean B-factor		
Crystal Structure	Light Chain	Heavy Chain - CDR H3	CDR H3	P-value*
14B7	11 ± 3	12 ± 3	12 ± 3	0.22
1H	13 ± 5	14 ± 6	16 ± 5	0.00016
M18	16 ± 6	16 ± 5	23 ± 5	7.0×10^{-19}

* Two-tailed t-test assuming unequal variances between CDR H3 and Heavy Chain - CDR H3

2.3.3 PAD4 structure

The structure of the Anthrax Protective Antigen (PA_{83} or, simply PA) has been solved previously at high resolution, both as the apo-protein (Petosa *et al.* 1997) and in

complex with the Anthrax toxin receptor (Santelli *et al.* 2004). The majority of contacts between PA_{83} and the CMG2 cellular receptor are made with PA domain 4 (PAD4), although some contacts with PA domain 2 are also seen. PAD4 consists of an initial β-hairpin and α-helix, followed by an immunoglobulin-like -sandwich composed of two 4-stranded antiparallel β-sheets. Residues 592-735 are observed for the four PAD4 monomers in the asymmetric unit of the PAD4-M18 crystal. A cartoon and surface

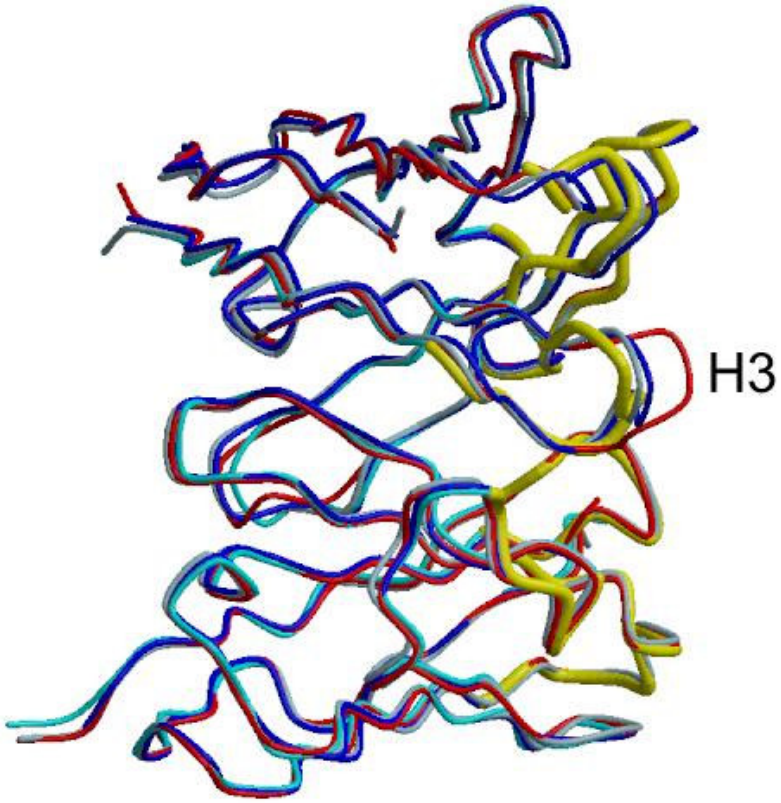

FIGURE 2.3 - SUPERPOSITION OF BACKBONE TRACES OF UNBOUND SCFV 14B7*, 1H, AND M18 ALONG WITH M18 FROM THE ANTIGEN-ANTIBODY COMPLEX. The trace of 14B7* is shown in dark blue, 1H in light blue, unbound M18 in red, and M18 from the complex in cyan. CDR loops from the bound M18 are shown thicker in yellow.

drawings of the PAD4-M18 complex are shown in Figures 2.4a and 2.4b. The PAD4 domain complexed with antibody is virtually identical to that from the unbound antigen (C rmsd of 0.7 Å), indicating that antibody binding does not cause significant conformational change in the antigen. A superposition of the C traces of the unbound and antibody-bound PAD4 is shown in Figure 2.4c.

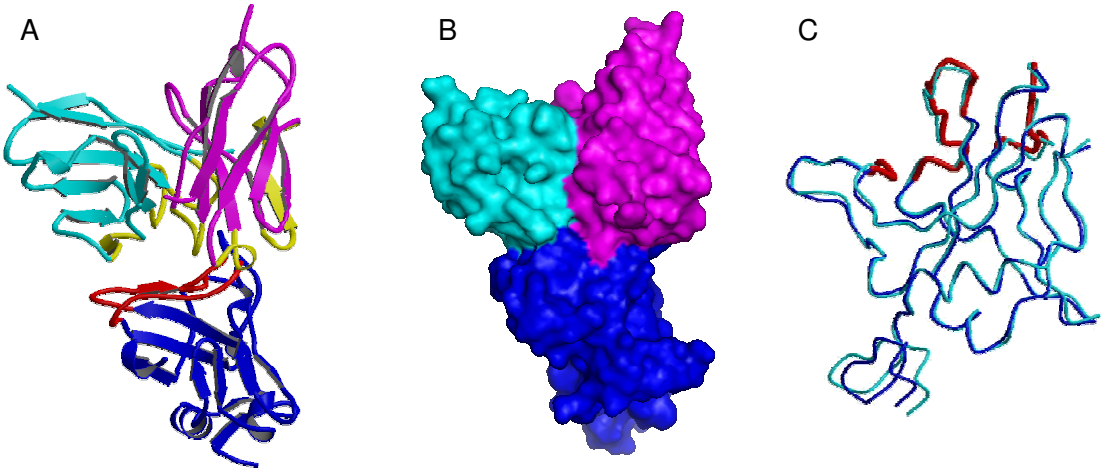

FIGURE 2.4 – REPRESENTATIONS OF THE PAD4-M18 COMPLEX. (a) Ribbon drawing of the PAD4-M18 complex. PAD4 is shown in blue, the M18 light chain in cyan, and the M18 heavy chain in magenta. The M18 CDR loops are shown in yellow; the PAD4 cell receptor binding loops are shown in red. (b) Surface view of PAD4-M18 structure with the same colors and orientation as (a). (c) Superposition of backbone traces of unbound PAD4 (Petosa *et al.* 1997) and PAD4 from the PAD4-M18 complex. PAD4 from the M18 complex is shown in cyan and unbound PAD4 in blue. The receptor binding loops are shown in red.

2.3.4 Antigen-antibody interface

The PAD4-M18 complex has a buried surface area of ~1700 Å^2. As expected, the CDRs of both the light and heavy chains of M18 face PAD4 in the antibody-antigen complex. All of the CDRs except L3 make some direct contact with PAD4, but the strongest interactions are made with H3 and L2. The major epitope of PAD4 is at an end of one of its β sheets (strands 5-6-9-10). There are three main contact loops: (1) β5-β6 (residues 646-658), comprised of the loop between strands 5 and 6, strand 6, and the loop immediately following strand 6; (2) β3-β9 (residues 683-694), the loop between helix 3 and strand 9; (3) pre-β10 (residues 716-719), the loop immediately preceding strand 10.

The M18 complex interface centers on PAD4 residues Y688 and L685. Y688 forms hydrophobic interactions with L2 residue Y49 and H3 residues L101 and L102, as shown in Figure 2.5a. L685 is a surface leucine, which upon binding with M18, is inserted into a pocket formed by CDRs H1 and H3 and the side chains of heavy chain residues W33 and L101. An additional hydrophobic interaction is formed between L652 and light chain residue Y50, and P686 also makes hydrophobic contact with heavy chain residue L101.

The complex is further stabilized by hydrophilic interactions, many of which are shown in Figure 2.5b. The hydroxyl of Y688 forms a hydrogen bond with the OE1 atom of L2 residue Q55. Several ion pairs are formed between PAD4 loops and CDRs L1, L2, and H2. These include D658 with L1 residue R30, D648 with L2 residue R53, D683 with H2 residue R50, and K684 with H2 residue D57. Several more hydrogen bonds are formed between all three PAD4 loops and CDR loops L1, L2, H1, and H3.

Previously, alanine-scanning experiments with residues 657 and 679-693 of PAD4 implicated N682, K684, L685, P686, L687, and Y688 as being significant for interactions with 14B7 (Rosovitz *et al.* 2003) (Figure 2.5c). By far, the largest effect on

14B7-binding was found for the L685A substitution, which showed a 10,000-fold decrease in binding affinity. It was also found that substitutions for N682, L687, and Y688 each reduced binding to 14B7 ~100-fold, while substitutions for K684 and P686 reduced binding affinity ~20-fold.

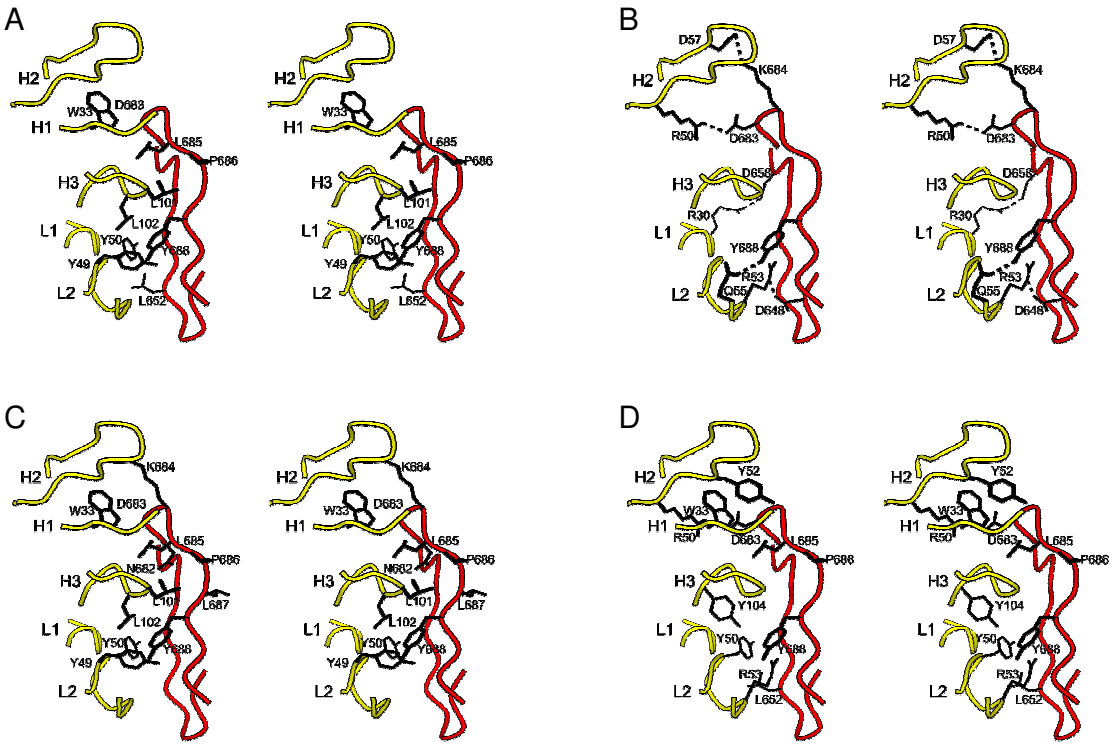

FIGURE 2.5 – THE PAD4-M18 INTERFACE. In these four panels, the M18 CDR loops are shown in yellow and labeled, and the PAD4 binding loops are shown in red. (a) Residues involved in specific hydrophobic interactions at the interface are shown. (b) Residues involved in hydrophilic interactions are shown. Hydrogen bonds are shown with a dashed line. (c) PAD4 residues indicated by alanine-scanning experiments to contribute to the binding of 14B7 (Rosovitz *et al.* 2003) are shown along with M18 residues observed to participate in hydrophobic interactions at the PAD4-M18 interface. (d) M18 residues indicated by alanine-scanning experiments to contribute to the binding

of PAD4 (Sivasubramanian *et al.* 2008) are shown with hydrophobic PAD4 residues observed to interact with M18. D683, known to interact with the MIDAS metal, is also shown.

In light of the PAD4-M18 structure, it is easy to rationalize the results found with PAD4 substitutions like K684A, L685A, P686A, and Y688A, each of which show clear interactions with M18 and significant buried surface area. Rationalizations for the reduced binding to 14B7 by the L687A and N682A variants are less obvious. L687 does not interact directly with the antibody, but may act as a key second shell residue, affecting the folding of PAD4 and the conformation of the epitope. L687 does form hydrophobic interactions with other PAD4 residues such as I646, I656, F678, and V696. N682 does not form any favorable interactions with PAD4 in the complex, but is pointed toward the backbone of heavy chain residues 101 and 102.

Previous results with alanine substitutions on the 14B7 structure are similarly easy to rationalize in large part (Sivasubramanian *et al.* 2008). Light chain residues Y50 and R53, as well as heavy chain residues W33, R50, Y52, and Y104 were found to be very important for binding, and these are all on the binding interface with PA (Figure 2.5d). Light chain residues W35, N92, and W96 were also found to be important in the alanine scan, but each of these are located within the interior of the light chain fold so they are likely key to establishing a stably folded structure.

2.3.5 Comparison to PAD4-CMG2 receptor interface

Previously, the structure of the complex of PA with the I domain of its host cell receptor, CMG2, was solved at 2.5 Å resolution (Santelli *et al.* 2004). There is a buried surface area of 1920 Å2 in the PA-CMG2 receptor complex, of which ~1360 $Å^2$ is buried

by the PAD4-receptor interface. The remainder is buried by the interface of the receptor with PA domain 2. There is no evidence that the 14B7 family of antibodies, including M18, contacts PA outside of domain 4. A superposition of the entire PA molecule (with domain 4 superimposed on that of our complex) indicates that M18 would contact only domain 4. That is, our complex represents the complete interaction of M18 with the PA protein.

Overall, the binding interfaces found in the PAD4-CMG2 and PAD4-M18 structures overlap well (Figure 2.6a). The CMG2 receptor interacts with the same three binding loops of PAD4 observed to make antibody contacts in the PAD4-M18 complex, and several of the PA residues are important in both cases (L682, P686, L687) based on alanine scanning results (Rosovitz *et al.* 2003). The binding interface between PAD4 and the CMG2 centers on a key interaction between D683 of PAD4 and a Mg atom bound in a so-called MIDAS (metal ion dependent adhesion site) motif of CMG2. In this way, the PA is mimicking the ligand recognition of integrins. Not surprisingly, when D683 is replaced by Ala, all PA toxicity is lost, presumably because the D683A variant cannot bind the CMG2 or other cellular receptors such as TEM8 (Rosovitz *et al.* 2003).

However, when D683 was converted to alanine, there was no measurable affect on the PAD4-14B7 interaction (Rosovitz *et al.* 2003). In the PAD4-M18 structure, D683 is found in the middle of the protein-protein interface, and makes a salt bridge with H2 residue R50 of M18 (Figure 2.5b). It is unclear why the loss of this ionic interaction should have so little effect on PAD4 antibody interaction. It is possible that a new hydrophobic contact is created in the D683A variant that adventitiously balances any binding energy lost with the elimination of the D683-R50 salt bridge.

There are some other clear differences between the PAD4-CMG2 and PAD4-M18 structural interactions. For example, the PAD4-CMG2 binding interface shows the

insertion of the CMG2 V115 side chain into a pronounced hydrophobic "socket" in PAD4 composed of I646, I656, and L687 (Figure 2.6b). In contrast, in the PAD4-M18 complex, this same PAD4 hydrophobic socket is not occupied by any antibody residue, hydrophobic or otherwise.

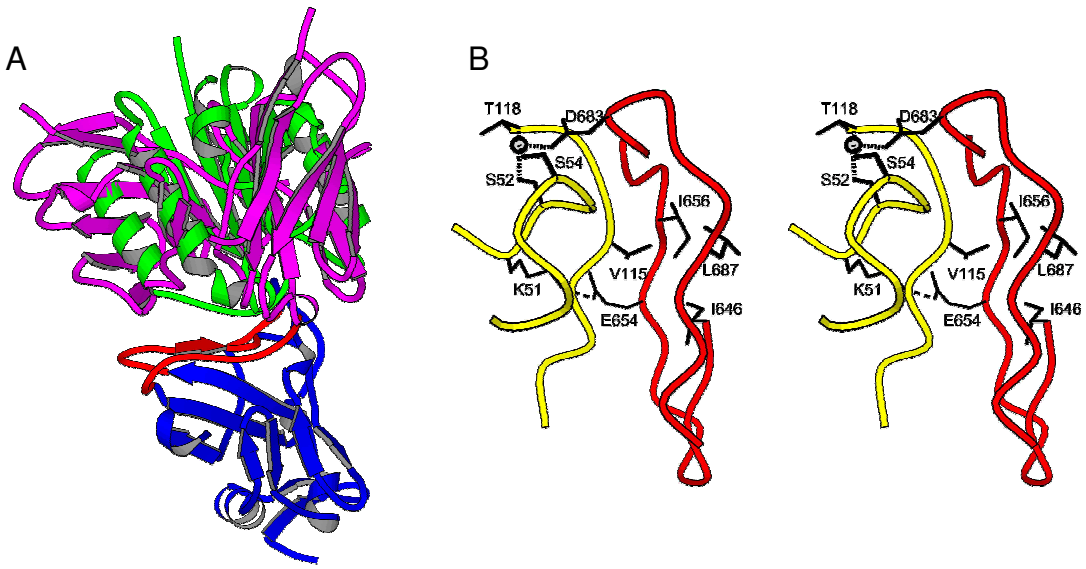

FIGURE 2.6 – PAD4-CMG2 COMPLEX IN RELATION TO THE PAD4-M18 COMPLEX. (a) Superposition of the PAD4-CMG2 receptor complex with the PAD4-M18 complex. PAD4 is shown in blue, the CMG2 receptor in green, and M18 in magenta. The receptor binding loops are shown in red. (b) PAD4-CMG2 receptor interface. Residues involved in specific interactions at the interface are shown, including the interaction of D683 with the MIDAS metal ion and the "hydrophobic socket". The PAD4 binding loops are shown in red, and the CMG2 receptor is in yellow. Coordinates were taken from the PAD4-CMG2 receptor complex (Santelli *et al.* 2004).

2.3.6 Structural aspects of 14B7 affinity maturation

In an effort to create a therapeutic anti-toxin antibody for use as a prophylactic as well as late stage treatment for anthrax, 14B7 was used as the platform for an antibody engineering effort. Initially, sequence randomization followed by phage display was used to affinity mature 14B7, resulting in 1H (250 pM) (Maynard *et al.* 2002). This approximately 20-fold affinity enhancement means that 1H has a higher affinity for PA than do the cellular receptors. Presumably for this reason, a humanized, whole IgG form of 1H, now called Anthim^{TM}, was shown to be an effective prophylactic and post-infection treatment for inhalation anthrax in animal models. Anthim^{TM} successfully completed a phase I clinical human safety trial and is currently in later stages of development.

The two key changes in 1H relative to 14B7 are light chain residues Q55L and S56P. Both changes increase hydrophobicity on the periphery of the binding interface with PA and, by analogy to the PAD4-M18 structure, will contact Y688 and S690 of PA. For example, the Cδ atom of P56 contacts Cα and Cβ of S690. It is tempting to ascribe the affinity enhancement to an increase in hydrophobic contacts.

The ultrahigh affinity variant M18 shares the S56P mutation with 1H and presumably makes similar interactions with the antigen. However, M18 does not contain the Q55L mutation. In the PAD4-M18 structure, only the polar –OH group of Y688 makes contact with the 55 and 56 side chains. In fact, in the case of Q55 of M18, there is a predicted hydrogen bond that will be lost upon replacement with leucine in 1H. Comparison of the 14B7 backbone conformation to that of 1H (and M18) in this region reveals no significant change in folded structure (Figure 2.3). Because the PAD4-M18 structure does not have the Q55L mutation, we can only speculate that there is some contribution from a hydrophobic contact with Y688 by L55 in 1H. Finally, considering

the constrained conformational dynamics of a proline moiety, it is worth considering that a major contribution of the S56P and possibly Q55L mutations could be to alter the dynamics of the L2 loop to be more favorable for binding.

Besides S56P, only the L46F mutation in M18 is located near the binding interface with PA (Figure 2.7). The role of L46 in affinity enhancement is not obvious, but may include a slight hydrophobic contact with Y688 of PA. The F46 Cα-Y688 Cα distance is 5.3 Å. F46 forms a stronger hydrophobic interaction with the side chain of L102 in the H3 loop; L102, in turn, is within 4 Å of the Y688 side chain so L46 may be acting to stabilize, indirectly, an important hydrophobic contact. In addition, the proximity of L46F to S56P might mean that they are working in concert to control subtle features of the conformation or dynamics of the L2 loop. Of course, we should not rule out the possibility that some of the other mutations in M18 contribute to an increase in affinity through subtle, indirect effects.

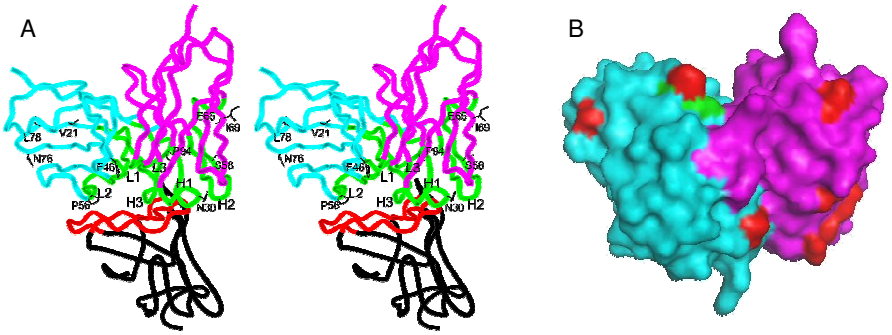

FIGURE 2.7 - AFFINITY MATURATION MUTATIONS OF M18 AND 1H. (a) The M18 light chain is shown in cyan, and the M18 heavy chain in magenta. The side chains of M18 variant residues are shown in black. The M18 CDR loops are shown in green and labeled. PAD4 is shown in black, and the PAD4 binding loops are shown in red. (b) The PAD4-binding face of M18 is shown. Mutations of M18 are shown in red. The Q55L mutation of 1H is shown in green.

Interestingly, the contributions of L46F, Q55L, and S56P appear to be additive based on a preliminary analysis. For example, adding the Q55L mutation to M18 (which already contains L46F and S56P) leads to a new variant called M18.1 that exhibits a dissociation constant of 21 pM, representing the highest affinity observed to date in the 14B7 family of engineered antibodies (Table 2.3). Unfortunately, this enhanced affinity comes at the expense of expression level as M18.1 expresses significantly more poorly than M18 in E. coli. Adding L46F to 14B7 enhances binding affinity by an order of magnitude, and removing L46F from M18 causes an analogous decrease in affinity (Table 2.3).

Table 2.3. Kinetic data for selected 14B7 and M18 variants

Clone	k_{off} (1/s, x10^{-5})	k_{on} (1/Ms, x10^{6})	K_D (pM)
14B7	390 ± 40	1.5 ± 0.3	2500 ± 600
14B7-L46F	40. ± 4	1 ± 1	300 ± 300
M18-F46L	32 ± 4	0.6 ± 0.4	500 ± 400
M18	5 ± 2	1.0 ± 0.6	50 ± 30

2.4 CONCLUSIONS

Overall the PAD4-M18 crystal structure can be used to nicely rationalize the extensive alanine scanning mutagenesis data available for this system. The one exception is the PA D683 position that would appear to make an important contribution to M18 binding, even though this is not reflected in the previously reported D683A variant of PA binding to 14B7. In addition, the results of affinity enhancements obtained by either phage panning (1H) or APEx (M18) can be rationalized as changes in key interactions in this same region of the interface, contacting Y688 and/or S690 of PA. However, a detailed explanation for the energetic contributions from other mutations in M18 known

to contribute to affinity enhancement, for example L46F, is not straightforward although it does appear to be operating in an additive fashion.

The PAD4-M18 structure can serve as the basis for engineering a new generation of ultrahigh affinity anti-PA antibodies. For example, using targeted mutagenesis, it may be possible to fill the hydrophobic "socket" in PAD4 composed of I646, I656, and L687 and thereby enhance the already very strong PA-antibody interaction. In addition, if a variant of PA is derived either from natural or deliberate variation, the PAD4-M18 structure will serve as an invaluable reference for designing targeted libraries that should be able to yield a high affinity therapeutic derivative of 14B7 in a timely fashion.

2.5 REFERENCES

Albrecht, M.T., Li, H., Williamson, E.D., LeButt, C.S., Flick-Smith, H.C., Quinn, C.P., Westra, H., Galloway, D., Mateczun, A., Goldman, S.*, et al.* 2007. Human monoclonal antibodies against anthrax lethal factor and protective antigen act independently to protect against Bacillus anthracis infection and enhance endogenous immunity to anthrax. *Infect Immun* **75:** 5425-5433.

Amit, A.G., Mariuzza, R.A., Phillips, S.E., and Poljak, R.J. 1986. Three-dimensional structure of an antigen-antibody complex at 2.8 A resolution. *Science* **233:** 747-753.

Bossart-Whitaker, P., Chang, C.Y., Novotny, J., Benjamin, D.C., and Sheriff, S. 1995. The crystal structure of the antibody N10-staphylococcal nuclease complex at 2.9 A resolution. *J Mol Biol* **253:** 559-575.

Braden, B.C., Fields, B.A., and Poljak, R.J. 1995. Conservation of water molecules in an antibody-antigen interaction. *J Mol Recognit* **8:** 317-325.

Braden, B.C., Souchon, H., Eisele, J.L., Bentley, G.A., Bhat, T.N., Navaza, J., and Poljak, R.J. 1994. Three-dimensional structures of the free and the antigen-complexed Fab from monoclonal anti-lysozyme antibody D44.1. *J Mol Biol* **243:** 767-781.

Breithaupt, C., Schubart, A., Zander, H., Skerra, A., Huber, R., Linington, C., and Jacob, U. 2003. Structural insights into the antigenicity of myelin oligodendrocyte glycoprotein. *Proc Natl Acad Sci U S A* **100:** 9446-9451.

Brossier, F., Levy, M., Landier, A., Lafaye, P., and Mock, M. 2004. Functional analysis of Bacillus anthracis protective antigen by using neutralizing monoclonal antibodies. *Infect Immun* **72:** 6313-6317.

Brunger, A.T. 1993. Assessment of phase accuracy by cross validation: the free R value. Methods and applications. *Acta Crystallogr D Biol Crystallogr* **49:** 24-36.

Brunger, A.T., Adams, P.D., Clore, G.M., DeLano, W.L., Gros, P., Grosse-Kunstleve, R.W., Jiang, J.S., Kuszewski, J., Nilges, M., Pannu, N.S., *et al.* 1998. Crystallography & NMR system: A new software suite for macromolecular structure determination. *Acta Crystallogr D Biol Crystallogr* **54 (Pt 5):** 905-921.

Chen, Z., Moayeri, M., Zhou, Y.H., Leppla, S., Emerson, S., Sebrell, A., Yu, F., Svitel, J., Schuck, P., St Claire, M., *et al.* 2006. Efficient neutralization of anthrax toxin by chimpanzee monoclonal antibodies against protective antigen. *J Infect Dis* **193:** 625-633.

Cho, H.S., Mason, K., Ramyar, K.X., Stanley, A.M., Gabelli, S.B., Denney, D.W., Jr., and Leahy, D.J. 2003. Structure of the extracellular region of HER2 alone and in complex with the Herceptin Fab. *Nature* **421:** 756-760.

Cirino, N.M., Sblattero, D., Allen, D., Peterson, S.R., Marks, J.D., Jackson, P.J., Bradbury, A., and Lehnert, B.E. 1999. Disruption of anthrax toxin binding with the use of human antibodies and competitive inhibitors. *Infect Immun* **67:** 2957-2963.

Colman, P.M., Laver, W.G., Varghese, J.N., Baker, A.T., Tulloch, P.A., Air, G.M., and Webster, R.G. 1987. Three-dimensional structure of a complex of antibody with influenza virus neuraminidase. *Nature* **326:** 358-363.

Corper, A.L., Sohi, M.K., Bonagura, V.R., Steinitz, M., Jefferis, R., Feinstein, A., Beale, D., Taussig, M.J., and Sutton, B.J. 1997. Structure of human IgM rheumatoid factor Fab bound to its autoantigen IgG Fc reveals a novel topology of antibody-antigen interaction. *Nat Struct Biol* **4:** 374-381.

Cote, C.K., Rossi, C.A., Kang, A.S., Morrow, P.R., Lee, J.S., and Welkos, S.L. 2005. The detection of protective antigen (PA) associated with spores of Bacillus anthracis and the effects of anti-PA antibodies on spore germination and macrophage interactions. *Microb Pathog* **38:** 209-225.

Cui, X., Li, Y., Moayeri, M., Choi, G.H., Subramanian, G.M., Li, X., Haley, M., Fitz, Y., Feng, J., Banks, S.M., *et al.* 2005. Late treatment with a protective antigen-directed monoclonal antibody improves hemodynamic function and survival in a lethal toxin-infused rat model of anthrax sepsis. *J Infect Dis* **191:** 422-434.

Davies, D.R., and Cohen, G.H. 1996. Interactions of protein antigens with antibodies. *Proc Natl Acad Sci U S A* **93:** 7-12.

Evans, E.J., Esnouf, R.M., Manso-Sancho, R., Gilbert, R.J., James, J.R., Yu, C., Fennelly, J.A., Vowles, C., Hanke, T., Walse, B., *et al.* 2005. Crystal structure of a soluble CD28-Fab complex. *Nat Immunol* **6:** 271-279.

Farady, C.J., Egea, P.F., Schneider, E.L., Darragh, M.R., and Craik, C.S. 2008. Structure of an Fab-protease complex reveals a highly specific non-canonical mechanism of inhibition. *J Mol Biol* **380:** 351-360.

Fields, B.A., Goldbaum, F.A., Ysern, X., Poljak, R.J., and Mariuzza, R.A. 1995. Molecular basis of antigen mimicry by an anti-idiotope. *Nature* **374:** 739-742.

Harvey, B.R., Georgiou, G., Hayhurst, A., Jeong, K.J., Iverson, B.L., and Rogers, G.K. 2004. Anchored periplasmic expression, a versatile technology for the isolation of high-affinity antibodies from Escherichia coli-expressed libraries. *Proc Natl Acad Sci U S A* **101:** 9193-9198.

Hayhurst, A., Happe, S., Mabry, R., Koch, Z., Iverson, B.L., and Georgiou, G. 2003. Isolation and expression of recombinant antibody fragments to the biological warfare pathogen Brucella melitensis. *J Immunol Methods* **276:** 185-196.

Huang, M., Syed, R., Stura, E.A., Stone, M.J., Stefanko, R.S., Ruf, W., Edgington, T.S., and Wilson, I.A. 1998. The mechanism of an inhibitory antibody on TF-initiated blood coagulation revealed by the crystal structures of human tissue factor, Fab 5G9 and TF.G9 complex. *J Mol Biol* **275:** 873-894.

Igonet, S., Vulliez-Le Normand, B., Faure, G., Riottot, M.M., Kocken, C.H., Thomas, A.W., and Bentley, G.A. 2007. Cross-reactivity studies of an anti-Plasmodium vivax apical membrane antigen 1 monoclonal antibody: binding and structural characterisation. *J Mol Biol* **366:** 1523-1537.

Jiao, G.S., Cregar, L., Wang, J., Millis, S.Z., Tang, C., O'Malley, S., Johnson, A.T., Sareth, S., Larson, J., and Thomas, G. 2006. Synthetic small molecule furin inhibitors derived from 2,5-dideoxystreptamine. *Proc Natl Acad Sci U S A* **103:** 19707-19712.

Jones, T.A., Zou, J.Y., Cowan, S.W., and Kjeldgaard, M. 1991. Improved methods for building protein models in electron density maps and the location of errors in these models. *Acta Crystallogr A* **47 (Pt 2):** 110-119.

Karginov, V.A., Robinson, T.M., Riemenschneider, J., Golding, B., Kennedy, M., Shiloach, J., and Alibek, K. 2004. Treatment of anthrax infection with combination of ciprofloxacin and antibodies to protective antigen of Bacillus anthracis. *FEMS Immunol Med Microbiol* **40:** 71-74.

Kelly, C.D., O'Loughlin, C., Gelder, F.B., Peterson, J.W., Sower, L.E., and Cirino, N.M. 2007. Rapid generation of an anthrax immunotherapeutic from goats using a novel non-toxic muramyl dipeptide adjuvant. *J Immune Based Ther Vaccines* **5:** 11.

Kissinger, C.R., Gehlhaar, D.K., Smith, B.A., and Bouzida, D. 2001. Molecular replacement by evolutionary search. *Acta Crystallogr D Biol Crystallogr* **57:** 1474-1479.

Kjer-Nielsen, L., Dunstone, M.A., Kostenko, L., Ely, L.K., Beddoe, T., Mifsud, N.A., Purcell, A.W., Brooks, A.G., McCluskey, J., and Rossjohn, J. 2004. Crystal structure of the human T cell receptor CD3 epsilon gamma heterodimer complexed to the therapeutic mAb OKT3. *Proc Natl Acad Sci U S A* **101:** 7675-7680.

Kobiler, D., Gozes, Y., Rosenberg, H., Marcus, D., Reuveny, S., and Altboum, Z. 2002. Efficiency of protection of guinea pigs against infection with Bacillus anthracis spores by passive immunization. *Infect Immun* **70:** 544-560.

Lee, J.E., Fusco, M.L., Hessell, A.J., Oswald, W.B., Burton, D.R., and Saphire, E.O. 2008. Structure of the Ebola virus glycoprotein bound to an antibody from a human survivor. *Nature* **454:** 177-182.

Li, H., Dunn, J.J., Luft, B.J., and Lawson, C.L. 1997. Crystal structure of Lyme disease antigen outer surface protein A complexed with an Fab. *Proc Natl Acad Sci U S A* **94:** 3584-3589.

Li, M., Gustchina, A., Alexandratos, J., Wlodawer, A., Wunschmann, S., Kepley, C.L., Chapman, M.D., and Pomes, A. 2008. Crystal structure of a dimerized cockroach allergen Bla g 2 complexed with a monoclonal antibody. *J Biol Chem* **283:** 22806-22814.

Li, S., Schmitz, K.R., Jeffrey, P.D., Wiltzius, J.J., Kussie, P., and Ferguson, K.M. 2005. Structural basis for inhibition of the epidermal growth factor receptor by cetuximab. *Cancer Cell* **7:** 301-311.

Li, Y., Li, H., Yang, F., Smith-Gill, S.J., and Mariuzza, R.A. 2003. X-ray snapshots of the maturation of an antibody response to a protein antigen. *Nat Struct Biol* **10:** 482-488.

Little, S.F., Ivins, B.E., Fellows, P.F., and Friedlander, A.M. 1997. Passive protection by polyclonal antibodies against Bacillus anthracis infection in guinea pigs. *Infect Immun* **65:** 5171-5175.

Little, S.F., Leppla, S.H., and Cora, E. 1988. Production and characterization of monoclonal antibodies to the protective antigen component of Bacillus anthracis toxin. *Infect Immun* **56:** 1807-1813.

Liu, H., Smith, T.J., Lee, W.M., Mosser, A.G., Rueckert, R.R., Olson, N.H., Cheng, R.H., and Baker, T.S. 1994. Structure determination of an Fab fragment that neutralizes human rhinovirus 14 and analysis of the Fab-virus complex. *J Mol Biol* **240:** 127-137.

Lok, S.M., Kostyuchenko, V., Nybakken, G.E., Holdaway, H.A., Battisti, A.J., Sukupolvi-Petty, S., Sedlak, D., Fremont, D.H., Chipman, P.R., Roehrig, J.T.*, et al.* 2008. Binding of a neutralizing antibody to dengue virus alters the arrangement of surface glycoproteins. *Nat Struct Mol Biol* **15:** 312-317.

Mabry, R., Rani, M., Geiger, R., Hubbard, G.B., Carrion, R., Jr., Brasky, K., Patterson, J.L., Georgiou, G., and Iverson, B.L. 2005. Passive protection against anthrax by using a high-affinity antitoxin antibody fragment lacking an Fc region. *Infect Immun* **73:** 8362-8368.

Maynard, J.A., Maassen, C.B., Leppla, S.H., Brasky, K., Patterson, J.L., Iverson, B.L., and Georgiou, G. 2002. Protection against anthrax toxin by recombinant antibody fragments correlates with antigen affinity. *Nat Biotechnol* **20:** 597-601.

McCoy, A.J. 2007. Solving structures of protein complexes by molecular replacement with Phaser. *Acta Crystallogr D Biol Crystallogr* **63:** 32-41.

Menez, R., Michel, S., Muller, B.H., Bossus, M., Ducancel, F., Jolivet-Reynaud, C., and Stura, E.A. 2008. Crystal structure of a ternary complex between human prostate-

specific antigen, its substrate acyl intermediate and an activating antibody. *J Mol Biol* **376:** 1021-1033.

Moayeri, M., and Leppla, S.H. 2004. The roles of anthrax toxin in pathogenesis. *Curr Opin Microbiol* **7:** 19-24.

Mohamed, N., Clagett, M., Li, J., Jones, S., Pincus, S., D'Alia, G., Nardone, L., Babin, M., Spitalny, G., and Casey, L. 2005. A high-affinity monoclonal antibody to anthrax protective antigen passively protects rabbits before and after aerosolized Bacillus anthracis spore challenge. *Infect Immun* **73:** 795-802.

Muller, Y.A., Chen, Y., Christinger, H.W., Li, B., Cunningham, B.C., Lowman, H.B., and de Vos, A.M. 1998. VEGF and the Fab fragment of a humanized neutralizing antibody: crystal structure of the complex at 2.4 A resolution and mutational analysis of the interface. *Structure* **6:** 1153-1167.

Mylvaganam, S.E., Paterson, Y., and Getzoff, E.D. 1998. Structural basis for the binding of an anti-cytochrome c antibody to its antigen: crystal structures of FabE8-cytochrome c complex to 1.8 A resolution and FabE8 to 2.26 A resolution. *J Mol Biol* **281:** 301-322.

Otwinowski, Z., and Minor, W. 1997. Processing of X-ray diffraction data collected in oscillation mode. *Methods Enzymol* **27:** 307-326.

Padlan, E.A., Silverton, E.W., Sheriff, S., Cohen, G.H., Smith-Gill, S.J., and Davies, D.R. 1989. Structure of an antibody-antigen complex: crystal structure of the HyHEL-10 Fab-lysozyme complex. *Proc Natl Acad Sci U S A* **86:** 5938-5942.

Pelat, T., Hust, M., Laffly, E., Condemine, F., Bottex, C., Vidal, D., Lefranc, M.P., Dubel, S., and Thullier, P. 2007. High-affinity, human antibody-like antibody fragment (single-chain variable fragment) neutralizing the lethal factor (LF) of

Bacillus anthracis by inhibiting protective antigen-LF complex formation. *Antimicrob Agents Chemother* **51:** 2758-2764.

Perrakis, A., Sixma, T.K., Wilson, K.S., and Lamzin, V.S. 1997. wARP: improvement and extension of crystallographic phases by weighted averaging of multiple-refined dummy atomic models. *Acta Crystallogr D Biol Crystallogr* **53:** 448-455.

Peterson, J.W., Comer, J.E., Noffsinger, D.M., Wenglikowski, A., Walberg, K.G., Chatuev, B.M., Chopra, A.K., Stanberry, L.R., Kang, A.S., Scholz, W.W.*, et al.* 2006. Human monoclonal anti-protective antigen antibody completely protects rabbits and is synergistic with ciprofloxacin in protecting mice and guinea pigs against inhalation anthrax. *Infect Immun* **74:** 1016-1024.

Petosa, C., Collier, R.J., Klimpel, K.R., Leppla, S.H., and Liddington, R.C. 1997. Crystal structure of the anthrax toxin protective antigen. *Nature* **385:** 833-838.

Prabakaran, P., Gan, J., Feng, Y., Zhu, Z., Choudhry, V., Xiao, X., Ji, X., and Dimitrov, D.S. 2006. Structure of severe acute respiratory syndrome coronavirus receptor-binding domain complexed with neutralizing antibody. *J Biol Chem* **281:** 15829-15836.

Prasad, L., Waygood, E.B., Lee, J.S., and Delbaere, L.T. 1998. The 2.5 A resolution structure of the jel42 Fab fragment/HPr complex. *J Mol Biol* **280:** 829-845.

Read, R.J. 1986. Improved Fourier coefficients for maps using phases from partial structures with errors. *Acta Crystallog. sect. A* **42:** 140-149.

Rivera, J., Nakouzi, A., Abboud, N., Revskaya, E., Goldman, D., Collier, R.J., Dadachova, E., and Casadevall, A. 2006. A monoclonal antibody to Bacillus anthracis protective antigen defines a neutralizing epitope in domain 1. *Infect Immun* **74:** 4149-4156.

Rosovitz, M.J., Schuck, P., Varughese, M., Chopra, A.P., Mehra, V., Singh, Y., McGinnis, L.M., and Leppla, S.H. 2003. Alanine-scanning mutations in domain 4 of anthrax toxin protective antigen reveal residues important for binding to the cellular receptor and to a neutralizing monoclonal antibody. *J Biol Chem* **278:** 30936-30944.

Santelli, E., Bankston, L.A., Leppla, S.H., and Liddington, R.C. 2004. Crystal structure of a complex between anthrax toxin and its host cell receptor. *Nature* **430:** 905-908.

Sawada-Hirai, R., Jiang, I., Wang, F., Sun, S.M., Nedellec, R., Ruther, P., Alvarez, A., Millis, D., Morrow, P.R., and Kang, A.S. 2004. Human anti-anthrax protective antigen neutralizing monoclonal antibodies derived from donors vaccinated with anthrax vaccine adsorbed. *J Immune Based Ther Vaccines* **2:** 5.

Sellman, B.R., Mourez, M., and Collier, R.J. 2001. Dominant-negative mutants of a toxin subunit: an approach to therapy of anthrax. *Science* **292:** 695-697.

Shoop, W.L., Xiong, Y., Wiltsie, J., Woods, A., Guo, J., Pivnichny, J.V., Felcetto, T., Michael, B.F., Bansal, A., Cummings, R.T.*, et al.* 2005. Anthrax lethal factor inhibition. *Proc Natl Acad Sci U S A* **102:** 7958-7963.

Sivasubramanian, A., Maynard, J.A., and Gray, J.J. 2008. Modeling the structure of mAb 14B7 bound to the anthrax protective antigen. *Proteins* **70:** 218-230.

Steiniger, S.C., Altobell, L.J., 3rd, Zhou, B., and Janda, K.D. 2007. Selection of human antibodies against cell surface-associated oligomeric anthrax protective antigen. *Mol Immunol* **44:** 2749-2755.

Su, H.P., Golden, J.W., Gittis, A.G., Hooper, J.W., and Garboczi, D.N. 2007. Structural basis for the binding of the neutralizing antibody, 7D11, to the poxvirus L1 protein. *Virology* **368:** 331-341.

Subramanian, G.M., Cronin, P.W., Poley, G., Weinstein, A., Stoughton, S.M., Zhong, J., Ou, Y., Zmuda, J.F., Osborn, B.L., and Freimuth, W.W. 2005. A phase 1 study of PAmAb, a fully human monoclonal antibody against Bacillus anthracis protective antigen, in healthy volunteers. *Clin Infect Dis* **41:** 12-20.

Thomas, R., Patenaude, S.I., MacKenzie, C.R., To, R., Hirama, T., Young, N.M., and Evans, S.V. 2002. Structure of an anti-blood group A Fv and improvement of its binding affinity without loss of specificity. *J Biol Chem* **277:** 2059-2064.

Turk, B.E., Wong, T.Y., Schwarzenbacher, R., Jarrell, E.T., Leppla, S.H., Collier, R.J., Liddington, R.C., and Cantley, L.C. 2004. The structural basis for substrate and inhibitor selectivity of the anthrax lethal factor. *Nat Struct Mol Biol* **11:** 60-66.

Vagin, A., and Teplyakov, A. 1997. MOLREP: an automated program for molecular replacement. *J. Appl. Cryst.* **30:** 1022-1025.

Vitale, L., Blanset, D., Lowy, I., O'Neill, T., Goldstein, J., Little, S.F., Andrews, G.P., Dorough, G., Taylor, R.K., and Keler, T. 2006. Prophylaxis and therapy of inhalational anthrax by a novel monoclonal antibody to protective antigen that mimics vaccine-induced immunity. *Infect Immun* **74:** 5840-5847.

Wedemayer, G.J., Patten, P.A., Wang, L.H., Schultz, P.G., and Stevens, R.C. 1997. Structural insights into the evolution of an antibody combining site. *Science* **276:** 1665-1669.

Wild, M.A., Xin, H., Maruyama, T., Nolan, M.J., Calveley, P.M., Malone, J.D., Wallace, M.R., and Bowdish, K.S. 2003. Human antibodies from immunized donors are protective against anthrax toxin in vivo. *Nat Biotechnol* **21:** 1305-1306.

Young, J.A., and Collier, R.J. 2007. Anthrax toxin: receptor binding, internalization, pore formation, and translocation. *Annu Rev Biochem* **76:** 243-265.

Zhou, T., Xu, L., Dey, B., Hessell, A.J., Van Ryk, D., Xiang, S.H., Yang, X., Zhang, M.Y., Zwick, M.B., Arthos, J.*, et al.* 2007. Structural definition of a conserved neutralization epitope on HIV-1 gp120. *Nature* **445:** 732-737.

CHAPTER 3

Structure-Based Engineering of an Enhanced Antibody to a Protective Antigen Variant

3.1 INTRODUCTION

Bacillus anthracis is the gram-positive, spore forming bacterium that is the causative agent of the zoonotic disease, anthrax (Moayeri and Leppla 2004; Young and Collier 2007). Unfortunately, because of its robust spore, ease of production, and associated fatality when inhaled or eaten, this disease has long been feared as a potentially very effective bioweapon. The inadvertent release of spores from Sverdlosk in 1979, and the resulting 77 human deaths, revealed how efficient *B. anthracis* can be as a bioweapon (Meselson *et al.* 1994), and the Anthrax letter attacks of 2001 serve to illustrate the fear, confusion, and chaos that can be created by such an asymmetric threat.

The current anthrax vaccine has significant side effects that make it unlikely to be used to vaccinate the entire American public, and there is a large amount of research being carried out to create a new, safer vaccine. Because there is a gap in coverage, and thus the opportunity for a similar or worse outcome than in 2001, our laboratory and others have worked to produce therapeutics that can treat anthrax (Little *et al.* 1988; Cirino *et al.* 1999; Sellman *et al.* 2001; Kobiler *et al.* 2002; Maynard *et al.* 2002; Wild *et al.* 2003; Brossier *et al.* 2004; Harvey *et al.* 2004; Sawada-Hirai *et al.* 2004; Turk *et al.* 2004; Mabry *et al.* 2005; Mohamed *et al.* 2005; Shoop *et al.* 2005; Subramanian *et al.* 2005; Chen *et al.* 2006; Jiao *et al.* 2006; Peterson *et al.* 2006; Rivera *et al.* 2006; Vitale *et al.* 2006; Albrecht *et al.* 2007; Pelat *et al.* 2007; Steiniger *et al.* 2007). Several of these

therapies have even been shown to be very effective in animal models (Little *et al.* 1997; Karginov *et al.* 2004; Cui *et al.* 2005; Vitale *et al.* 2006; Kelly *et al.* 2007).

However, what is not well understood is whether these therapeutics would be useful in the face of natural or deliberate variation of the anthrax toxin genes. In fact, alanine scanning of the protective antigen revealed several mutations that prevented the 14B7 family of antibodies from binding and neutralizing the toxin, and some of these variants still retained their toxic activity (Rosovitz *et al.* 2003). This underlines the importance of, first, uncovering the method and mechanism of interaction of these various therapeutics with the toxin; second, understanding the limitations of these therapeutics based upon these molecular constraints; and third, developing a second generation of therapeutics that can counter any perceived threats.

The ideal antibody countermeasure to anthrax would provide a general solution even against altered toxins. With this in mind, our approach was to utilize the crystallographic characterization of the interaction of first-generation anthrax therapeutics to enable the development of potential second generation countermeasures. As a starting point, our laboratory had previously undertaken to evolve an antibody fragment from the 14B7 family of antibodies that could bind to PA-Y688A, a point mutant of PA that greatly reduced binding affinity of 14B7 (>100-fold) while retaining its toxic activity. In the absence of the crystallographic model of interaction, all attempts had failed to develop a 14B7 variant with enhanced affinity to PA-Y688A. Error-prone libraries and very large saturation mutagenesis libraries did not yield affinity-improved binders (Jeong, K.J., unpublished data). Our new effort, which turned out to be successful, used key information from the structure of the M18-PAD4 interaction to create focused libraries that allowed for the isolation of variants with enhanced affinity for PAD4-Y688A.

3.2 MATERIALS AND METHODS

3.2.1 PAD4 Construction

PAD4 was cloned into pET17b under the control of a T7 promoter with an *N*-terminal 3xFlag tag and a *C*-terminal 6xHis tag between the NdeI and BamHI sites. PCR was performed on the PAD4 gene to introduce these features utilizing the following primers: forward GGCGGCGGCCATATGGATTATAAAGATCATGATGGCGATTATAAAGATCATG ATATTGATTATAAAGATGATGATGATAAATTCCACTACGATCGTAACAATATC GCGG, and reverse GGCGGCGGCGGATCCTTATTAGTGATGGTGATGATGATGACCAATTTCATAG CCCTTTTTGCTAAAAATCAGG.

PAD4-Y688A was constructed using site-directed mutagenesis via overlap PCR. First, two PCR reactions were carried out to synthesize two fragments of the gene of interest with the internal primers containing the codon changing residue 688 from tyrosine to alanine (Outer primers--Fragment 1 forward primer: TAATACGACTCACTATAGGG, Fragment 2 reverse primer: GCTAGTTATTGCTCAGCGG; Inner primers-- Fragment 1 reverse primer: CGTTCACTTCGTAGTTTGGATTGCTGATCGCCAGCGGCAATTTGTCGTTGTAC, Fragment 2 forward primer: GCGATCAGCAATCCAAACTACGAAGTGAACG). These two PCR fragments were purified by agarose gel electrophoresis, and mixed together as template for a second PCR reaction to yield the full-length gene fragment. Only the outer primers were used for amplification of this second reaction. Digestion of this fragment was accomplished with NdeI and BamHI and subjected to agarose gel

electrophoresis, which was then ligated with pET17b vector that had been cleaved with NdeI and BamHI. Ligations were desalted using Millipore desalting membrane for 1 hr. Reactions were subsequently transformed via electroporation into Jude-1 cells and plated on LB-Agar with 2% glucose and Ampicillin at 100 μg/mL and grown overnight at 37°C. Individual colonies were picked and grown overnight in liquid culture of LB with 2% glucose and Ampicillin at 100 μg/mL at 37°C. Plasmid was isolated from each culture by Miniprep (Qiagen), and sequencing was performed on individual clones by the ICMB Sequencing Core Facility.

After the correct sequence was determined for each construct, plasmid was transformed by electroporation into KRX cells (Promega), which were plated on LB-Agar with 2% glucose and Ampicillin at 100 μg/mL and grown overnight at 37°C. Individual colonies were picked and grown overnight in liquid culture of LB with 2% glucose and Ampicillin at 100 μg/mL at 37°C. Frozen stocks were made by mixing liquid culture with 50% glycerol 2:1, for a final glycerol concentration of 16%; cells were frozen at -80°C.

3.2.2 PAD4 Expression and Purification

Overnight cultures 40 mL in volume of TB with 2% glucose and Ampicillin at 100 μg/mL were inoculated from frozen stocks and incubated at 37°C. The next day, this culture was used to inoculate 1 L of TB with Ampicillin at 100 μg/mL, which was incubated at 37°C for 4 hours, then 1 g of L-rhamnose (Sigma) was added to each liter of culture and induction was allowed to continue overnight. The following morning, cells were pelleted and resuspended in 50 mL of 50 mM Tris, pH 8.0, 500 mM NaCl, 10 mM imidazole. Cells were lysed by sonication (Probe dismembrator, Fisher Scientific) on ice in 5 mL aliquots by 3 cycles of 30 s at level 5 followed by 30 s off. Membranes were

pelleted by centrifugation at 8,000 rpm for 20 minutes. Supernatant was equilibrated with 1 mL Ni-NTA Agarose (Qiagen) per liter of culture that had been washed three times in binding buffer. The cell lysate-bead mixture was mixed on ice for one hour. The Ni-NTA agarose beads were washed twice in batch by centrifugation at 3,000 rpm for 5 minutes, decanting of supernatant, followed by resuspension in 50 mM Tris, pH 8.0, 500 mM NaCl, 20 mM imidazole. The washed beads were then placed in a disposable polypropylene column (Pierce), and protein was eluted by addition of 4- 1 mL fractions of 50 mM Tris, pH 8.0, 500 mM NaCl, 250 mM imidazole. The eluent was dialyzed and concentrated into 50 mM Tris, pH 8.0, 150 mM NaCl buffer using an Amicon Ultra 15, 10,000 MWCO filter. Protein concentrations were assessed using the BCA assay (Pierce) with BSA as a control.

3.2.3 M18-NNS Library Construction

Overlap PCR, as described above, was used to construct both the NNS3 and NNS8 libraries. As there were two locations in the primary sequence where diversity was to be introduced, three segments were amplified initially (NNS3/NNS8 Outside primers—Fragment 1 forward primer: CGGATAACAATTTCACACAGG, Fragment 3 reverse primer: CGCAGTAGCGGTAAACGGC; NNS3 Internal primers--Fragment 1 reverse primer: TAATCTTGATGTGTAGTAGATCAGGAATTTAACAGTTCCGTCTGG, Fragment 2 forward primer: CCAGACGGAACTGTTAAATTCCTGATCTACTACACATCAAGATTANNSNNSGG AGTCCCATCAAGGTTCAGTGGC, Fragment 2 reverse primer: CCCCGATCTTGCACAGAAATAGACCG, Fragment 3 forward primer: CGGTCTATTTCTGTGCAAGATCGGGGNNSCTACGTTATGCTATGGACTACTGG

GGTCAAGG; NNS8 Internal primers—Fragment 1 reverse primer: TTTAACAGTTCCGTCTGGTTTCTGCTGATACC, Fragment 2 forward primer: GGTATCAGCAGAAACCAGACGGAACTGTTAAANNSCTGATCNNSTACACATC ANNSTTANNSNNSGGAGTCCCATCAAGGTTCAGTGGC, Fragment 2 reverse primer: CCCCGATCTTGCACAGAAATAGACCG, Fragment 3 forward primer: CGGTCTATTTCTGTGCAAGATCGGGGNNSNNSCGTTATGCTATGNNSTACTGG GGTCAAGGAACCTCAGTCACC). After agarose gel electrophoresis, the purified fragments were mixed and amplified with only the outside forward primer from fragment 1, and the outside reverse primer from fragment 3. After purification by PCR cleanup (Zymo Research), the PCR fragment was digested with SfiI. Agarose gel electrophoresis was used to purify the restricted fragment, and the insert was ligated into previously SfiI-digested pAPEx1 plasmid for 4 hours at room temperature. After desalting for one hour, MC1061 cells were transformed with the desalted ligation reaction via electroporation and grown for one hour in SOC media with 2% glucose at 37°C. These cells were then plated on TB-Agar with 2% glucose and chloramphenicol at 30 μg/mL and grown overnight at 30°C before being scraped and frozen away at -80°C in TB media with 16% glycerol.

3.2.4 Library Sorting

Screening of libraries was carried out using the APEx protocol (Harvey *et al.* 2004). Overnight cultures or frozen cells were used to seed 40 mL of TB with 2% glucose and 40μg/mL chloramphenicol at an OD_{600} of 0.2. Cultures were grown at 37°C for 4 hours, centrifuged for 6 minutes at 3,500 rpm, and resuspended in 40 mL of TB with 1 mM IPTG and 40μg/mL chloramphenicol. Induced cultures were shaken at 25°C

for 4 hours. An equivalent volume of cells to 1 mL at OD_{600} of 3.0 was taken for spheroplasting and labeling.

Spheroplasting was accomplished by resuspending cells in 350 µL of 100 mM Tris, pH 7.5, 750 mM sucrose, mixing with 700 µL 1 mM EDTA and 40 µL of 20 mg/mL hen egg lysozyme and mixing for 20 minutes at room temperature. 50 µL of 0.5 M $MgCl_2$ was added and the cell suspension was placed on ice for 10 minutes. Spheroplasts were centrifuged for 6 minutes at 10,000 rpm and resuspended in 500µL 1xPBS with 2% BSA. 125µL of spheroplasts were subjected to various labeling concentrations of either wild-type PAD4 or PAD4-Y688A, and allowed to shake in the dark for one hour at room temperature. Spheroplasts were then pelleted again at 10,000 rpm for 6 minutes, resuspended in 100 µL of 20 µg/mL anti-Flag-PE, and shaken in the dark for one hour at room temperature.

Labeled samples were then diluted into 1xPBS with 2% BSA and sorted on a MoFlo (Dako) fluorescence activated cell sorter using the 488 nm Argon laser line for excitation, and a 570/40 nm bandpass filter to observe emission of PE. Spheroplasts were sorted at a rate of 30,000 events per second, and approximately the top 2% most fluorescent of gated spheroplasts were collected. Collected spheroplasts were subjected to an immediate re-sort utilizing the same gates as the initial sort.

Colony PCR was carried out on re-sorted spheroplasts to amplify the scFv genes (forward primer: CGGATAACAATTTCACACAGG, reverse primer: CGCAGTAGCGGTAAACGGC). After purification using a PCR cleanup kit (Zymo Research), the PCR fragments were digested with SfiI, purified by agarose gel electrophoresis, and ligated into pAPEx1 previously excised with SfiI. After desalting for one hour, MC1061 cells were transformed with the desalted ligation reaction via electroporation and grown for one hour in SOC media with 2% glucose at 37° C. These

cells were then plated on TB-Agar with 2% glucose and chloramphenicol at 30 μg/mL and grown overnight at 30°C before being scraped and frozen away at -80°C in TB media with 16% glycerol. Aliquots of the library were prepared such that thawing and dilution into 40 mL of media would yield a cell suspension at an OD_{600} of 0.2. Frozen stocks of a round of sorting were used to inoculate subsequent cultures for additional rounds of sorting.

3.2.5 SINGLE WELL ELISA SCREENING

Initial ELISA screening was performed essentially as described by Mazor, et al (Nature Protocols, submitted). After four rounds of sorting, colony PCR was carried out on re-sorted spheroplasts to amplify the scFv genes (forward primer: CGGATAACAATTTCACACAGG, reverse primer: CGCAGTAGCGGTAAACGGC). After purification using a PCR cleanup kit (Zymo Research), the PCR fragments were digested with SfiI, purified by agarose gel electrophoresis, and ligated into pMoPac16 previously excised with SfiI. After desalting for one hour, MC1061 cells were transformed with the desalted ligation reaction via electroporation and plated on TB-Agar with 2% glucose and Ampicillin at 100 μg/mL and grown overnight at 30°C. Individual colonies were picked and used to inoculate 200 μL of LB media with 2% glucose and 100 μg/mL Ampicillin in 96 well plates, which were shaken at 30°C overnight. The next day, this master plate was wrapped in parafilm and stored at 4°C. 10 μL from each master plate was used to inoculate 190 μL of TB media with 2% glucose and 100 μg/mL Ampicillin, which was shaken at 30°C for 3 hours. Plates were then centrifuged at 4450 rpm for 15 minutes, supernatant was decanted, cells were resuspended in 200 μL of TB induction media with 1 mM IPTG and 100 μg/mL Ampicillin, and left to shake overnight

at room temperature. ELISA plates were then coated overnight at 4°C with 50 µL of 3 µg/mL PAD4-Y688A in PBS or 3 µg/mL human transferrin in PBS as a negative control.

After coating overnight, the ELISA plates were washed with PBS with 0.05% Tween-20 using a SkanWasher 300 (Molecular Devices); all subsequent washing was carried out using this instrument. ELISA plates were then blocked for 4 hours at room temperature in 2% milk in PBS. Cell plates that had incubated at room temperature overnight were centrifuged at 4450 rpm for 15 minutes, supernatant was decanted, cells were resuspended in 200 µL of 20% Bugbuster-HT in PBS, and shaken at room temperature for 1 hour. Cell debris was pelleted by centrifugation at 4450 rpm for 15 minutes, and 10 µL of scAb-containing supernatant was added to 90 µL of 2% milk in PBS. ELISA plates were then washed with PBS with 0.05% Tween-20. 100 µL of supernatant diluted in milk-PBS was applied to a well coated in PAD4-Y688A as well as one coated with human transferrin, and allowed to incubate at room temperature for 1 hour. ELISA plates were washed with PBS with 0.05% Tween-20, and then incubated with a 1:2500 dilution of anti-Human Kappa chain IgG-HRP in PBS with 2% milk for 1 hour at room temperature. ELISA plates were then washed with PBS with 0.05% Tween-20 and developed with 100 µL of TMB substrate. Development was quenched by adding 100 µL of 4.5 M H_2SO_4, mixing gently, and then was read at 450 nm using a 96-well plate reader.

3.2.6 scAb Expression and Purification for Plate ELISA Screening

Cultures 4 mL in volume of TB media with 2% glucose and 100 µg/mL Ampicillin were inoculated using 20 µL of selected clones from the master plate made during single well ELISA screening, and placed on a shaker at 37°C overnight. In the morning, the 4 mL culture was poured into 40 mL of TB media with 2% glucose and 100

μg/mL of Ampicillin and placed on a shaker at 37°C for 4 hours. The culture was centrifuged at 4500 rpm for 6 minutes, supernatant was decanted, cells were resuspended in 40 mL of TB media with 1 mM IPTG and 100 μg/mL of Ampicillin and placed on a shaker at room temperature for 4 hours. Cultures were then centrifuged at 4000 rpm for 15 minutes, supernatant was decanted, and cells were resuspended in 1 mL of 100 mM Tris, pH 7.5, 750 mM sucrose. Cells were mixed by swirling on ice while 2 mL of 1 mM EDTA was added dropwise, followed by addition of 0.1 mL of 10 mg/mL hen egg lysozyme. Cells were left to mix by swirling on ice for 30 minutes. Next, 140 μL of 0.5 M $MgCl_2$ was added to stabilize spheroplasts and chelate free EDTA, and the mixture was allowed to swirl on ice for 10 minutes. Spheroplasts were pelleted by centrifugation at 6000 rpm for 25 minutes; the scAb-containing supernatant was decanted into a new tube, 350 μL of 10x IMAC buffer (0.2 M Tris, pH 8.0, 5M NaCl, 0.1M imidazole, 1% Tween-20) was added and gently mixed, and then equilibrated with 0.5 mL Ni-NTA agarose beads washed 3 times with 1x IMAC buffer (20 mM Tris, pH 8.0, 500 mM NaCl, 10 mM imidazole, 0.1% Tween-20). The agarose beads were allowed to incubate on ice while shaking with the supernatant for one hour, and then they were pelleted at 3000 rpm for 5 minutes in a swinging bucket centrifuge. Beads were washed twice by addition of 50 mL of ice-cold 1x IMAC buffer, centrifugation at 3000 rpm for 5 minutes, and gentle decanting of the supernatant. Beads were placed in a 5 mL disposable polypropylene column (Pierce) and scAb was collected in four subsequent elutions of 1 mL each of 50 mM Tris, pH 8.0, 500 mM NaCl, and 250 mM imidazole. The eluent was dialyzed and concentrated into 50 mM Tris, pH 8.0, 150 mM NaCl buffer using an Amicon Ultra 15, 10,000 MWCO filter. Samples were then filtered using 0.22 μm Ultrafree-MC basket filters with PVDF membranes (Millipore). Protein concentrations were assessed using the BCA assay (Pierce) with BSA as a control; purity was assessed by PAGE.

3.2.7 Plate ELISA Screening

ELISA plate wells were coated with 100 µL of 3 µg/mL PAD4-Y688A in PBS overnight at 4°C. The following morning, the plates were washed with 1x PBS with 0.05% Tween-20 using a SkanWasher 300 and then allowed to block for 4 hours at room temperature with 2% milk in PBS. scAb's were diluted to 1 µM in 2% milk-PBS, loaded on to the plate, and subjected to 1:1 serial dilutions with 2% milk-PBS across the remaining 11 rows of the plate; 100 µL was left in each well. This was incubated at room temperature for one hour before washing with 0.05% Tween-20 in PBS. 100 µL of anti-Human Kappa chain IgG-HRP conjugate diluted 1:2500 into 2% milk-PBS was applied to each well and allowed to incubate at room temperature for 1 hour. ELISA plates were then washed with PBS with 0.05% Tween-20 and developed with 100 µL of TMB substrate. Development was quenched by adding 100 µL of 4.5 M H_2SO_4, mixing gently, and then was read at 450 nm using a 96-well plate reader.

3.2.8 Expression and Purification of scAb's for Kinetic Studies

Cultures 40 mL in volume of TB media with 2% glucose and 100 µg/mL Ampicillin were inoculated using 20 µL of selected clones from the master plate made during single well ELISA screening, and placed on a shaker at 37°C overnight. In the morning, the 40 mL culture was poured into 400 mL of TB media with 100 µg/mL of Ampicillin and placed on a shaker at 37°C for 4 hours. The culture was induced by addition of IPTG to 1 mM and placed on a shaker at room temperature for 4 hours. Cultures were then centrifuged at 7000 rpm for 10 minutes, supernatant was decanted, and cells were resuspended in 10 mL of 100 mM Tris, pH 7.5, 750 mM sucrose. Cells

were mixed by swirling on ice while 20 mL of 1 mM EDTA was added dropwise, followed by addition of 1 mL of 10 mg/mL hen egg lysozyme. Cells were left to mix by swirling on ice for 30 minutes. Next, 1.4 mL of 0.5 M $MgCl_2$ was added to stabilize spheroplasts and chelate free EDTA, and the mixture was allowed to swirl on ice for 10 minutes. Spheroplasts were pelleted by centrifugation at 8000 rpm for 20 minutes; the scAb-containing supernatant was decanted into a new tube, 3.5 mL of 10x IMAC buffer (0.2 M Tris, pH 8.0, 5M NaCl, 0.1M imidazole, 1% Tween-20) was added and gently mixed, and then equilibrated with 0.5 mL Ni-NTA agarose beads washed 3 times with 1x IMAC buffer (20 mM Tris, pH 8.0, 500 mM NaCl, 10 mM imidazole, 0.1% Tween-20). The agarose beads were allowed to incubate on ice while shaking with the supernatant for one hour, and then they were pelleted at 3000 rpm for 5 minutes in a swinging bucket centrifuge. Beads were washed twice by addition of 50 mL of ice-cold 1x IMAC buffer, centrifugation at 3000 rpm for 5 minutes, and gentle decanting of the supernatant. Beads were placed in a 5 mL disposable polypropylene column (Pierce) and scAb was collected in four subsequent elutions of 1 mL each of 50 mM Tris, pH 8.0, 500 mM NaCl, and 250 mM imidazole. The eluent was dialyzed and concentrated into 50 mM Tris, pH 8.0, 150 mM NaCl buffer using an Amicon Ultra 15, 10,000 MWCO filter. Samples were then filtered using 0.22 μm Ultrafree-MC basket filters with PVDF membranes (Millipore).

The scAb-containing eluent was then subjected to size exclusion chromatography on a Superdex 200 column (GE Healthcare), utilizing a fast performance liquid chromatography (FPLC) system (ÄKTA FPLC, GE Healthcare). Running buffer was 1x HBS-P (10 mM Hepes, pH 7.4, 150 mM NaCl, 0.005% Polysorbate-20), flow rate was 0.5 mL/min, and 0.5 mL fractions were collected. Fractions containing monomeric scAb based upon the FPLC profile as monitored by the 280 nm UV detector were combined

and concentrated using an Amicon Ultra 15, 10,000 MWCO filter. Samples were then filtered using 0.22 μm Ultrafree-MC basket filters with PVDF membranes (Millipore). Protein concentrations were assessed using the BCA assay (Pierce) with BSA as a control.

3.2.9 Kinetic Analysis by Surface Plasmon Resonance

Kinetic studies were carried out on scAb's using a Biacore 3000 (Biacore, Inc.) with a CM5 sensor chip. A mixture of 0.2 M 1-ethyl-3-(3-dimethylaminopropyl) carbodiimide hydrochloride (EDC) and 0.05 M N-hydroxysuccinimide (NHS) was injected across the carboxymethyl-dextran surface to activate it for protein immobilization. Next a 20 μg/mL protein solution in 10 mM sodium acetate buffer was injected across the surface so that NHS-esters could react with free amines on the surface of the protein to create more stable amide bonds. Deactivation of the remaining unreacted NHS-esters was accomplished by injecting 1 M ethanolamine-HCl, pH 8.5. An equal amount of resonance units of human transferrin was immobilized as a control in all experiments, and it was immobilized in 10 mM sodium acetate buffer, pH 5.0. PAD4-Y688A was coupled using 10 mM sodium acetate buffer, pH 4.0, with a target amount of 1000 resonance units. 750 resonance units was the targeted immobilization for both wild-type PA_{83} and PA_{83}-Y688A in 10 mM sodium acetate buffer, pH 5.0.

Concentration series were injected for each scAb to be analyzed; a flow rate of 100 μL/min was utilized. Studies performed against wild-type PA_{83} consisted of a 1 minute association phase and 15 minutes of dissociation in 1x HBS-P running buffer with concentration series of 5-20 nM for M18 and 10-40 nM for variants. Studies carried out with PA_{83}-Y688A utilized a 1 minute association and 3.5 minutes of dissociation in 1x HBS-P running buffer, with concentration series of 20-80 nM for M18 and 10-40 nM for

variants. Studies performed on PAD4-Y688A employed a 1 minute association phase and 3.5 minutes of dissociation in 1x HBS-EP running buffer (1x HBS-P with 3 mM EDTA); concentration series of 20-80 nM were used for M18 and 10-40 nM for variants. All surfaces were regenerated using a 30 second wash with 4 M $MgCl_2$ in running buffer.

3.3 RESULTS AND DISCUSSION

3.3.1 Construction of Saturation Mutagenesis Libraries

Elucidation of the interaction of the 14B7 family of antibodies with PA was instrumental in the construction of these libraries. Previous attempts in our laboratory at affinity maturation of an antibody toward the variant PA-Y688A had not met with success. Error-prone libraries of 14B7 and very large saturation mutagenesis libraries based upon computational docking models of the antibody-toxin interaction did not yield affinity-improved binders (Jeong, K.J., unpublished data). The approach described here utilized the crystal structure of the ultra-high affinity antibody fragment M18 in complex with domain 4 of protective antigen of *Bacillus anthracis*. Based upon this interaction model, residues in definitive spheres of interaction with PAD4-688 were selected for saturation mutagenesis. This approach allowed maximum library diversity to be focused on the precise area of contact with PAD4-688.

With this intention, two libraries were constructed. The first, denoted NNS3, utilized the NNS DNA codon (N signifying any base A, G, C, or T; S signifying G or C) to replace wild-type codons in M18 at 3 locations: the two residues that appear to directly interact with Y688 of PA (L Q55 and H L101), and the neighboring proline (L P56) that might modulate the conformation of the binding region CDR L2. Likewise, the second

library, NNS8, replaced wild-type codons with NNS for 8 residues, which encompass all surface exposed amino acids within 6 Å of the Y688 residue of PA (L F46, L Y49, L R53, L Q55, L P56, H L101, H L102, and H D107). This second library included all amino acids saturated in NNS3, and added 5 more residues. After construction by overlap PCR and electroporation into MC1061 cells, the NNS3 library exhibited 2 x 10^7 individual transformants, while 6 x 10^7 transformants were observed for the NNS8 library. It is important to note that the theoretical diversity at the DNA level for the NNS3 and NNS8 libraries were 3.3 x 10^4 and 1.1 x 10^{12}, respectively. Therefore, the theoretical diversity was covered almost 1000 times by the number of transformants produced in the NNS3 library, making it highly likely that every combination of mutations was represented at least once in this library. In contrast, the NNS8 library represents, at best, the coverage of 0.005% of the theoretical diversity of an 8-membered saturation mutagenesis library. Ten clones from each library were sequenced, and excellent diversity was observed in all expected codons.

3.3.2 Library Sorting

Prior to the first round of sorting, the NNS3 library was observed to have an obvious "tail" feature, while the NNS8 library appeared primarily negative with rare positive events. Both libraries were screened in parallel, and the first three rounds of selection were carried out by labeling with 1 μM PAD4-Y688A. The NNS8 library appeared to enrich after two rounds of sorting by the emergence of a tail; significant enrichment was observed in both libraries after three rounds of sorting. Because of this enrichment, a more stringent sort with labeling at 20 nM of PAD4-Y688A was carried out for the fourth round of sorting. After the fourth round, analysis was carried out on several isolated clones chosen at random from the selected pool.

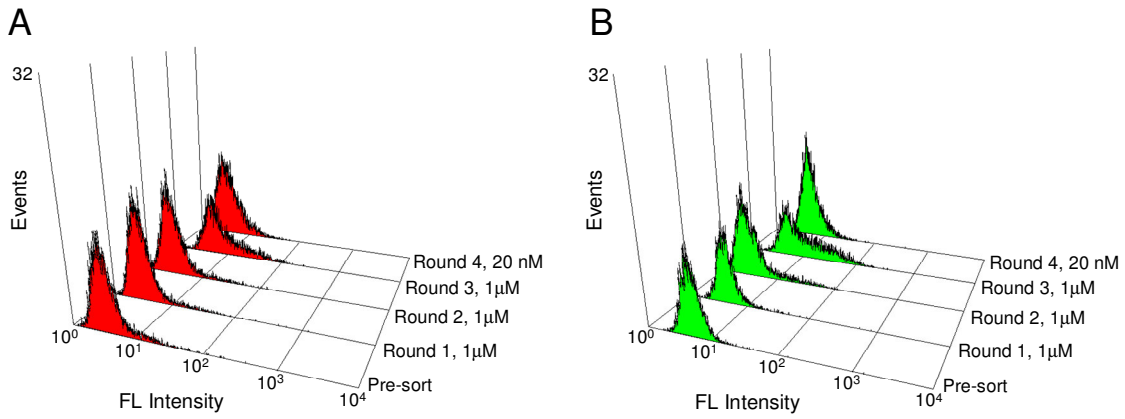

FIGURE 3.1. FACS SCREENING OF (A) NNS3 AND (B) NNS8 LIBRARIES. Y688A PAD4 labeling concentration is listed with the round of sorting.

3.3.3 Single Well ELISA Screening

Two 96-well plates were screened from each library, yielding a total of 384 individual clones screened (Figure 3.2). Based upon optimization experiments, the wild-type scAb M18 would have an absorbance of approximately 1. 43% of clones were considered positive (A_{450} above 0.5), and 36% of clones gave an equivalent or greater signal than that expected of M18 (A_{450} of 1.0 or above). The top ten percent of clones (A_{450} of 3.0 or above) were submitted for sequencing to determine whether a consensus sequence could be identified. Analysis revealed that these clones from the NNS3 library did not converge to a single sequence, as there was still variability among the twelve clones. Interestingly, the 27 clones from the NNS8 library produced several solutions, with a consensus forming of L Q55I, L P56S, and H L101M for 20 of 27 clones; however, only three of these clones had any variation from wild-type at any of the other five locations targeted in the NNS8 library, and this was exhibited as H L102V (CTA

GTC) in one clone and a silent codon change at L R53 (AGA AGG) in two clones. The top nine clones with the greatest absorbances (greater than A_{450} of 3.9) were well separated from the remaining clones. Thus, these were taken to the next round of screening by scale-up expression, purification, and ELISA titration.

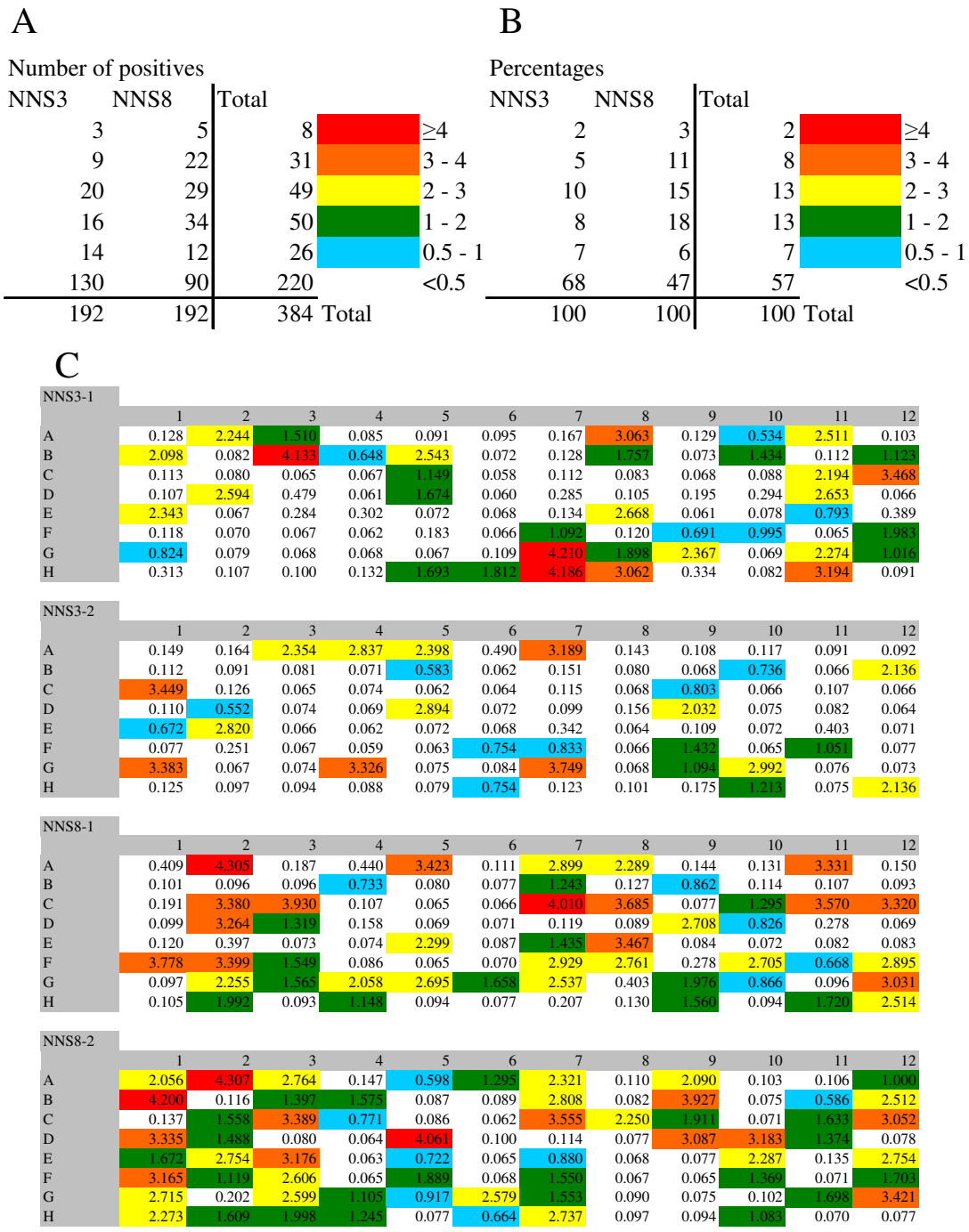

A

Number of positives

NNS3	NNS8	Total	
3	5	8	≥4
9	22	31	3 - 4
20	29	49	2 - 3
16	34	50	1 - 2
14	12	26	0.5 - 1
130	90	220	<0.5
192	192	384	Total

B

Percentages

NNS3	NNS8	Total	
2	3	2	≥4
5	11	8	3 - 4
10	15	13	2 - 3
8	18	13	1 - 2
7	6	7	0.5 - 1
68	47	57	<0.5
100	100	100	Total

C

NNS3-1

	1	2	3	4	5	6	7	8	9	10	11	12
A	0.128	2.244	1.510	0.085	0.091	0.095	0.167	3.063	0.129	0.534	2.511	0.103
B	2.098	0.082	4.133	0.648	2.543	0.072	0.128	1.757	0.073	1.434	0.112	1.123
C	0.113	0.080	0.065	0.067	1.149	0.058	0.112	0.083	0.068	0.088	2.194	3.468
D	0.107	2.594	0.479	0.061	1.674	0.060	0.285	0.105	0.195	0.294	2.653	0.066
E	2.343	0.067	0.284	0.302	0.072	0.068	0.134	2.668	0.061	0.078	0.793	0.389
F	0.118	0.070	0.067	0.062	0.183	0.066	1.092	0.120	0.691	0.995	0.065	1.983
G	0.824	0.079	0.068	0.068	0.067	0.109	4.210	1.898	2.367	0.069	2.274	1.016
H	0.313	0.107	0.100	0.132	1.693	1.812	4.186	3.062	0.334	0.082	3.194	0.091

NNS3-2

	1	2	3	4	5	6	7	8	9	10	11	12
A	0.149	0.164	2.354	2.837	2.398	0.490	3.189	0.143	0.108	0.117	0.091	0.092
B	0.112	0.091	0.081	0.071	0.583	0.062	0.151	0.080	0.068	0.736	0.066	2.136
C	3.449	0.126	0.065	0.074	0.062	0.064	0.115	0.068	0.803	0.066	0.107	0.066
D	0.110	0.552	0.074	0.069	2.894	0.072	0.099	0.156	2.032	0.075	0.082	0.064
E	0.672	2.820	0.066	0.062	0.072	0.068	0.342	0.064	0.109	0.072	0.403	0.071
F	0.077	0.251	0.067	0.059	0.063	0.754	0.833	0.066	1.432	0.065	1.051	0.077
G	3.383	0.067	0.074	3.326	0.075	0.084	3.749	0.068	1.094	2.992	0.076	0.073
H	0.125	0.097	0.094	0.088	0.079	0.754	0.123	0.101	0.175	1.213	0.075	2.136

NNS8-1

	1	2	3	4	5	6	7	8	9	10	11	12
A	0.409	4.305	0.187	0.440	3.423	0.111	2.899	2.289	0.144	0.131	3.331	0.150
B	0.101	0.096	0.096	0.733	0.080	0.077	1.243	0.127	0.862	0.114	0.107	0.093
C	0.191	3.380	3.930	0.107	0.065	0.066	4.010	3.685	0.077	1.295	3.570	3.320
D	0.099	3.264	1.319	0.158	0.069	0.071	0.119	0.089	2.708	0.826	0.278	0.069
E	0.120	0.397	0.073	0.074	2.299	0.087	1.435	3.467	0.084	0.072	0.082	0.083
F	3.778	3.399	1.549	0.086	0.065	0.070	2.929	2.761	0.278	2.705	0.668	2.895
G	0.097	2.255	1.565	2.058	2.695	1.658	2.537	0.403	1.976	0.866	0.096	3.031
H	0.105	1.992	0.093	1.148	0.094	0.077	0.207	0.130	1.560	0.094	1.720	2.514

NNS8-2

	1	2	3	4	5	6	7	8	9	10	11	12
A	2.056	4.307	2.764	0.147	0.598	1.295	2.321	0.110	2.090	0.103	0.106	1.000
B	4.200	0.116	1.397	1.575	0.087	0.089	2.808	0.082	3.927	0.075	0.586	2.512
C	0.137	1.558	3.389	0.771	0.086	0.062	3.555	2.250	1.911	0.071	1.633	3.052
D	3.335	1.488	0.080	0.064	4.061	0.100	0.114	0.077	3.087	3.183	1.374	0.078
E	1.672	2.754	3.176	0.063	0.722	0.065	0.880	0.068	0.077	2.287	0.135	2.754
F	3.165	1.119	2.606	0.065	1.889	0.068	1.550	0.067	0.065	1.369	0.071	1.703
G	2.715	0.202	2.599	1.105	0.917	2.579	1.553	0.090	0.075	0.102	1.698	3.421
H	2.273	1.609	1.998	1.245	0.077	0.664	2.737	0.097	0.094	1.083	0.070	0.077

FIGURE 3.2. SINGLE WELL ELISA SCREENING OF ISOLATED CLONES. Listed values are 450 nm absorbances. (A) Aggregate data and (B) percentage analysis of (C) actual single well ELISA data.

3.3.4 Plate ELISA Screening

The top nine clones from the previous round of screening were prepared in pure form along with M18 scAb, which served as an important control. When these were analyzed for affinity by tittering on ELISA, the observed EC50's of the mutant clones were all better than that of M18 (Figure 3.3). The best binding curves reflected EC50's of approximately 7-8 fold improved over the wild-type (~10 nM vs. ~70 nM). The top four clones were then examined by surface plasmon resonance (SPR) to determine kinetic parameters more accurately.

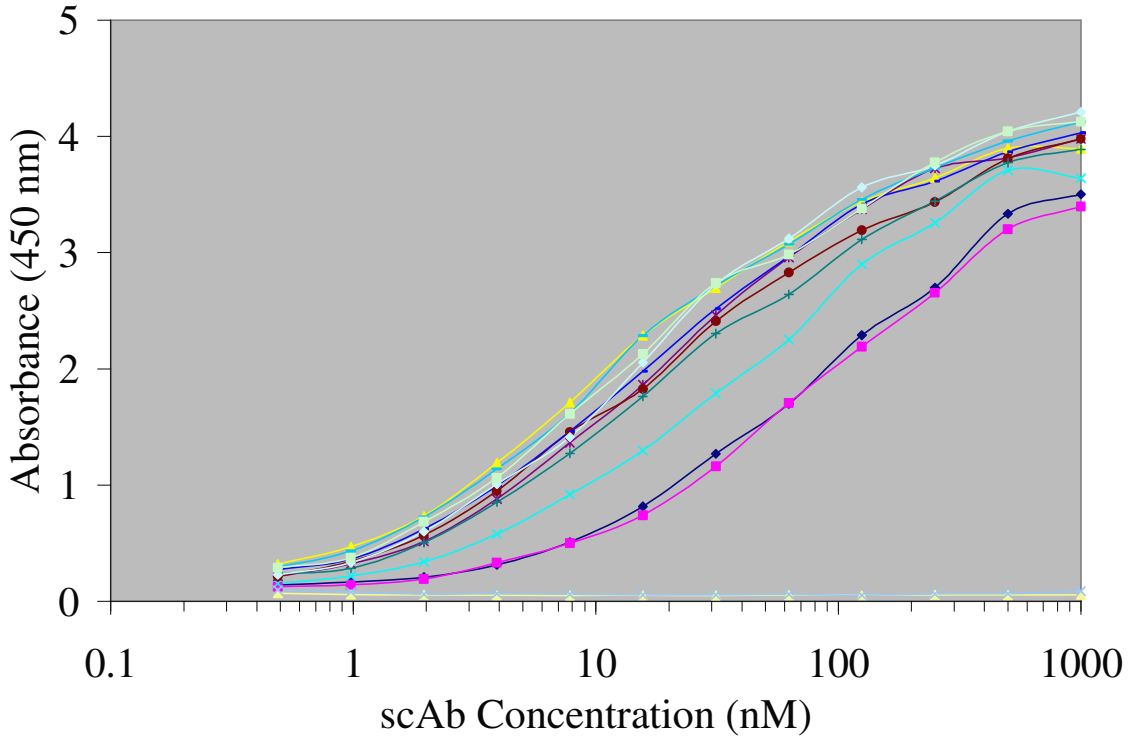

FIGURE 3.3. TITERED PLATE ELISAS FOR THE TOP NINE PAD4-Y688A BINDERS. (—, —, M18; —, —, no scAb (negative); —, 31B3; —, 31G7; —, 81A2; —, 81C3; —, 81C7; —, 82A2; —, 82B1; —, 82B9; —, 82D5.)

3.3.5 Kinetic Studies

Initially, all four clones and M18 scAb were screened by SPR to determine their kinetic constants with PAD4-Y688A. Results can be seen in Table 1. The affinity of M18 for PAD4-Y688A was found to be 73.8 nM, more than 2000 times lower affinity than M18 binding wild-type PA. The best of the affinity enhanced clones, 82B9, exhibited an apparent affinity of 10.5 nM for PAD4-Y688A, which is approximately 7-fold better than M18. SPR analysis was also carried out for M18 and 82B9 interacting with full-length PA_{83}-Y688A to confirm that the absence of domains 1-3 did not have any unintended effects. M18 and 82B9 were observed to have affinities of 60 nM and 8 nM, respectively, consistent with affinities acquired using PAD4-Y688A. When the interaction between 82B9 and wild-type PA83 was probed, an affinity of 740 pM was observed, an approximate 20-fold loss of affinity relative to M18.

3.3.6 Analysis of Clones

Inspection of the sequences of the 39 highest performing clones (Figure 3.4) in the single well ELISA assay revealed that one clone was the result of contamination from a neighboring well, as the sequence was that of the negative control, 26-10. Of the remaining 38 clones, twenty displayed the variation L-Q55I, L-P56S, and H-L101M with minor variations in sequence throughout. This represents 53% of total clones sequenced, and 74% of clones sequenced from the NNS8 library. Clones from the NNS3 library were much more variable in sequence composition. However, no additional mutations approached fixation within the remaining scFv proteins.

Figure 3.4. Primary sequence of 38 highest clones from the single well ELISA assay.

Analysis of the four best variants (Figure 3.5) revealed that increased bulk and hydrophobicity were selected at locations L 55, L 56, and H 101. In fact, in the best clone, 82B9, the bulky and hydrophobic amino acids L Q55W and H L101H create an aromatic "knob" that most likely fills the space vacated in the Y688A mutation. Other variants incorporated valine or isoleucine at L 55, which are both bulky and hydrophobic. Only one of the four clones retained the proline at L 56, and the three best clones had substitutions of serine, histidine, and leucine, respectively. Because proline restricts conformation, it appears that the increased flexibility associated with these other amino acids is preferable for binding to the Y688A variant.

It is also interesting to note that while three of the four best antibody variants isolated were from the NNS8 library, all four antibodies exhibited completely wild-type codons at the DNA level for the five residues covered in the NNS8 library that were not in the NNS3 library. Thus, it is not clear if these three genes were actually selected from the initial NNS8 library, or if they were the product of cross contamination from the NNS3 library. While efforts were made at every step to eliminate cross contamination, both libraries were sorted and cloned in parallel. As mentioned earlier, there were clones isolated from the NNS8 library within the top 10% of single well ELISA binders that did contain diversity in these five codons, which might imply that these four were faithfully selected from the NNS8 library and that there was great selective pressure for the wild-type residues at these locations, although the presence of wild-type codons would be highly coincindental.

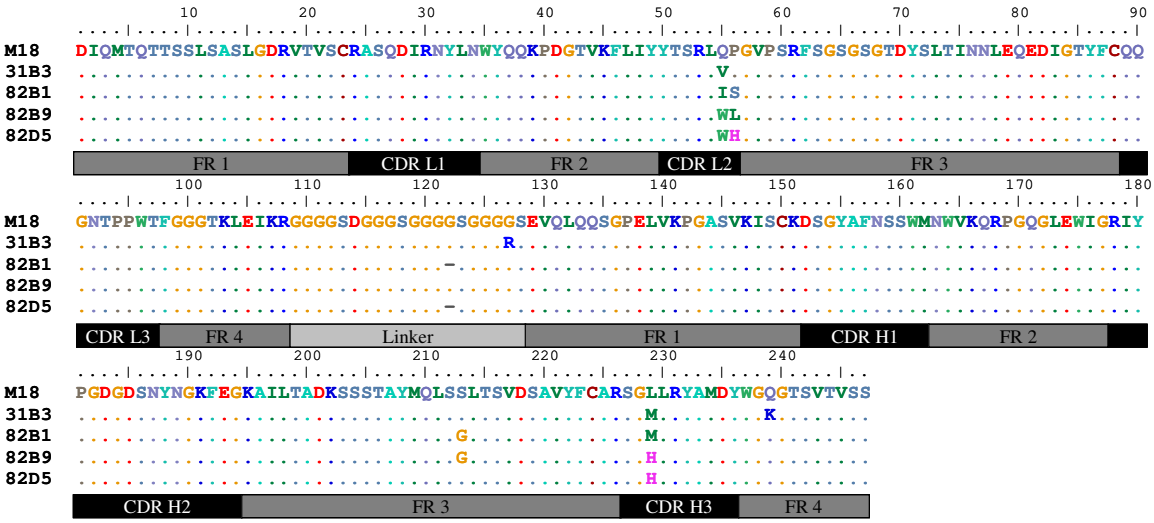

FIGURE 3.5. PROTEIN SEQUENCES OF FOUR BEST BINDING CLONES FOR PAD4-Y688A ALIGNED WITH M18. Framework (FR) and complementarity-determining regions (CDR's) are denoted in gray and black, respectively.

3.4 CONCLUSIONS

The recovery of 82B9 represents the first affinity improved antibody fragment to an altered anthrax toxin. It is clear that the elucidation of the co-crystal structure of M18 in complex with PAD4 provided the foundational difference for resolution of this problem. Being able to focus maximum diversity through saturation mutagenesis into a very small area yielded the only improvement to date. The retrieval of several clones that exhibit similar selected tendencies, that is hydrophobic, aromatic, and bulky side chains, mesh well with the idea that gains in affinity were the result of complementation for the loss of the tyrosine on the surface of protective antigen. While this does represent a success, continuing to evolve this clone until a potential therapeutic level (K_D ~ 50 pM) is reached is still underway.

3.5 REFERENCES

Albrecht, M.T., Li, H., Williamson, E.D., LeButt, C.S., Flick-Smith, H.C., Quinn, C.P., Westra, H., Galloway, D., Mateczun, A., Goldman, S.*, et al.* 2007. Human monoclonal antibodies against anthrax lethal factor and protective antigen act independently to protect against Bacillus anthracis infection and enhance endogenous immunity to anthrax. *Infect Immun* **75:** 5425-5433.

Brossier, F., Levy, M., Landier, A., Lafaye, P., and Mock, M. 2004. Functional analysis of Bacillus anthracis protective antigen by using neutralizing monoclonal antibodies. *Infect Immun* **72:** 6313-6317.

Chen, Z., Moayeri, M., Zhou, Y.H., Leppla, S., Emerson, S., Sebrell, A., Yu, F., Svitel, J., Schuck, P., St Claire, M.*, et al.* 2006. Efficient neutralization of anthrax toxin by chimpanzee monoclonal antibodies against protective antigen. *J Infect Dis* **193:** 625-633.

Cirino, N.M., Sblattero, D., Allen, D., Peterson, S.R., Marks, J.D., Jackson, P.J., Bradbury, A., and Lehnert, B.E. 1999. Disruption of anthrax toxin binding with the use of human antibodies and competitive inhibitors. *Infect Immun* **67:** 2957-2963.

Cui, X., Li, Y., Moayeri, M., Choi, G.H., Subramanian, G.M., Li, X., Haley, M., Fitz, Y., Feng, J., Banks, S.M.*, et al.* 2005. Late treatment with a protective antigen-directed monoclonal antibody improves hemodynamic function and survival in a lethal toxin-infused rat model of anthrax sepsis. *J Infect Dis* **191:** 422-434.

Harvey, B.R., Georgiou, G., Hayhurst, A., Jeong, K.J., Iverson, B.L., and Rogers, G.K. 2004. Anchored periplasmic expression, a versatile technology for the isolation of high-affinity antibodies from Escherichia coli-expressed libraries. *Proc Natl Acad Sci U S A* **101:** 9193-9198.

Jiao, G.S., Cregar, L., Wang, J., Millis, S.Z., Tang, C., O'Malley, S., Johnson, A.T., Sareth, S., Larson, J., and Thomas, G. 2006. Synthetic small molecule furin inhibitors derived from 2,5-dideoxystreptamine. *Proc Natl Acad Sci U S A* **103:** 19707-19712.

Karginov, V.A., Robinson, T.M., Riemenschneider, J., Golding, B., Kennedy, M., Shiloach, J., and Alibek, K. 2004. Treatment of anthrax infection with combination of ciprofloxacin and antibodies to protective antigen of Bacillus anthracis. *FEMS Immunol Med Microbiol* **40:** 71-74.

Kelly, C.D., O'Loughlin, C., Gelder, F.B., Peterson, J.W., Sower, L.E., and Cirino, N.M. 2007. Rapid generation of an anthrax immunotherapeutic from goats using a novel non-toxic muramyl dipeptide adjuvant. *J Immune Based Ther Vaccines* **5:** 11.

Kobiler, D., Gozes, Y., Rosenberg, H., Marcus, D., Reuveny, S., and Altboum, Z. 2002. Efficiency of protection of guinea pigs against infection with Bacillus anthracis spores by passive immunization. *Infect Immun* **70:** 544-560.

Little, S.F., Ivins, B.E., Fellows, P.F., and Friedlander, A.M. 1997. Passive protection by polyclonal antibodies against Bacillus anthracis infection in guinea pigs. *Infect Immun* **65:** 5171-5175.

Little, S.F., Leppla, S.H., and Cora, E. 1988. Production and characterization of monoclonal antibodies to the protective antigen component of Bacillus anthracis toxin. *Infect Immun* **56:** 1807-1813.

Mabry, R., Rani, M., Geiger, R., Hubbard, G.B., Carrion, R., Jr., Brasky, K., Patterson, J.L., Georgiou, G., and Iverson, B.L. 2005. Passive protection against anthrax by using a high-affinity antitoxin antibody fragment lacking an Fc region. *Infect Immun* **73:** 8362-8368.

Maynard, J.A., Maassen, C.B., Leppla, S.H., Brasky, K., Patterson, J.L., Iverson, B.L., and Georgiou, G. 2002. Protection against anthrax toxin by recombinant antibody fragments correlates with antigen affinity. *Nat Biotechnol* **20:** 597-601.

Meselson, M., Guillemin, J., Hugh-Jones, M., Langmuir, A., Popova, I., Shelokov, A., and Yampolskaya, O. 1994. The Sverdlovsk anthrax outbreak of 1979. *Science* **266:** 1202-1208.

Moayeri, M., and Leppla, S.H. 2004. The roles of anthrax toxin in pathogenesis. *Curr Opin Microbiol* **7:** 19-24.

Mohamed, N., Clagett, M., Li, J., Jones, S., Pincus, S., D'Alia, G., Nardone, L., Babin, M., Spitalny, G., and Casey, L. 2005. A high-affinity monoclonal antibody to anthrax protective antigen passively protects rabbits before and after aerosolized Bacillus anthracis spore challenge. *Infect Immun* **73:** 795-802.

Pelat, T., Hust, M., Laffly, E., Condemine, F., Bottex, C., Vidal, D., Lefranc, M.P., Dubel, S., and Thullier, P. 2007. High-affinity, human antibody-like antibody fragment (single-chain variable fragment) neutralizing the lethal factor (LF) of Bacillus anthracis by inhibiting protective antigen-LF complex formation. *Antimicrob Agents Chemother* **51:** 2758-2764.

Peterson, J.W., Comer, J.E., Noffsinger, D.M., Wenglikowski, A., Walberg, K.G., Chatuev, B.M., Chopra, A.K., Stanberry, L.R., Kang, A.S., Scholz, W.W.*, et al.* 2006. Human monoclonal anti-protective antigen antibody completely protects rabbits and is synergistic with ciprofloxacin in protecting mice and guinea pigs against inhalation anthrax. *Infect Immun* **74:** 1016-1024.

Rivera, J., Nakouzi, A., Abboud, N., Revskaya, E., Goldman, D., Collier, R.J., Dadachova, E., and Casadevall, A. 2006. A monoclonal antibody to Bacillus anthracis protective antigen defines a neutralizing epitope in domain 1. *Infect Immun* **74:** 4149-4156.

Rosovitz, M.J., Schuck, P., Varughese, M., Chopra, A.P., Mehra, V., Singh, Y., McGinnis, L.M., and Leppla, S.H. 2003. Alanine-scanning mutations in domain 4 of anthrax toxin protective antigen reveal residues important for binding to the cellular receptor and to a neutralizing monoclonal antibody. *J Biol Chem* **278:** 30936-30944.

Sawada-Hirai, R., Jiang, I., Wang, F., Sun, S.M., Nedellec, R., Ruther, P., Alvarez, A., Millis, D., Morrow, P.R., and Kang, A.S. 2004. Human anti-anthrax protective antigen neutralizing monoclonal antibodies derived from donors vaccinated with anthrax vaccine adsorbed. *J Immune Based Ther Vaccines* **2:** 5.

Sellman, B.R., Mourez, M., and Collier, R.J. 2001. Dominant-negative mutants of a toxin subunit: an approach to therapy of anthrax. *Science* **292:** 695-697.

Shoop, W.L., Xiong, Y., Wiltsie, J., Woods, A., Guo, J., Pivnichny, J.V., Felcetto, T., Michael, B.F., Bansal, A., Cummings, R.T.*, et al.* 2005. Anthrax lethal factor inhibition. *Proc Natl Acad Sci U S A* **102:** 7958-7963.

Steiniger, S.C., Altobell, L.J., 3rd, Zhou, B., and Janda, K.D. 2007. Selection of human antibodies against cell surface-associated oligomeric anthrax protective antigen. *Mol Immunol* **44:** 2749-2755.

Subramanian, G.M., Cronin, P.W., Poley, G., Weinstein, A., Stoughton, S.M., Zhong, J., Ou, Y., Zmuda, J.F., Osborn, B.L., and Freimuth, W.W. 2005. A phase 1 study of PAmAb, a fully human monoclonal antibody against Bacillus anthracis protective antigen, in healthy volunteers. *Clin Infect Dis* **41:** 12-20.

Turk, B.E., Wong, T.Y., Schwarzenbacher, R., Jarrell, E.T., Leppla, S.H., Collier, R.J., Liddington, R.C., and Cantley, L.C. 2004. The structural basis for substrate and inhibitor selectivity of the anthrax lethal factor. *Nat Struct Mol Biol* **11:** 60-66.

Vitale, L., Blanset, D., Lowy, I., O'Neill, T., Goldstein, J., Little, S.F., Andrews, G.P., Dorough, G., Taylor, R.K., and Keler, T. 2006. Prophylaxis and therapy of inhalational anthrax by a novel monoclonal antibody to protective antigen that mimics vaccine-induced immunity. *Infect Immun* **74:** 5840-5847.

Wild, M.A., Xin, H., Maruyama, T., Nolan, M.J., Calveley, P.M., Malone, J.D., Wallace, M.R., and Bowdish, K.S. 2003. Human antibodies from immunized donors are protective against anthrax toxin in vivo. *Nat Biotechnol* **21:** 1305-1306.

Young, J.A., and Collier, R.J. 2007. Anthrax toxin: receptor binding, internalization, pore formation, and translocation. *Annu Rev Biochem* **76:** 243-265.

CHAPTER 4

Toward the Engineering of a Photoresponsive Antibody

4.1 INTRODUCTION

Antibodies have for thousands of years provided protection against disease and infection as part of our immune system. With their high affinities and specificity to their intended target, they have proved resilient to some of humankind's most overwhelming illnesses (Lee *et al.* 2008; Yu *et al.* 2008). As scientists and physicians began to understand their structure and function, they sought to use them as therapeutics, diagnostics, and laboratory reagents, because of the same qualities that made them indispensable to the immune system: affinity and specificity. Currently there are 26 antibodies approved by the FDA for use as therapeutics or diagnostics for a variety of different ailments from Crohn's disease to cancer (Pavlou and Belsey 2005).

The creation of a reversible, photoresponsive antibody would be of great utility because it would allow both temporal and spatial control of molecular machinery utilizing only light. This could aid in the development of better therapeutics, reusable biosensors and protein arrays, and novel reagents in molecular biology. Recently, a photo-activatable antibody was constructed for treatment of cancer utilizing folate-tagged anti-CD3 antibodies (Thompson *et al.* 2008). Folate binds to cancer cells expressing folate receptor, and antibodies to CD3 attract killer T-cells to these cancer cells. The photo-activatable portion of this therapeutic was the appending of 1-(2-nitrophenyl)ethanol moieties to the antibody that rendered it inactive until they were removed upon irradiation with UV light (Self and Thompson 1996). This is certainly a

functional system, but it is not reversible because the antibody cannot be rendered inactive after cleavage of the photoactive groups. A reversible, photoresponsive system would provide utility in multiple arenas.

Previous work has characterized photoisomerizable dyes that can reversibly transition between states that differ in shape and polarity (Sakata *et al.* 2005b; 2005a). The nitrospirobenzopyran (BIPS) molecule can reversibly transition between a colorless spiro (SP) state and a colored merocyanine (MC) state upon exposure to different wavelengths of light. The SP to MC transition occurs upon irradiation with UV light (365 nm), and irradiation with visible light (546 nm) causes transition from MC back to the SP state. If this small molecule could be placed at or near the binding site, perhaps it could alter the interaction of antibody with antigen differently in each state, which could lead to a differential effect on binding.

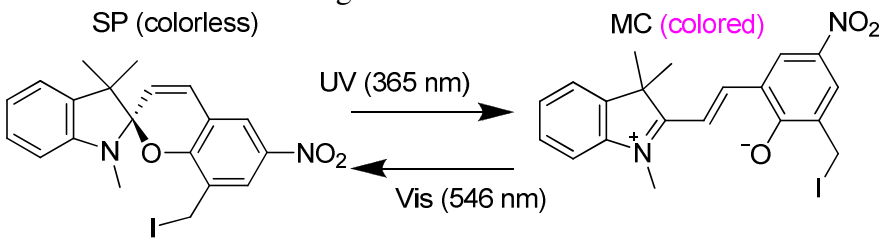

Figure 4.1. Photoisomerization of 8-I-BIPS.

A second approach is to utilize a larger appendage to interrupt binding of antibody to antigen. Previous studies revealed the engineering of "smart" polymer-protein conjugates that could alter enzymatic activity or streptavidin binding based upon polymer structure in response to light modulation (Shimoboji *et al.* 2001; Shimoboji *et al.* 2002a; Shimoboji *et al.* 2002b; Shimoboji *et al.* 2003). The polymer was a co-polymer primarily made up of dimethylacrylamide, with azobenzene moieties dispersed

throughout. These polymers exhibited an unfurled state after exposure to one wavelength of light, and subsequently underwent aggregation at the protein surface after exposure to a second wavelength of light. This aggregation covered the active site or binding site, thus rendering the protein inactive. Reversion back to the unfurled state restored activity. In much the same way, positioning a photoresponsive polymer near the binding site of an antibody might allow the specific obstruction of the antibody-antigen interaction.

The antibody-antigen pair that is to be used in this study is that of the M18 scFv with protective antigen (PA) of *Bacillus anthracis*. M18 is an ultra-high affinity variant from the 14B7 family of neutralizing antibodies directed at PA (Harvey *et al.* 2004). Earlier work has revealed the individual and complex structures of M18 with PA domain IV, and the 14B7 family has been amenable to engineering in several systems (Harvey *et al.* 2004; Jeong *et al.* 2007).

4.2 MATERIALS AND METHODS

4.2.1 Optimization of UV Dye Isomerization

8-Iodo-BIPS was a kind gift from Dr. Gerard Marriott at the University of Wisconsin-Madison. 8-I-BIPS was dissolved in dimethylformamide (DMF) at a concentration of 10 mM, and then diluted into 1x-HBS-E (10 mM Hepes, pH 7.4, 150 mM NaCl, 3 mM EDTA) at various concentrations. An apparatus was constructed to provide a consistent scaffold for irradiation of samples with UV light. A UV hand lamp was mounted to an enclosure such that a cuvette could be reproducibly placed at 1 cm distance from the center of the light source, while ambient light was blocked. Samples were placed in a quartz cuvette and irradiated with UV light (365 nm) for specified

amounts of time, at which point the absorbance at 546 nm was measured with a UV-1600 UV-Vis spectrophotometer (Shimadzu).

4.2.2 Site Directed Mutagenesis

M18 variants were constructed using site-directed mutagenesis via overlap PCR. The following variants were constructed: H-V93C, H-N59C, H-S75C, L-Q55C, H-Y100C, L-F46C, L-Y32C, and H-Y52C. First, two PCR reactions were carried out to synthesize two fragments of the gene of interest with the internal primers containing the codon changing residue. These two PCR fragments were purified by agarose gel electrophoresis, and mixed together as template for a second PCR reaction to yield the full-length gene fragment. Only the outer primers were used for amplification of this second reaction. Digestion of this fragment was accomplished with SfiI and subjected to agarose gel electrophoresis, which was then ligated with pAK400 vector that had previously been cleaved with SfiI. Ligations were desalted using Millipore desalting membrane for 1 hr. Reactions were subsequently transformed via electroporation into Jude-1 cells and plated on LB-Agar with 2% glucose and chloramphenicol at 30 μg/mL and grown overnight at 37°C. Individual colonies were picked and grown overnight in liquid culture of LB with 2% glucose and chloramphenicol at 30 μg/mL at 37°C. Plasmid was isolated from each culture by Miniprep (Qiagen), and sequencing was performed on individual clones by the ICMB Sequencing Core Facility.

After the correct sequence was determined for each construct, plasmid was transformed by electroporation into Jude-1 cells, which were plated on LB-Agar with 2% glucose and chloramphenicol at 30 μg/mL and grown overnight at 37°C. Individual colonies were picked and grown overnight in liquid culture of LB with 2% glucose and chloramphenicol at 30 μg/mL at 37°C. Frozen stocks were made by mixing liquid

culture with 50% glycerol 2:1, for a final glycerol concentration of 16%; cells were frozen at -80°C.

4.2.3 Protein Expression and Purification

Overnight cultures 40 mL in volume of TB with 2% glucose and cloramphenicol at 30 μg/mL were inoculated from frozen stocks and incubated at 37°C. The next day, this culture was used to inoculate 1 L of TB with chloramphenicol at 30 μg/mL, which was incubated at 37°C for 4 hours, then IPTG was added to 1 mM and induction was allowed to continue overnight. The following morning, cells were pelleted and resuspended in 50 mL of 50 mM Tris, pH 8.0, 500 mM NaCl, 10 mM imidazole. Cells were lysed by sonication (Probe dismembrator, Fisher Scientific) on ice in 5 mL aliquots by 3 cycles of 30 s at level 5 followed by 30 s off. Membranes were pelleted by centrifugation at 8,000 rpm for 20 minutes. Supernatant was equilibrated with 1 mL Ni-NTA Agarose (Qiagen) per liter of culture that had been washed three times in binding buffer. The cell lysate-bead mixture was mixed on ice for one hour. The Ni-NTA agarose beads were washed twice in batch by centrifugation at 3,000 rpm for 5 minutes, decanting of supernatant, followed by resuspension in 50 mM Tris, pH 8.0, 500 mM NaCl, 20 mM imidazole. The washed beads were then placed in a disposable polypropylene column (Pierce), and protein was eluted by addition of 4- 1 mL fractions of 50 mM Tris, pH 8.0, 500 mM NaCl, 250 mM imidazole. The eluent was dialyzed and concentrated into 10 mM Hepes, pH 7.4, 150 mM NaCl, 3 mM EDTA buffer using an Amicon Ultra 15, 10,000 MWCO filter.

The scFv-containing eluent was then subjected to size exclusion chromatography on a Superdex 200 column (GE Healthcare), utilizing a fast performance liquid chromatography (FPLC) system (ÄKTA FPLC, GE Healthcare). Running buffer was 1x

HBS-E (10 mM Hepes, pH 7.4, 150 mM NaCl, 3 mM EDTA), flow rate was 0.5 mL/min, and 0.5 mL fractions were collected. Fractions containing monomeric scFv based upon the FPLC profile as monitored by the 280 nm UV detector were combined and concentrated using an Amicon Ultra 15, 10,000 MWCO filter. Samples were then filtered using 0.22 μm Ultrafree-MC basket filters with PVDF membranes (Millipore). Protein concentrations were assessed using the BCA assay (Pierce) with BSA as a control.

4.2.4 Expression and Purification of M18-Y52C

After overnight cultivation of *E. coli* XL1-Blue containing plasmid pAK400-M18-Y52C in shake flask, cells were transferred into a 1 L flask containing 150 mL of R/2 medium (Jeong and Lee 1999) plus 2% (w/v) glucose. After 8 hr cultivation at 37^{o}C, cells were inoculated into fermentor. Fed-Batch fermentations were conducted in a 3.5 L Bioflo 300 fermentor (New Brunswick Scientific Co., Edison, NJ) containing 0.75 liter of same R/2 medium plus 2% (w/v) glucose. The pH was controlled at 6.8 by the addition of 28% (v/v) ammonia water. The dissolved oxygen concentration (DOC) was controlled at 40% of air saturation by automatically increasing the agitation speed up to 1,000 rpm and by the change of pure oxygen percentage. Two nutrient feeding solutions were added into the fermentor by pH-stat feeding strategy. Firstly, defined feeding solution (700 g/L glucose plus 20 g/L $MgSO_4 \cdot 7H_2O$) was used during pre-induction period. When the pH rose to a value greater than its set point (6.8) by 0.08 due to the depletion of glucose, the appropriate volume of feeding solution was automatically added to increase the glucose concentration in the culture broth. Secondly, complex feeding solution (500 g/L glucose, 100 g/L yeast extract and 20 g/L $MgSO_4 \cdot 7H_2O$) was used for enhancing protein production and cell growth during post-induction period. Before induction, culture

temperature was maintained at 37°C but, when cell density reached OD_{600} of 60, temperature was set to 25°C for 30 min and then induction with 1 mM IPTG were done and temperatures were maintained at 25°C during post-induction period for correct folding of scFv in periplasm. Cell growth was monitored by measuring the optical density (OD) at 600nm using an Ultraspec 3000 spectrophotometer (Shimazu, Japan). Culture samples were collected periodically by centrifugation and cell pellets and supernatants were stored at -20°C for further analysis. After finishing fermentation, 1.5 L culture was collected by centrifugation (6,500 rpm, for 20 min at 4°C) and cell paste was stored -20°C for purification of scFv.

Cells were thawed and resuspended in 1,250 mL of lysis buffer (50 mM Tris, pH 8.0, 500 mM NaCl, 10 mM imidazole), then they were lysed by two passes through a flow-through microfluidics homogenizer set at 10,000 psi. Cell lysates were then centrifuged for 30 minutes at 8,000 rpm, and the scFv-containing supernatant was retained. 4 mL of Ni-NTA agarose beads (Qiagen) were pre-washed with lysis buffer, and then mixed with the supernatant at 4°C for one hour. The Ni-NTA agarose beads were then collected on a column and washed with 40 mL of lysis buffer. Purified protein was then eluted in 8 mL of 50 mM Tris, pH 8.0, 500 mM NaCl, 250 mM imidazole. The column eluent was then dialyzed against 10 mM Tris, pH 8.0 overnight at 4°C using a 2,000 MWCO Slide-A-Lyzer dialysis cassette (Pierce).

The dialyzed sample was then subjected to anion exchange chromatography on a Mono Q 5/5 column (GE Healthcare), utilizing a fast performance liquid chromatography (FPLC) system (ÄKTA FPLC, GE Healthcare). The initial running buffer was 10 mM Tris, pH 8.0 (Buffer A), and the gradient buffer was 10 mM Tris, pH 8.0 with 800 mM NaCl (Buffer B). The flow rate was 0.5 mL/min throughout, and 1 mL fractions were collected during the run. The sample was injected on to the column and allowed to reach

equilibrium with running buffer of 100% Buffer A before a gradient was begun to reach 20% Buffer B after 50 minutes; pure scFv typically eluted between 8-10% Buffer B based upon UV absorbance as monitored by the 280 nm detector . Fractions containing scFv were buffer exchanged and concentrated into 10 mM Tris, pH 8.0 with 150 mM NaCl using an Amicon Ultra 15, 10,000 MWCO filter. Samples were then filtered using 0.22 μm Ultrafree-MC basket filters with PVDF membranes (Millipore). Protein concentrations were assessed using the BCA assay (Pierce) with BSA as a control.

4.2.5 Conjugation of Small Molecules to Proteins

8-I-BIPS or 5-iodoacetamidofluorescein (5-IAF) was added to protein solutions in a 4- to 8-fold molar excess of protein, and was placed in the dark at 4°C overnight. Free dye was removed by centrifugation for 1 minute at 12,000 rpm followed by thorough washing of the supernatant containing protein-dye conjugate with 1x HBS-EP buffer (10 mM Hepes, pH 7.4, 150 mM NaCl, 3 mM EDTA, 0.005% Polysorbate-20) by diafiltration utilizing an Amicon Ultra 15, 10,000 MWCO filter. Protein concentrations were assessed using the BCA assay (Pierce) with BSA as a control, dye concentrations were measured at 350 nm (35,000 $M^{-1}cm^{-1}$) using a Nanodrop 1000 spectrophotometer, and the percent conjugation was calculated by taking the ratio of these two concentrations.

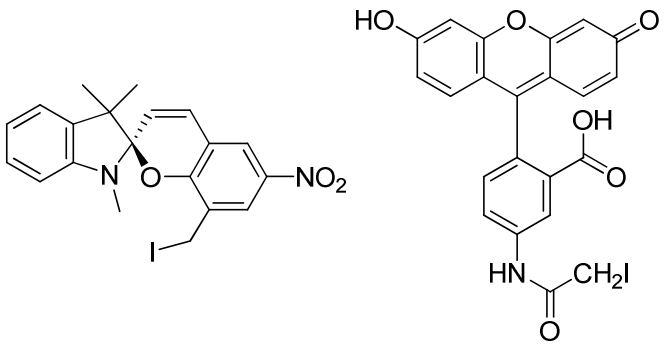

Figure 4.2. Structures of 8-I-BIPS (left), and 5-iodoacetamidofluorescein (right).

4.2.6 ELISA Screening of scFv-8-I-BIPS conjugates

ELISA plate wells were coated with 100 µL of 3 µg/mL PA_{83} in PBS overnight at 4°C. The following morning, the plates were washed with 1x PBS with 0.05% Tween-20 using a SkanWasher 300 and then allowed to block for 4 hours at room temperature with 2% milk in PBS. scFv-dye conjugates, while still in concentrated solution, were given no treatment, UV irradiation, or UV irradiation followed by irradiation by visible light. They were then diluted to 600 nM in 2% milk-PBS, loaded on to the plate, and subjected to 1:1 serial dilutions with 2% milk-PBS across the remaining 11 rows of the plate; 100 µL was left in each well. M18 was used as a positive control, and was diluted to 62.5 nM in 2% milk-PBS and treated similarly as samples. This was incubated at room temperature for one hour before washing with 0.05% Tween-20 in PBS. 100 µL of anti-His-tag IgG-HRP conjugate diluted 1:2500 into 2% milk-PBS was applied to each well and allowed to incubate at room temperature for 1 hour. ELISA plates were then washed with PBS with 0.05% Tween-20 and developed with 100 µL of TMB substrate. Development was quenched by adding 100 µL of 4.5 M H_2SO_4, mixing gently, and then was read at 450 nm using a 96-well plate reader.

4.2.7 Temperature Stability ELISA for M18-Y52C

ELISA plate wells were coated with 100 µL of 3 µg/mL PA_{83} in PBS overnight at 4°C. The following morning, the plates were washed with 1x PBS with 0.05% Tween-20 using a SkanWasher 300 and then allowed to block for 4 hours at room temperature with 2% milk in PBS. M18-Y52C scFv aliquots were placed at a range of temperatures for 15 minutes, and then diluted to 600 nM in 2% milk-PBS, loaded on to the plate, and subjected to 1:1 serial dilutions with 2% milk-PBS across the remaining 11 rows of the plate; 100 µL was left in each well. This was incubated at room temperature for one hour before washing with 0.05% Tween-20 in PBS. 100 µL of anti-His-tag IgG-HRP conjugate diluted 1:2500 into 2% milk-PBS was applied to each well and allowed to incubate at room temperature for 1 hour. ELISA plates were then washed with PBS with 0.05% Tween-20 and developed with 100 µL of TMB substrate. Development was quenched by adding 100 µL of 4.5 M H_2SO_4, mixing gently, and then was read at 450 nm using a 96-well plate reader.

4.2.8 Fluorescent Plate Assay for M18-Y52C scFv-IAF Conjugates

Various concentrations of PA_{83} were mixed with a set concentration of M18-Y52C-IAF in a black 96 well plate and allowed to incubate at room temperature for 45 minutes. The plate was then read using a BioTek SynergyHT plate reader for fluorescein fluorescence with 485/20 nm excitation and 530/25 nm emission.

4.2.9 Synthesis of Azobenzene Acrylate Monomer

The synthesis of 4-phenylazophenyl acrylate was carried out essentially as described by Shimoboji *et al.* 4-phenylazophenol was recrystallized in ethanol and dried overnight under vacuum. Acryloyl chloride was distilled under vacuum, and triethylamine was distilled prior to use. Dry diethyl ether was obtained from a solvent delivery system. 0.2 mol of 4-phenylazophenol and 0.26 mol triethylamine were dissolved in 200 mL diethyl ether and placed under argon at 0°C. 0.24 mol acryloyl chloride was added dropwise while stirring, then the ice bath was removed and the reaction was allowed to equilibrate to room temperature overnight. The reaction was then filtered to remove triethylammonium salts, washed with base, water, and brine, then dried with sodium sulfate and filtered. The remaining solution was evaporated and ^{1}H NMR in deuterated-DMSO confirmed the presence and purity of product. 1H NMR (DMSO) δ 7.95 (m, 2H), 7.87 (m, 2H), 7.57 (m, 3H), 7.41 (m, 2H), 6.56 (dd, J_{large} = 17.2 Hz, J_{small} = 1.2 Hz, 1H), 6.42 (dd, J_{large} = 17.2 Hz, J_{small} = 10.4 Hz, 1H), 6.17 (dd, J_{large} = 10.4 Hz, J_{small} = 1.2 Hz, 1H) ppm. Product was stored at -20°C in the dark to await further use.

4.2.10 Synthesis of Azobenzene-Dimethylacrylamide Co-polymer

Again, synthesis of this polymer was modeled after the synthesis of Shimoboji *et al.* Dimethylacrylamide, the co-polymer monomer, and β-mercaptoethanol, the chain transfer reagent, were distilled under reduced pressure immediately prior to use. 2,2'-azobisbutyronitrile (AIBN), the radical initiatior, was recrystallized from acetone and was a kind gift of the laboratory of Dr. Grant Willson. Dry dimethylformamide was obtained from a solvent delivery system. As this was a co-polymer, the total monomer concentration (4-phenylazophenol acrylate and dimethylacrylamide) was 2 M, and the

basic ratio of monomer:AIBN:β-mercaptoethanol was 100:1:0.2 for all syntheses. The reaction was prepared and then subjected to three cycles of freeze-pump-thaw to remove oxygen from solution; it was then placed at 60°C under argon for 20 hours to polymerize. The reaction was then either evaporated and solubilized in tetrahydrofuran (THF), or mixed 1:1 with THF and precipitated into 10 volumes of 33% diethyl ether in hexanes (v/v); the reaction was then filtered and dried under vacuum overnight. Gel permeation chromatography was utilized to determine the molecular weight of the polymer, and ^{1}H NMR in deuterated-DMSO was used to reveal the percent incorporation of the azobenzene monomer within the co-polymer by comparing the ratio of the proton integrations of aliphatic to aromatic signals, while subtracting out signals due to the protons in the acrylic backbone based upon their prevalence in the monomers. Co-polymers were stored in the dark at room temperature awaiting further use.

4.2.11 Synthesis of Vinyl Sulfone-capped Co-polymer

Co-polymer synthesized with the aid of the chain transfer agent β-mercaptoethanol contained a terminal hydroxyl group on one end of the polymer. Divinyl sulfone was reacted with that hydroxyl group in order to append a moiety that could covalently attach to a free cysteine located on a protein. Approximately 1 gram of co-polymer was dissolved in 20 mL of either dichloromethane or THF with 10-fold molar excess of divinyl sulfone and 2.5-fold molar excess of potassium *tert*-butoxide. The solution was allowed to react under argon while stirring overnight at room temperature. Reactions in dichloromethane were evaporated and solubilized in THF; then, the reaction solution in THF was precipitated into 10 volumes of 33% diethyl ether in hexanes (v/v), filtered, and dried overnight under vacuum. Gel permeation chromatography was utilized to determine the molecular weight of the co-polymer, and FT-IR was used to confirm the

presence of a sulfone in the co-polymer. The product was then stored in the dark at room temperature while awaiting use.

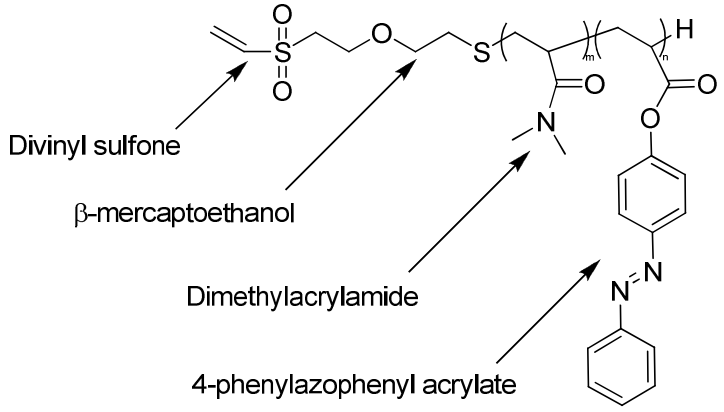

Figure 4.3. Structure of vinyl sulfone-capped co-polymer, with the respective precursor groups labeled below.

4.2.12 Lower Critical Solution Temperature (LCST) Measurements

Co-polymer was dissolved in aqueous solvent at a concentration of 2mg/mL, loaded into a microcuvette, and exposed to visible or UV light. LCST measurements were then made on samples using a Beckman DU 700 UV-Vis spectrophotometer with a peltier temperature controlled cuvette holder. Data was collected for 600 nm absorbance at 0.2°C increments, and a temperature gradient of 0.5°C/min was maintained throughout.

4.3 RESULTS AND DISCUSSION

4.3.1 Optimization of UV Dye Isomerization

In order to carry out photoisomerization studies with 8-I- BIPS appended to proteins on a free cysteine, it was necessary to first understand how this dye responded to

UV light using our instrumentation. The photoisomerization of this molecule has been carried out extensively in previous work (Sakata *et al.* 2005b; 2005a). Irradiation with UV light results in scission of a C-O bond, which induces an absorbance in the visible range and makes the compound colored. Irradiation with visible light causes reversion back to the uncolored state. Analysis in this laboratory revealed that an exposure to UV light for 2 minutes resulted in greater than 90% conversion of dye to the colored state; additionally, the response of the dye appeared to be concentration independent.

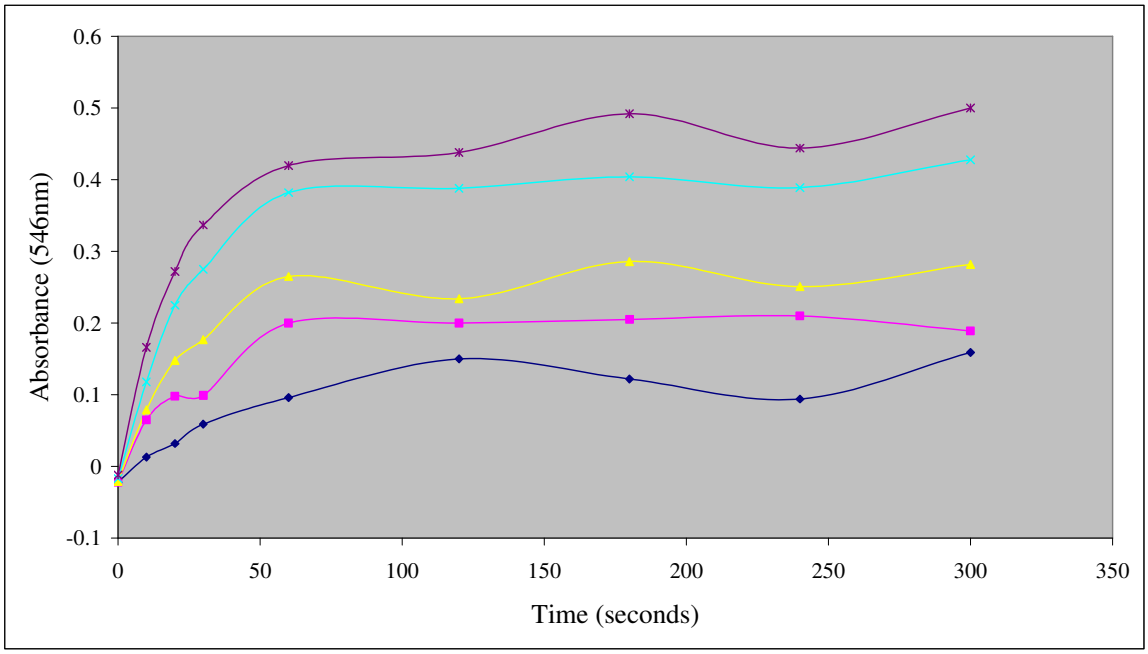

FIGURE 4.4. UV OPTIMIZATION OF 8-I-BIPS PHOTOISOMERIZATION, by concentration of 8-I-BIPS listed here. —□—, 5 µM; —□—, 7.5 µM; —□—, 10 µM; —X—, 15 µM; —*—, 20 µM.

4.3.2 Protein Expression and Purification

Eight variants of M18 were constructed with an additional cysteine placed using site-directed mutagenesis: H-V93C, H-N59C, H-S75C, L-Q55C, H-Y100C, L-F46C, L-Y332C, and H-Y52C. These mutations were placed at locations around the antibody fragment to determine a location optimal for manipulation of the antibody affinity by the photoreactive group. Of note, H-Y100C was in the center of bindng site, and H-Y52C was at the edge of the binding site with PA. With the addition of this extra cysteine, it was hypothesized that additional misfolding might occur, which could decrease the protein yield. This appeared to be the case, because mutation of M18 scFv, which routinely yields 4-8 mg/L of culture, resulted in variants that routinely produced less that 0.1 mg/L of culture. Because of the poor yields, it was at times necessary to carry out multiple preparations of a given protein in order to characterize it in more than one assay. It was also observed that levels of contaminating proteins within preparations could vary, such that an alternate form of purification might be preferable for additional studies.

4.3.3 Expression and Purification of M18-Y52C scFv

While hampered in earlier efforts with poor protein production, a fermentor was utilized to produce a greater amount of protein to prevent the time consuming effort and variation in purity of preparations that were prevalent using other techniques. A retrospective analysis is presented in Figure 4.5 for the preparation of M18-Y52C utilizing fermentation.

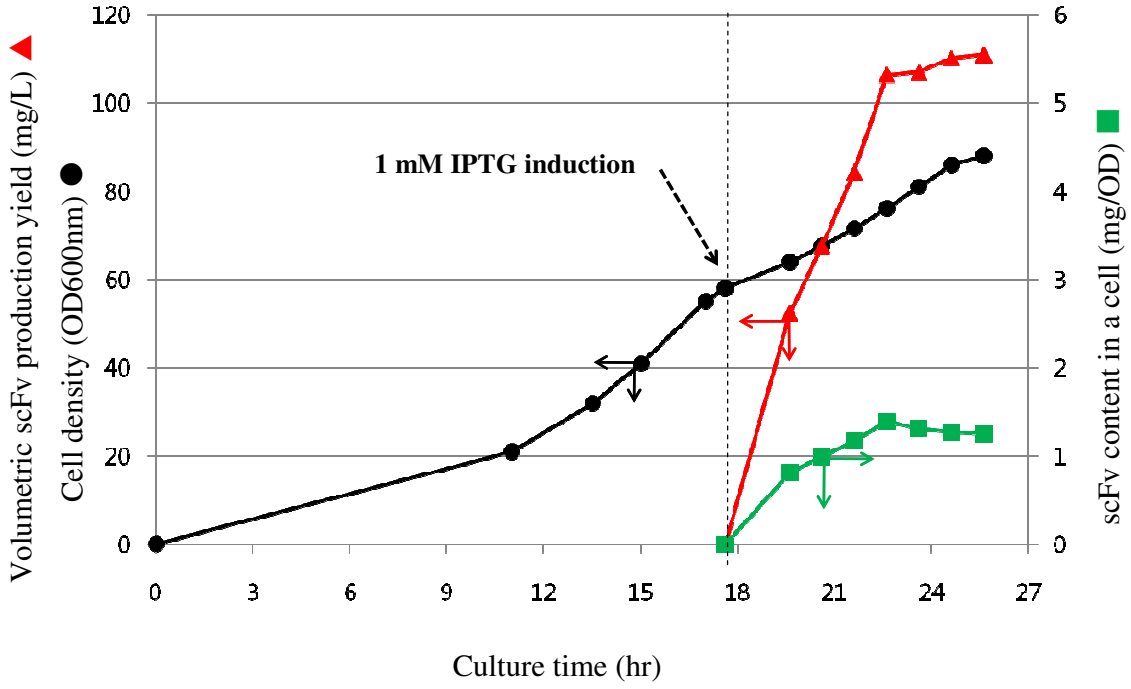

Figure 4.5. Analysis of M18-Y52C scFv fermentor run.

As observed in previous preparations, contaminating proteins hindered the isolation of pure M18 variants. Protein sequencing revealed the identity of contaminant proteins (glmS and slyD), and the isoelectric point of each of the contaminants was computationally determined to reside between 5 and 6. The M18 scFv and its variants exhibit a significantly higher pI between 7 and 8. The disparity of isoelectric points was utilized by anion exchange chromatography to remove these contaminants to yield pure M18-Y52C. The final yield of M18-Y52C was 21.4 mg from 1.25L of culture. This purification was carried out under limiting Ni-NTA agarose bead conditions to maintain maximum purity, but it appears based upon the retrospective analysis that less than 20%

of the total M18-Y52C was recovered. However, 21.4 mg of protein was more than enough for its intended purposes.

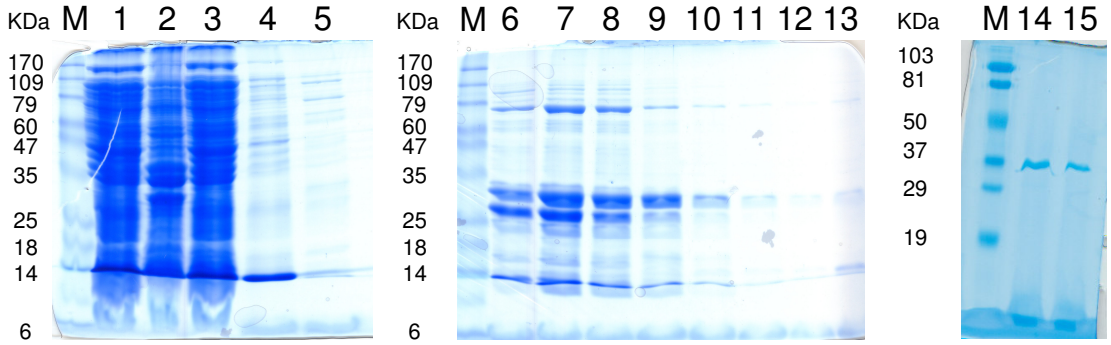

FIGURE 4.6. PAGE ANALYSIS OF M18-Y52C PROTEIN PURIFICATION. Lane labels: M- molecular weight marker; 1- pre-Ni-NTA soluble fraction; 2- insoluble fraction; 3- Ni-NTA column flow-through; 4- Ni-NTA column wash 1; 5- Ni-NTA column wash 2; 6-13- Ni-NTA column elutions 1-8; 14 and 15- M18-Y52C after ion exchange chromatography.

4.3.4 Conjugation of Small Molecules to Proteins

Both compounds that were to be appended to proteins were iodinated, so an S_N2 reaction with a free cysteine should proceed spontaneously, given that the sulfur is in a deprotonated state. The pK_a of cysteine is 8.3, so the reaction was carried out in buffer with pH as close to that as possible (pH of 7.4 to 8.0) to increase efficiency of attack. While it was expected that reactions of cysteines placed in different locations might have different efficiencies of conjugation, and this appeared to be the case, these conjugation efficiencies are very rough approximations and do not carry much meaning. When the M18 variants H-V93C, L-Q55C, and H-Y100C were coupled with 8-I-BIPS they yielded 25%, 23%, and 30% conjugation efficiencies, respectively; when H-Y52C was coupled

with 5-IAF it yielded 18% conjugation efficiency by the ratio of spectroscopically determined dye concentration to the protein concentration determined by BCA assay.

4.3.5 ELISA of 8-I-BIPS Conjugates

It was found that when careful titration using multi-channel pipettes and utilization of the SkanWasher 300 for washes were combined during ELISA, that plate-to-plate variation was minimized on a given day. It appeared that H-N59C and L-Q55C exhibited reproducible changes in ELISA binding curves when exposed to UV light relative to non-irradiated samples. When subsequently exposing L-Q55C to visible light in order to restore the BIPS dye to its three-ringed "ground" state, there appeared to be no reversion to the untreated curve. However, H-Y100C, which is located directly in the binding interface of the M18-PA complex, did appear to have a slight light-dependent, reversible effect based upon ELISA binding curves. This effect seemed to be reproducible, though statistically insignificant.

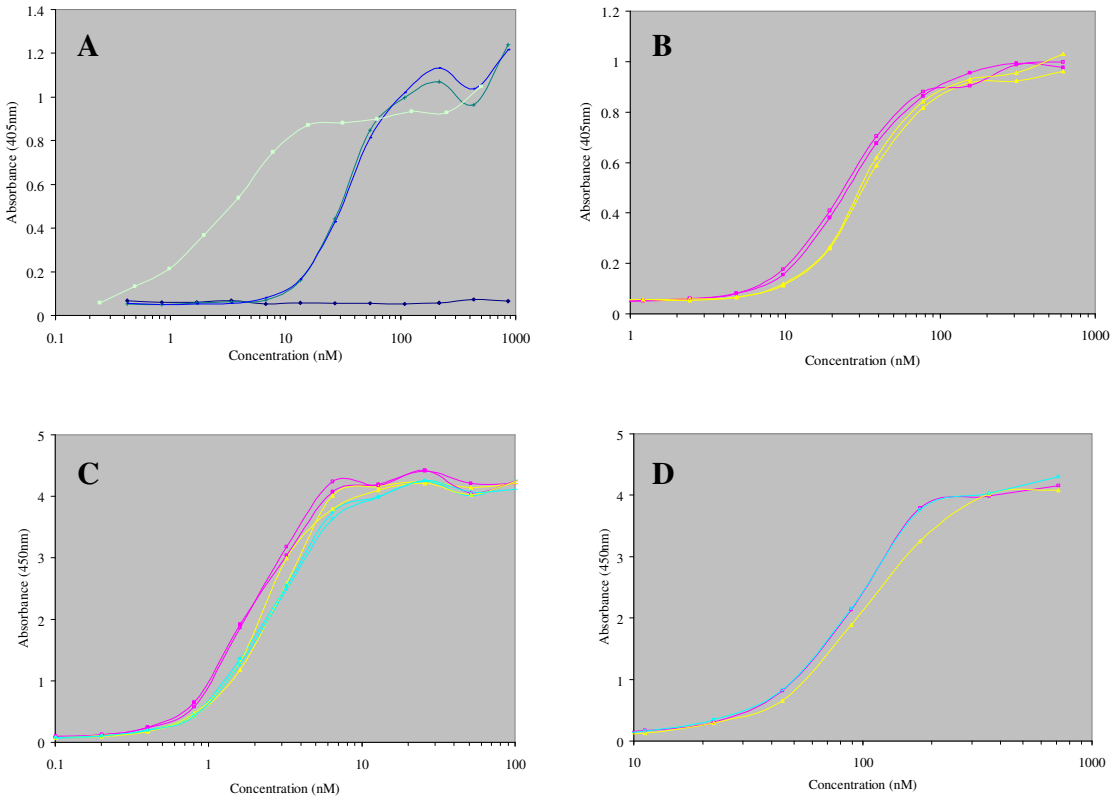

FIGURE 4.7. ELISA CURVES FOR SCFV-BIPS CONJUGATES. (A) Controls: , M18 scFv (positive); , Negative; , N59C unconjugated; , N59C unconjugated + UV. (B) N59C-BIPS: , no treatment; , UV. (C) Q55C-BIPS: , no treatment; , UV; , UV + Vis. (D) Y100C-BIPS: , no treatment; , UV; , UV + Vis.

This effect is likely negligible because it was an attempt to utilize a relatively small molecule with a slight structural deviation to effect a quantifiable change on a large binding surface. In light of this, the use of a much larger photoactive moiety was intended to prevent problems associated with the earlier approach. Earlier work undertaken at the University of Washington indicated the synthesis of photoactive

polymers that could be appended to proteins might be a valid approach (Shimoboji *et al.* 2002a; Shimoboji *et al.* 2002b). To begin this effort, a location on the M18 scFv was sought after that would be suitable for the placement of such a polymer.

4.3.6 Plate Assay for M18-Y52C-IAF

Based upon crystallographic studies of the M18-PA binding interface, it was determined that the heavy chain residue Y52, which resides at the beginning of the CDR H2 loop, might be a residue that would be close enough to the binding site to allow the photoresponsive polymer to interrupt the interaction between M18 and PA while not abrogating binding completely. Because these are also requirements for a fluorescent environmental sensor (Owenius *et al.* 1999; de Lorimier *et al.* 2002; Renard *et al.* 2003; Thomas *et al.* 2006), the successful development of a PA-detecting fluorescent sensor utilizing the M18 scFv scaffold might be used to determine whether H-Y52C would be a suitable candidate for location of the photopolymer.

After scale-up, purification of M18-Y52C, and conjugation to 5-IAF, ELISA was carried out on the unconjugated and conjugated forms of M18-Y52C to verify that there was still adequate binding activity. Then, a constant amount of M18-Y52C-AF was aliquoted into a 96 well plate and mixed with varying concentrations of PA in order to determine whether differential fluorescence could be observed based upon PA concentration. While trying to correct for the amount of fluorescence added into each well when using different protein-fluor preparations, a titration curve was reproduced using fluor-protein conjugate made from different protein preparations and conjugation reactions. Initial single concentration optimization experiments revealed that 970 nM M18-Y52C-AF conjugate exhibited differential fluorescence in the presence of 1.1 μM PA, while an equal concentration of BSA did not have an effect. With a probable

location for conjugation of the photopolymer identified, synthesis of a suitable photopolymer was undertaken after temperature stability was determined for the M18-Y52C scFv.

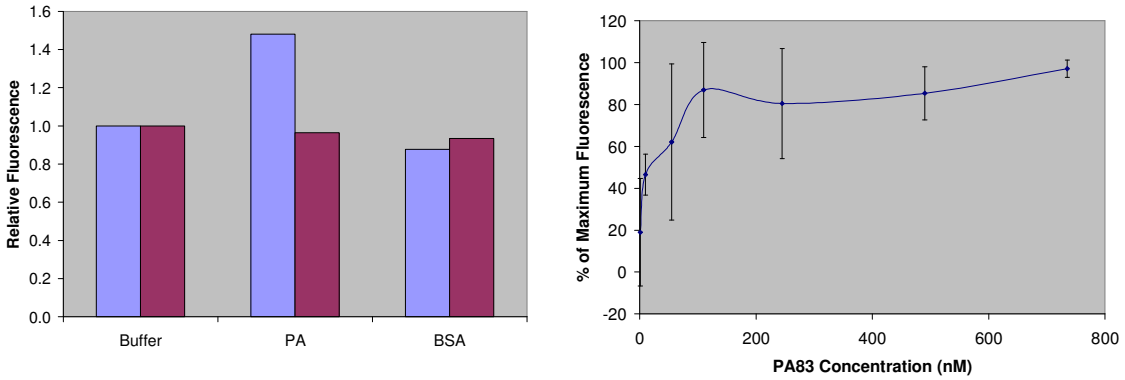

FIGURE 4.8. ENVIRONMENTAL BIOSENSOR ACTIVITY OF M18-Y52C-AF. Left: Optimization of environmental sensor at (▯) 0.97 µM M18-Y52C-AF mixed with 1.1 µM of PA or BSA; (▯) 0.92 µM M18-Y100C-AF (non-sensing) with 1.1 µM of PA or BSA for comparison. Right: Environmental biosensor M18-Y52C-AF with several concentrations of PA83.

4.3.7 Temperature Stability of M18-Y52C scFv

An ELISA assay to determine the maximum temperature for an experiment using M18-Y52C was developed because of the nature of the photopolymer that would be used. UV irradiation causes an upward shift in the LCST of the polymer with respect to polymer irradiated with visible light. This LCST is a measurement of aggregation of the polymer, and the differential effect of light irradiation is elicited through the trans to cis transition of azobenzene with UV irradiation, with the cis form causing the LCST transition to occur at a higher temperature (Shimoboji *et al.* 2002a). The utility of a photo-reactive transition between the two states of linear to aggregated polymer could

then be carried out at a constant temperature just below where aggregation begins to occur for the UV irradiated polymer. In that case visible irradiation would cause precipitation of the polymer which might then block the binding site of the M18-Y52C scFv, rendering it unable to bind PA; subsequent irradiation with UV light would restore the polymer to its linear form and allow the scFv to bind PA. In order to determine the requirements of the polymer, the temperature stability of the scFv must be assessed.

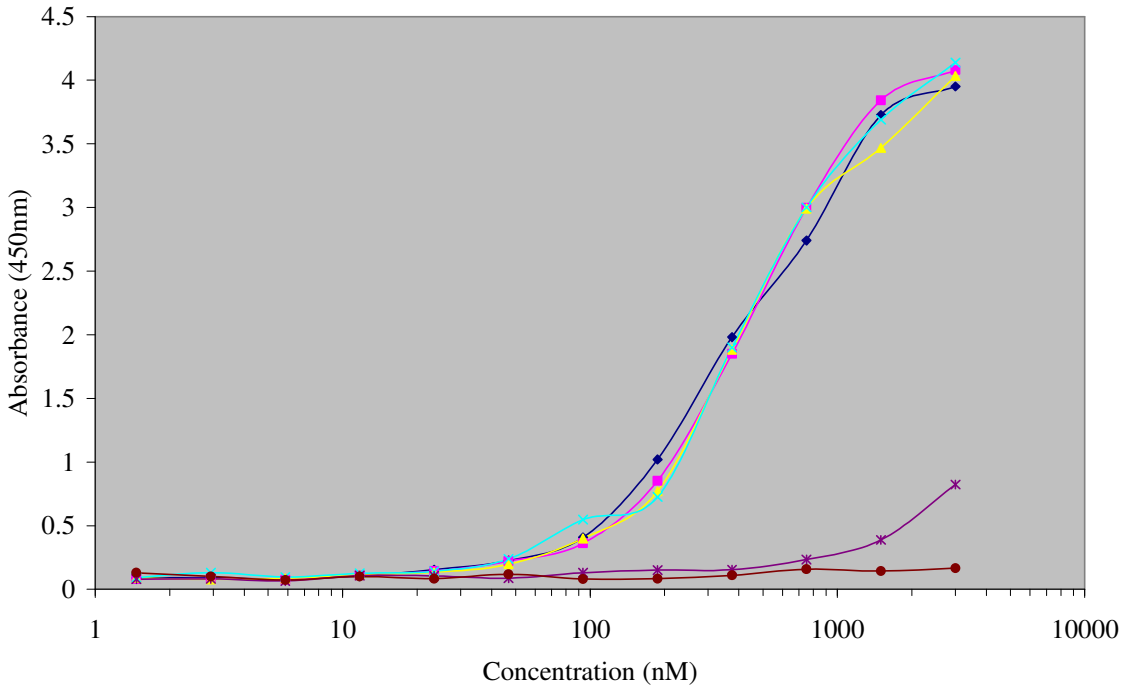

FIGURE 4.9. TEMPERATURE STABILITY ELISA OF M18-Y52C AT 15 MINUTES EXPOSURE TO EACH TEMPERATURE. —□—, 25°C; —□—, 30°C; —□—, 37°C; —X—, 45°C; —*—, 55°C; —□—, Negative.

Analysis of the ELISA determined that a maximum of 15 minutes at 45°C could be sustained by the antibody fragment; in fact, precipitation was observed in the 45°C sample when mixing with milk-PBS to apply to the ELISA plate. It is inferred that more time at that temperature would presumably render the scFv inactive. Therefore, it would be preferred that the isotherm at which an experiment were run at would be below 40°C, and lower temperatures than this would be preferable.

4.3.8 Synthesis of Azobenzene-Acrylate Monomer

Utilizing Shimoboji *et al.* as a guide, synthesis of the ester-linked azobenzene-acrylate monomer was quite straightforward. The reaction occurring was of an acid chloride with an alcohol to create an ester. The only alteration from the previous protocol was that recrystallization after formation of the acrylate monomer was omitted, because unwanted polymerization appeared to occur upon heating of the monomer in ethanol. Characterization by ^{1}H-NMR agreed well with the expected product.

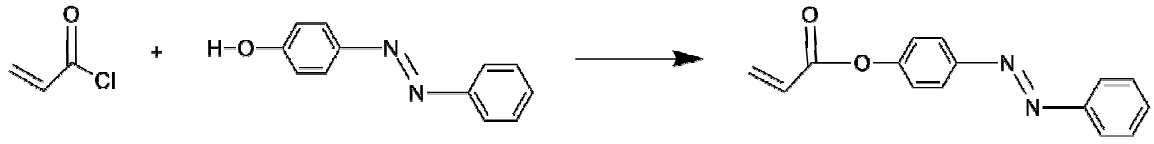

Figure 4.10. Synthesis of 4-phenylazophenyl acrylate.

4.3.9 Synthesis of Azobenzene-Dimethylacrylamide Co-polymer

Synthesis of the co-polymer required more alterations to the originally published protocol than synthesis of the azobenzene monomer. Polymerization conditions were maintained essentially as described in Shimoboji *et al.*, with the addition of three freeze-

pump-thaw cycles after preparation of the reaction. Following polymerization, precipitation using previously described conditions was found to be insufficient. Evaporation followed by resuspension in THF or dilution 1:1 in THF followed by precipitation into 1:2 diethyl ether:hexanes produced much more efficient precipitation of the co-polymer. ^{1}H-NMR revealed approximately 10% incorporation of the photoactive azobenzene monomer into the co-polymer utilizing the reaction composition of the earlier work, and gel permeation chromatography (GPC) analysis yielded M_w=26,900 and M_n=13,200. LCST analysis revealed a steep A_{600} curve that began to rise from baseline at approximately 48^{o}C, and UV irradiation caused a successful shift of the A_{600} curve to roughly 55^{o}C in 10 mM Tris, pH 8.0. While this represented a successful construction of a photoresponsive co-polymer, it was not a polymer that conformed to the temperature constraints of the M18-Y52C scFv.

Previous studies in dimethylacrylamide co-polymers reveal that in order to lower the LCST, an increase in the aromatic monomer incorporation is necessary (Miyazaki and Kataoka 1996). Therefore, an attempt to increase incorporation to 15% was initiated. This was accomplished by increasing the amount of monomeric azobenzene-acrylate ester in the polymerization reaction. GPC analysis revealed M_w=20,900 and M_n=12,700, while ^{1}H-NMR yielded a molar incorporation of 18% for azobenzene monomer. This polymer was so hydrophobic that it could not be dissolved in aqueous buffers at room temperature and a concentration of 2 mg/mL for LCST testing at this stage, although more polymer appeared to dissolve into aqueous buffer when the undissolved suspension was placed at 4^{o}C. This might imply that the LCST is lower than room temperature for this preparation of polymer.

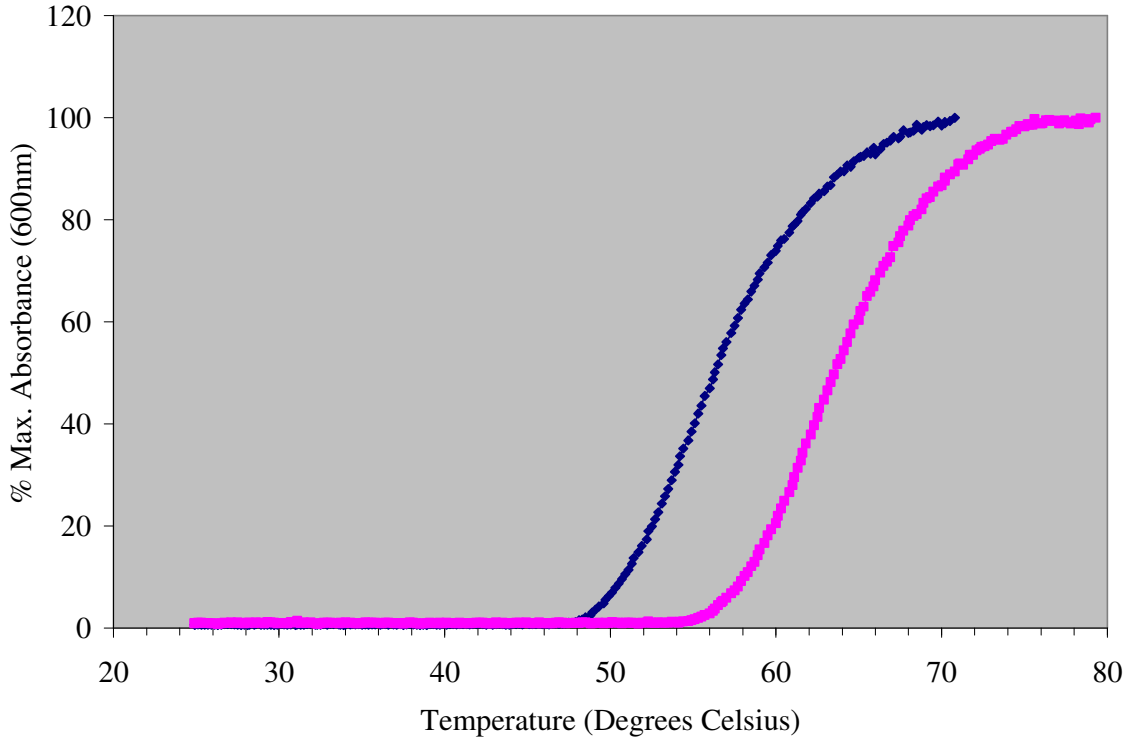

Figure 4.11. LCST curves for co-polymer with 10% azobenzene monomer incorporation. —□—, visible irradiated; —□—, UV irradiated.

4.3.10 Synthesis of Vinyl Sulfone-capped Co-polymer

Polymer that was synthesized in the previous step was purposefully made using the chain transfer agent β-mercaptoethanol so that a hydroxyl group would reside on one of the ends of the polymer chains. Divinyl sulfone was reacted in a Michael addition in high molar excess to place the vinyl sulfone as an end group which will allow the polymer chains to append to a free cysteine on a protein. Potassium *tert*-butoxide was used to quantitatively deprotonate the hydroxyl, which should then react by attacking one

of the alkenes in 1,4 addition fashion. Reactions were carried out overnight at room temperature in DCM or THF, and the choice of solvent did not seem to have an effect over that duration. Precipitation conditions had to be altered from Shimoboji *et al.*, as DCM precipitated into diethyl ether was not optimal. Yield from each reaction was 80-90% for both 10% and 15% azobenzene monomer-incorporated polymers, and sulfone bands were observed using FT-IR, which were not present before the addition. However, GPC analysis of each polymer revealed molecular weights significantly lower than those of the original co-polymers. M_w=8,600 and M_n=5,200 were observed for the vinyl sulfone-co-polymer with 10% incorporation (VS-10), and Mw=11,600 and Mn=5,900 were obtained for the 18% azobenzene incorporation co-polymer (VS-18). LCST curves revealed the initial aggregation for visible light-irradiated polymer of both VS-10 and VS-18 were at approximately 58°C. UV irradiation of the VS-10 polymer gave a characteristic upward shift of aggregation initiation to approximately 63°C, while similar treatment of the VS-18 polymer actually decreased the initial aggregation temperature to approximately 55°C. This later result was unexpected.

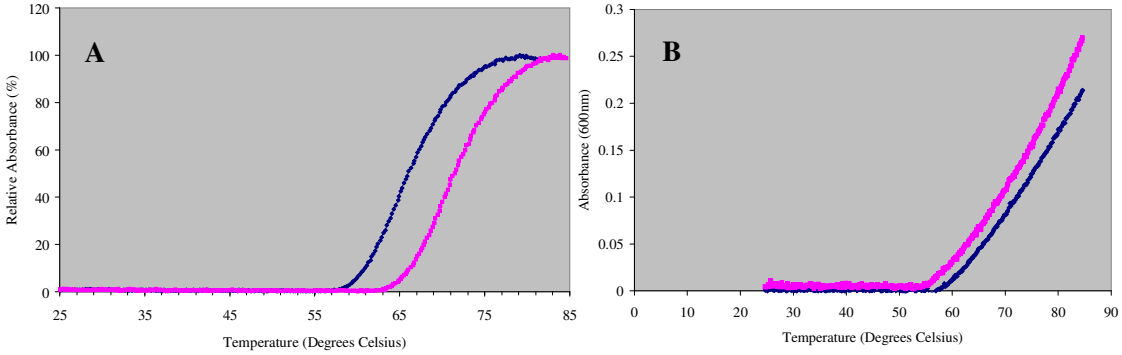

FIGURE 4.12. LCST CURVES FOR VINYL SULFONE-CAPPED CO-POLYMERS. (A) VS-10: ⊟, visible irradiated; ⊟, UV irradiated. (B) VS-18: ⊟, visible irradiated; ⊟, UV irradiated.

While it is possible that capping with vinyl sulfone caused the apparent molecular weights to shift downward by GPC, this was such a significant shift that it is not likely to be the case. Other possibilities are that there is actually cleavage of the polymer backbone during the reaction, or that the precipitation conditions are selectively precipitating only the lower molecular weight polymer chains.

4.4 CONCLUSIONS

The purpose of this work is to move toward the creation of a generalizable engineering solution to the challenge of producing a photoresponsive antibody. In this study, two different attempts at photoresponsive elements were utilized. First was the use of a photoisomerizable small molecule at the binding interface, and the second was the synthesis of a photoreactive polymer that would cover the binding interface. The former system yielded equivocal results, and it is probable that requiring a small molecule to alter the binding interface in a significant way so as to perturb the interaction was energetically beyond the reach of the system. The latter system appears to show some promise as the photoreactive polymer could be reproduced and yielded differential LCST curves for visible- and UV-irradiated samples. However, several hurdles need to be cleared in order to bring this system to fruition. First, a polymer must be synthesized that meets the temperature needs of the M18-Y52C scFv, which is an assay temperature of less than 40^{o}C and preferably very close to room temperature. It must also have differential response to UV and visible irradiation. This will most likely require an empirical approach utilizing the previous conditions as guidelines for synthesis of the next round of co-polymers. Second, conditions for precipitation of the polymer after appending the vinyl sulfone moiety must be optimized such that the distribution of molecular weights of the polymer is not skewed significantly in the process. If this is not

the reason for decrease in molecular weight, then additional insight is needed to resolve the basis for this decline. Despite the intrinsic difficulties of working through these obstacles, the use of photoresponsive polymers appears to hold great promise for the application to modulation of antibody binding based upon its successes in other systems.

4.5 REFERENCES

de Lorimier, R.M., Smith, J.J., Dwyer, M.A., Looger, L.L., Sali, K.M., Paavola, C.D., Rizk, S.S., Sadigov, S., Conrad, D.W., Loew, L.*, et al.* 2002. Construction of a fluorescent biosensor family. *Protein Sci* **11:** 2655-2675.

Harvey, B.R., Georgiou, G., Hayhurst, A., Jeong, K.J., Iverson, B.L., and Rogers, G.K. 2004. Anchored periplasmic expression, a versatile technology for the isolation of high-affinity antibodies from Escherichia coli-expressed libraries. *Proc Natl Acad Sci U S A* **101:** 9193-9198.

Jeong, K.J., and Lee, S.Y. 1999. High-level production of human leptin by fed-batch cultivation of recombinant Escherichia coli and its purification. *Appl Environ Microbiol* **65:** 3027-3032.

Jeong, K.J., Seo, M.J., Iverson, B.L., and Georgiou, G. 2007. APEx 2-hybrid, a quantitative protein-protein interaction assay for antibody discovery and engineering. *Proc Natl Acad Sci U S A* **104:** 8247-8252.

Lee, J.E., Fusco, M.L., Hessell, A.J., Oswald, W.B., Burton, D.R., and Saphire, E.O. 2008. Structure of the Ebola virus glycoprotein bound to an antibody from a human survivor. *Nature* **454:** 177-182.

Miyazaki, H., and Kataoka, K. 1996. Preparation of polyacrylamide derivatives showing thermo-reversible coacervate formation and their potential application to two-phase separation processes. *Polymer* **37:** 681-685.

Owenius, R., Osterlund, M., Lindgren, M., Svensson, M., Olsen, O.H., Persson, E., Freskgard, P.O., and Carlsson, U. 1999. Properties of spin and fluorescent labels at a receptor-ligand interface. *Biophys J* **77:** 2237-2250.

Pavlou, A.K., and Belsey, M.J. 2005. The therapeutic antibodies market to 2008. *Eur J Pharm Biopharm* **59:** 389-396.

Renard, M., Belkadi, L., and Bedouelle, H. 2003. Deriving topological constraints from functional data for the design of reagentless fluorescent immunosensors. *J Mol Biol* **326:** 167-175.

Sakata, T., Yan, Y., and Marriott, G. 2005a. Family of site-selective molecular optical switches. *J Org Chem* **70:** 2009-2013.

Sakata, T., Yan, Y., and Marriott, G. 2005b. Optical switching of dipolar interactions on proteins. *Proc Natl Acad Sci U S A* **102:** 4759-4764.

Self, C.H., and Thompson, S. 1996. Light activatable antibodies: models for remotely activatable proteins. *Nat Med* **2:** 817-820.

Shimoboji, T., Ding, Z., Stayton, P.S., and Hoffman, A.S. 2001. Mechanistic investigation of smart polymer-protein conjugates. *Bioconjug Chem* **12:** 314-319.

Shimoboji, T., Ding, Z.L., Stayton, P.S., and Hoffman, A.S. 2002a. Photoswitching of ligand association with a photoresponsive polymer-protein conjugate. *Bioconjug Chem* **13:** 915-919.

Shimoboji, T., Larenas, E., Fowler, T., Hoffman, A.S., and Stayton, P.S. 2003. Temperature-induced switching of enzyme activity with smart polymer-enzyme conjugates. *Bioconjug Chem* **14:** 517-525.

Shimoboji, T., Larenas, E., Fowler, T., Kulkarni, S., Hoffman, A.S., and Stayton, P.S. 2002b. Photoresponsive polymer-enzyme switches. *Proc Natl Acad Sci U S A* **99:** 16592-16596.

Thomas, K.J., Sherman, D.B., Amiss, T.J., Andaluz, S.A., and Pitner, J.B. 2006. A long-wavelength fluorescent glucose biosensor based on bioconjugates of galactose/glucose binding protein and Nile Red derivatives. *Diabetes Technol Ther* **8:** 261-268.

Thompson, S., Dessi, J., and Self, C.H. 2008. The construction and in vitro testing of photo-activatable cancer targeting folated anti-CD3 conjugates. *Biochem Biophys Res Commun* **366:** 526-531.

Yu, X., Tsibane, T., McGraw, P.A., House, F.S., Keefer, C.J., Hicar, M.D., Tumpey, T.M., Pappas, C., Perrone, L.A., Martinez, O.*, et al.* 2008. Neutralizing antibodies derived from the B cells of 1918 influenza pandemic survivors. *Nature* **Advance online publication**.

CHAPTER 5

Structure and Function of an RNA Thermosensor in *Yersinia pestis*

5.1 BACKGROUND

Yersinia pestis is a gram negative pathogenic bacterium that is the causative agent of plague. It is estimated to have killed approximately 200 million people over recorded history, and in the mid 14th century it wiped out approximately 40% of the European populace (Duplaix 1988). Outbreaks as recently as 1994 reveal that *Y. pestis* is still a health threat, and its ability to cause fear and panic make it an ideal agent for bioterrorism attacks (Perry and Fetherston 1997).

Y. pestis persists through cyclic infection of rodents and their fleas. Over 31 species of fleas have been proven to be vectors, while it is thought that any of the other 1,500 species could carry the bacterium under the proper conditions (Perry and Fetherston 1997). It is also known that over 200 mammalian species can become infected by the bacterium (Perry and Fetherston 1997). Mammalian blood can contain high concentrations of bacteria during infection, which are passed to fleas when they feed on their mammalian hosts. The bacteria then create an obstruction in the proventriculus of the flea, which prevents the flea from feeding. However, these fleas then try to feed continually, and transmit *Y. pestis* to another mammalian host while doing so (Bacot 1914). Rodents are the primary mammals utilized in the transmission cycle of *Y. pestis*, while humans usually represent an unproductive infection for the bacterium.

Mammalian virulence of *Y. pestis*, and related pathogenic species *Y. enterocolitica* and *Y. pseudotuberculosis*, are very complex. Approximately 50 genes are

involved. These genes are located on a roughly 70 kb plasmid, named pCD1 in *Y. pestis* (Hu *et al.* 1998; Perry *et al.* 1998). Virulence effectors, secretion machinery, translocation machinery, chaperones, and virulence regulators are all encoded within this virulence plasmid (Konkel and Tilly 2000). In general, effector proteins are named as Yops ("*Yersinia* outer protein"), secretion machinery are labeled as Yscs ("Yop secretion"), and chaperones are regarded as Sycs ("Specific Yop chaperone").

Approximately half of the virulence genes are under the control of LcrF, a member of the AraC transcription activator family (Cornelis *et al.* 1998). The members of this family comprise two groups, catabolic regulators and virulence regulators. LcrF is a 31 kDa protein that exhibits a remarkable 98% similarity to VirF of *Y. enterocolitica* (Hoe *et al.* 1992). These proteins have a putative helix-turn-helix motif, which is implicated in DNA binding (Caron *et al.* 1989). Expression of both of these proteins is also regulated by temperature. At low temperatures around 26^{o}C, expression is very low, while protein levels are markedly higher at 37^{o}C. This temperature switch is thought to be the main regulatory mechanism by which the bacterium is alerted that it is in its mammalian host.

Two different models have been put forth for the temperature regulation of LcrF and VirF. First, VirF transcription in *Y. enterocolitica* is thought to be controlled by bent DNA (Rohde *et al.* 1999). At low temperatures, the intrinsic bend prevents transcription, while shifting the temperature up to 37^{o}C relieves the bent structure, allowing transcription to occur. The second model, from *Y. pestis*, speculates that RNA secondary structure within the 5' UTR of the lcrF mRNA sequesters the Shine-Dalgarno (SD) sequence at low temperatures, preventing translation. At 37^{o}C, the secondary structure unfolds and allows translation to take place (Hoe and Goguen 1993).

The first model has been experimentally tested in *Y. enterocolitica*, and it appears to have merit. Other systems that seem to exhibit this type of control appear in *Shigella* and *E. coli* (Tanaka *et al.* 1991; Prosseda *et al.* 2004). Previously, temperature regulation of LcrF by an RNA thermosensor was proposed as a theoretical model in 1993, and it has remained untested for more than 10 years. Other organisms that have been found to use this type of control are *E. coli*, *Listeria monocytogenes*, and *Bradyrhizobium japonicum* (Morita *et al.* 1999a; Morita *et al.* 1999b; Nocker *et al.* 2001; Johansson *et al.* 2002).

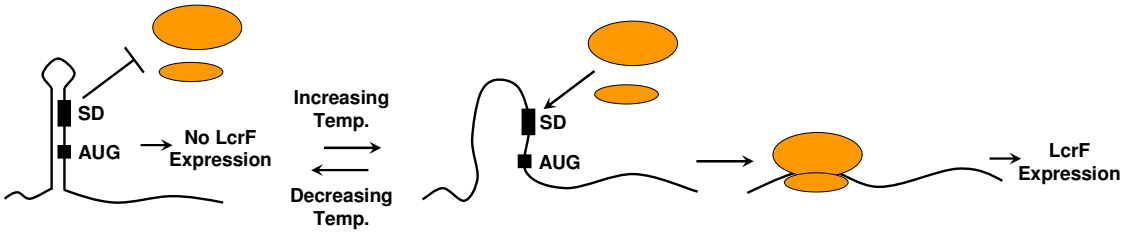

FIGURE 5.1. POST-TRANSCRIPTIONAL PROTEIN REGULATION OF LCRF. RNA thermosensor model of Yersinia pestis LcrF post-transcriptional regulation. At low temperatures, the RNA hairpin prevents the ribosome from binding the Shine-Dalgarno (SD) sequence. At higher temperatures, the hairpin unfolds and allows access to the ribosome. Adapted from Johansson *et al.*, 2003.

Although the LcrF RNA thermosensor has never been analyzed for these properties, it is widely proposed that LcrF protein expression is modulated by this post-transcriptional phenomenon, even being included as a foundational member of a class of RNA thermometers (Waldminghaus *et al.* 2007). There is also speculation that both mechanisms could function together to regulate LcrF/VirF at both the transcriptional and translational level (Cornelis *et al.* 1998). Although there is evidence that post-transcriptional regulation is occurring, a rigorous test of the validity of an LcrF RNA thermosensor model should be carried out before it becomes so firmly rooted in dogma.

5.2 MATERIALS AND METHODS

5.2.1 Construction of Plasmids

The 5' UTR of LcrF (NCBI Nucleotide accession number M86690, Hoe *et al.* 1992) was constructed using PCR with overlapping primers (Sandhu *et al.* 1992), and placed on the *N*- terminus of GFPm2 (Tabor *et al.* 2008) with 24 nucleotides from pGFPUV (ATGACCATGATTACGCCAAGCTTT, Clonetech) in between. This construct was introduced into the arabinose-inducible, ampicillin resistant pBAD18 vector (Guzman *et al.* 1995) between the KpnI and SphI restriction sites of the Multiple Cloning Site (MCS) to create pBAD18-LcrF-GFP. Mutants 1, 2, 3, 5, 6, 7, and G178C were constructed using the QuikChange® procedure (Stratagene). pBAD33-CFP was created by inserting the eCFP gene with a strong ribosomal binding site from the MIT registry of standard biological parts (http://parts.mit.edu, part number BBa_I15012) at the KpnI site and sequencing to confirm proper orientation.

5.2.2 In-line Probing

RNA structure assays utilizing in-line probing were performed on the wild-type LcrF 5' UTR. PCR was utilized to create the template for run-off transcription by amplifying with primers truncating the 5' UTR for optimal resolution based upon optimization of the assay. The forward primer introduced a T7 promoter (lcrF.gfpm2b.inline.F, TTCTAATACGACTCACTATAGGGCATAATAACTCAATACA) and the reverse primer truncated the transcript at the first codon of GFPm2 (lcrF.gfpm2b.inline.R,

CATAAAGCTTGGCGTAATCAT). PCR products were transcribed using a T7 RNA transcription kit (Epicentre). The resulting RNA was purified by denaturing polyacrylamide gel electrophoresis (PAGE), dephosphorylated, radiolabeled using T4 polynucleotide kinase (NEB), and subjected to a second round of denaturing PAGE. In-line probing was performed at 25°C for 48 hours and at 37°C for 24 hours, resolved by denaturing PAGE, and imaged using a phosphorimager.

5.2.3 Fluorescence Assays

Jude-1 cells (Kawarasaki *et al.* 2003) were electroporated with one of the pBAD18-LcrF-GFP variants in combination with pBAD33-CFP and plated on selective media (100 μg/mL ampicillin and 30 mg/μL chloramphenicol). Colonies were picked, grown in liquid culture overnight at 37°C, and frozen at -80°C in LB with 15% glycerol. Frozen stocks were used to inoculate 3 mL cultures of LB selective media and were grown overnight at 37°C. These cultures were placed on ice for 15 minutes and used to inoculate inducing media (LB with 0.2% arabinose, 100 μg/mL ampicillin, and 30 mg/μL chloramphenicol) or non-inducing media (LB with 100 μg/mL ampicillin and 30 mg/μL chloramphenicol) at an OD of 0.05. Samples were grown in triplicate in a 96 well plate and monitored in real-time for OD at 600 nm, GFP fluorescence, and CFP fluorescence using a Synergy-HT plate reader (Bio-Tek) at specified temperatures. Fluorescence results from the onset of stationary phase were utilized for analysis.

5.2.4 Real-Time PCR Assays

Samples were subjected to similar treatment for fluorescence assays at 25°C and 37°C and then placed at -80°C to prevent RNA degradation until processing. RNA was

isolated using an RNeasy mini kit (Qiagen) in conjunction with DNase digestion to eliminate DNA contamination of samples. Reverse transcription of the samples to produce cDNA was carried out using SuperScript II reverse transcriptase (Invitrogen) with a mixture of the reverse primers of the real-time PCR sets for each gene. Real-time PCR assays were performed in triplicate for each sample using an Applied Biosystems 7900HT real-time PCR machine for GFP, CFP, and 16S rRNA. 2x qPCR master mix (Applied Biosystems) and 1 ng of cDNA template was used for each reaction, and primers and probes for each gene are listed. GFP forward primer- GATGGCCCTGTCCTTTTACCA, GFP reverse primer- TTTTCGTTGGGATCTTTCGAA, and GFP Taqman probe- 6FAM/ACAACCATTACCTGTCCACACAATCTGCC/BHQ1; CFP forward primer- CATCGACTTCAAGGAGGAC, CFP reverse primer- CTTGATGCCGTTCTTCTG, and CFP Taqman probe- 6FAM/GTACAACTACATCAGCCACAACGTCTATAT/BHQ1; 16S rRNA forward primer- CGTGTTGTGAAATGTTGGGTTAA, 16S rRNA reverse primer- ACCGCTGGCAACAAAAGATAA, and 16S rRNA Taqman probe- 6FAM/ TCCCGCAACGAGCGCAACC/BHQ1, where BHQ1 is Black Hole Quencher 1 (Integrated DNA Technologies). The ratio of Cycle Threshold values (C(T)s) at 25°C and 37°C of the 16S rRNA were used as a multiplier to normalize GFP and CFP C(T)s. Average C(T) values reported for each sample were calculated from 3 independent cultures grown in parallel.

5.3 RESULTS AND DISCUSSION

5.3.1 In-line Probing

Hoe and Goguen uncovered indirect evidence of posttranscriptional regulation of LcrF in 1993. Our initial direction was to show structural proof of a hairpin that occluded the Shine-Dalgarno region of the LcrF 5' UTR that was predicted from our mfold calculations. We chose to use in-line probing as our method of detection.

RNA bases that are in unstructured regions (i.e., single stranded RNA) will be susceptible to a spontaneous 2'-3' cyclic phosphate transesterification of the RNA backbone, which is the normal method of RNA degradation (Fig. 5.2). This cleavage reaction can occur when the 2' hydroxyl of the ribose lies in the same plane as the adjacent P-O 5' bond. RNA bases lying in an A-form helix are prohibited from adopting the "in-line" conformation and are resistant to this cleavage. Hence, unpaired bases are represented by bands present in denaturing PAGE, and absence of banding represents double stranded RNA.

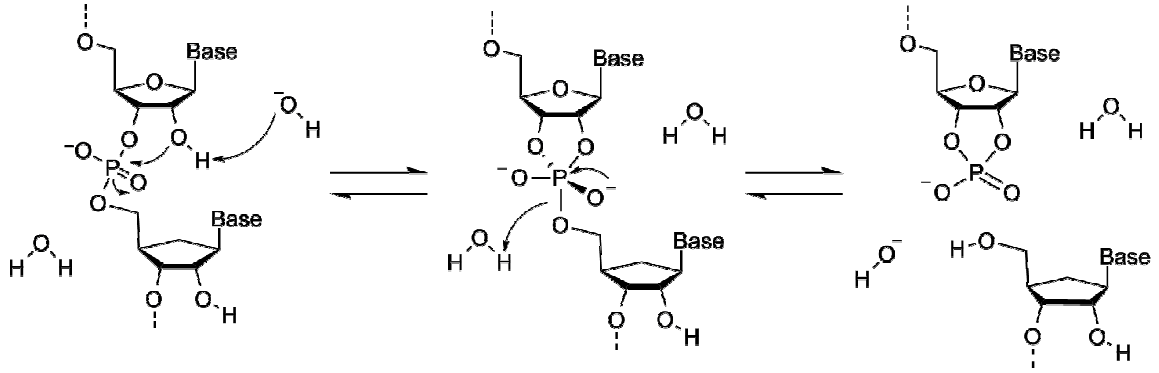

FIGURE 5.2. MECHANISM OF IN-LINE PROBING. The 2' hydroxyl group attacks the 3' phosphate group when the 5' P-O bond of the next base is in the same plane as the 2' hydroxyl, with the downstream base acting as the leaving group. This is how spontaneous degradation of RNA occurs. Adapted from Soukup and Breaker, 2003.

In-line probing was carried out on ^{32}P-end labeled RNA as described previously (Soukup and Breaker 1999; Winkler *et al.* 2002; Sudarsan *et al.* 2003). Alkaline hydrolysis (every base) and RNase T1 (G-specific) cleavage ladders were prepared using protocols from Soukup and Breaker (Soukup and Breaker 1999). Predicted and actual data are shown below, and they coincide very well (Figure 5.3). Increased banding of the 37°C sample was not observed as was hypothesized, although this is not inconsistent with previous studies as structural analysis has been reported at the lower temperature only.

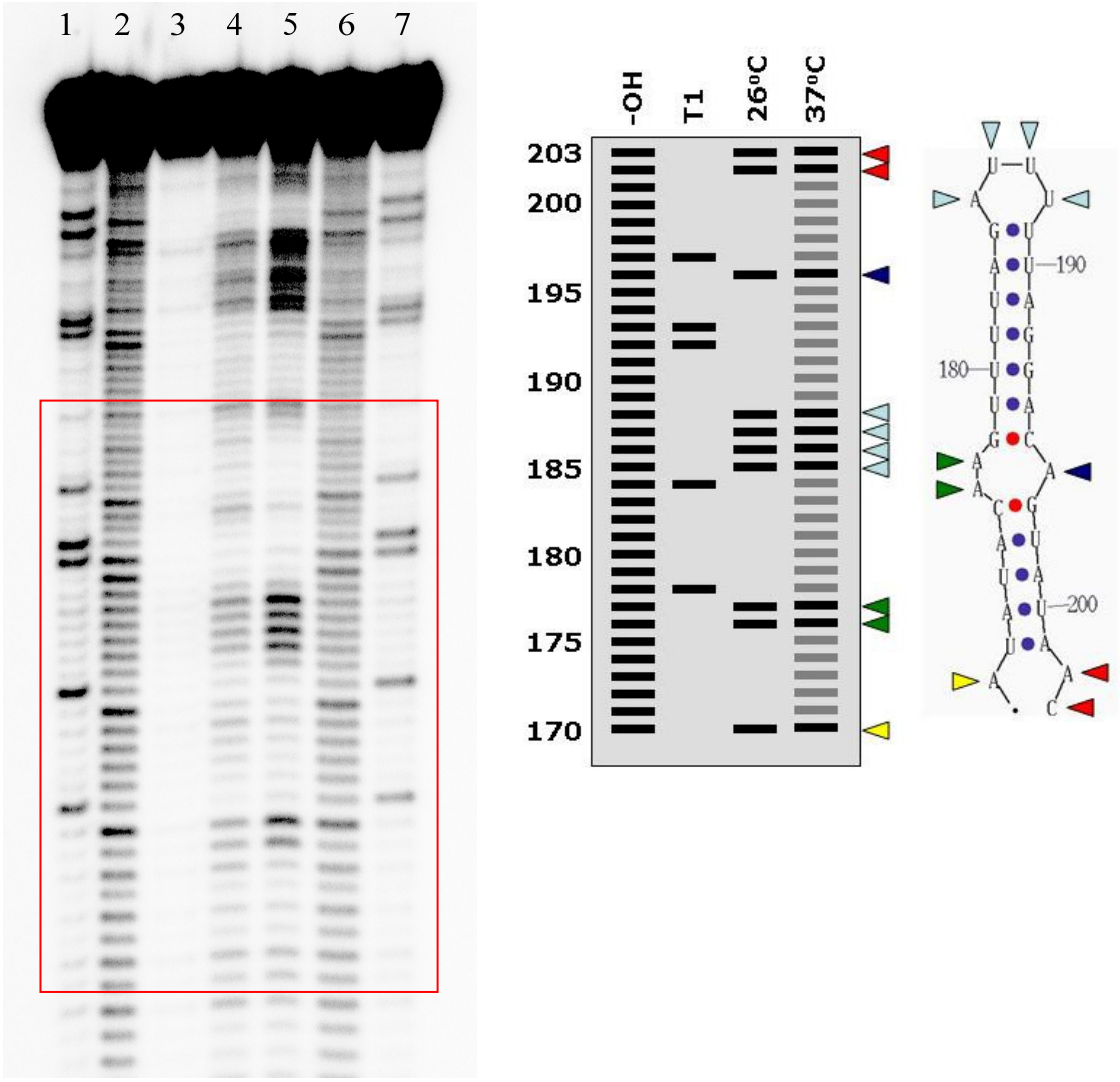

FIGURE 5.3. IN-LINE PROBING OF THE LCRF 5'UTR. Actual results are to the left, boxed in red for emphasis. Predicted results are to the right, with a stem-loop structure illustrated to aid interpretation. Lanes 1 and 7-RNase T1 digested; Lanes 2 and 6-alkaline hydrolysis; Lane 3-no digestion; Lane 4-25°C; Lane 5-37°C.

5.3.2 Fluorescence Assays

In order to determine whether the lcrF 5' UTR behaved as a thermosensor, it was necessary to make mutations to the stem-loop structure that would have predictable outcomes if the structure was in fact sensing temperature and folding accordingly. We made 7 mutant forms of the thermosensor which would have a destabilizing, stabilizing, or no effect on the stem loop structure (Figure 5.4). Destabilizing mutants should exhibit higher protein expression at lower temperatures, while stabilizing mutants should have low protein expression at both low and high temperatures.

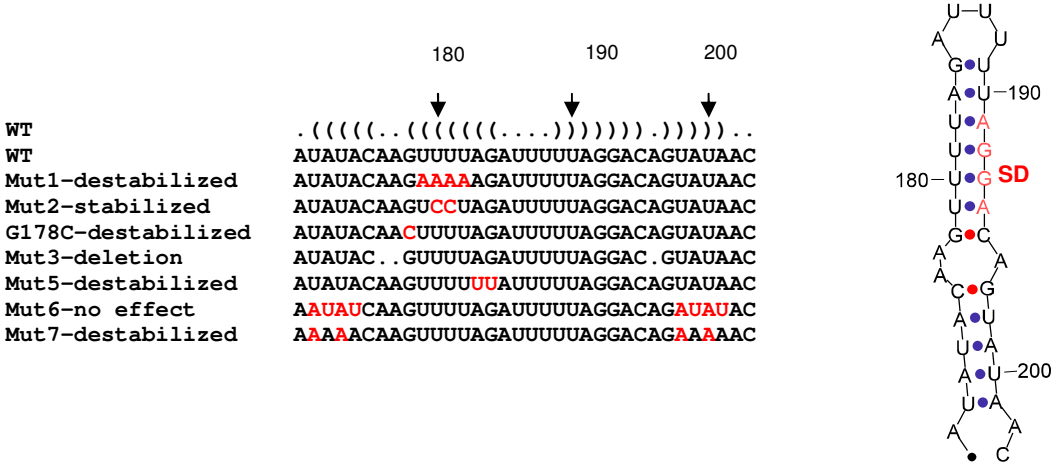

Figure 5.4. LcrF 5' UTR Mutants.

A reporter system was constructed for our purpose. The lcrF 5' UTR and the 7 mutants were placed upstream of GFP mutant 2b in pBAD18, while eCFP was cloned into pBAD33. These two plasmids were co-transformed into Jude-1 cells, and double selection was performed. After stable lines were confirmed by sequencing, all lines were subcultured at an OD 600 of 0.05 and grown at the specified temperature while OD 600, GFP, and CFP fluorescence were monitored. Data shown below are the ratios of

GFP/CFP for Induced/Non-induced cells. Cells were plated out in triplicate, and the statistics from those replicates are shown in the error bars below (Figure 5.5).

Consistent with our hypothesis, variants possessing stabilizing mutations did not exhibit GFP/CFP fluorescence ratio changes across the temperatures assayed. One destabilizing mutation, G178C, exhibited increased protein expression across all temperatures relative to the wild-type 5' UTR. All other destabilizing mutations exhibited similar fluorescence as wild-type at higher temperatures, while fluorescence at lower temperatures appeared to be higher than those observed for the wild-type 5' UTR.

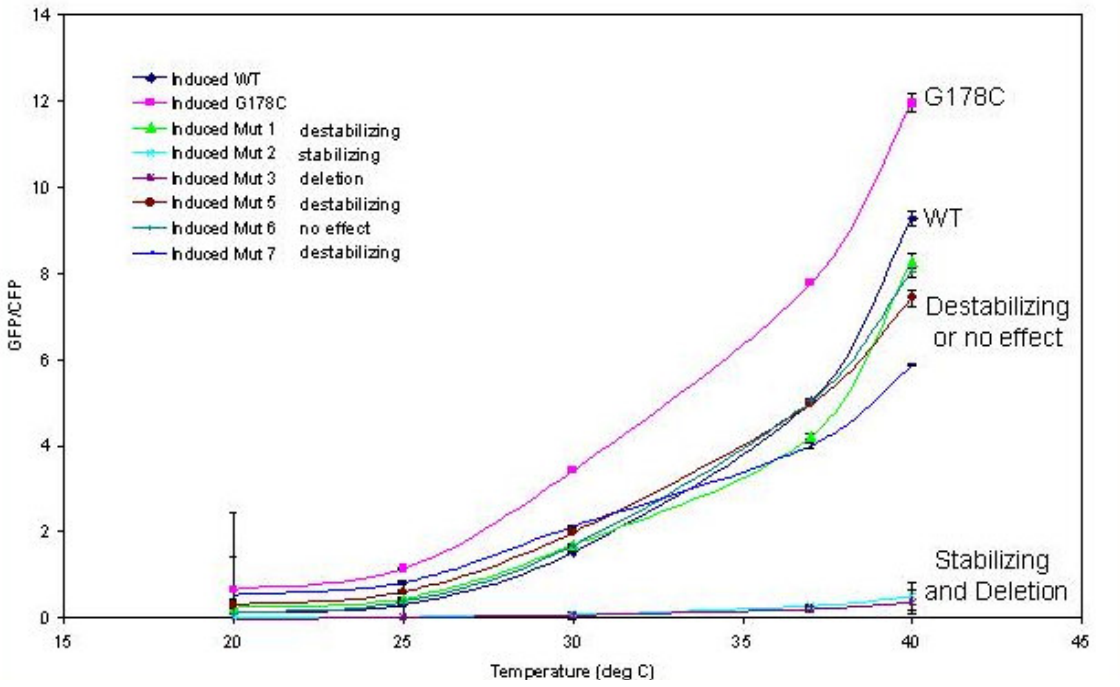

Figure 5.5. GFP/CFP ratios for LcrF 5' UTR mutants at specified temperatures.

5.3.3 Real-Time PCR Assays

RNA levels were examined using RNeasy (Qiagen) to isolate RNA, reverse transcription, and real-time PCR for GFP, CFP, and 16S rRNA. 16S rRNA C(T) ratios for 25°C and 37°C were used to normalize GFP and CFP measurements. Results are shown below in Table 5.1.

		C(T) Values	
		25°C	37°C
WT	CFP	19.79 ± 0.15	19.92 ± 0.27
	GFP	20.47 ± 0.05	20.13 ± 0.50
Mut 2	CFP	19.88 ± 0.71	20.54 ± 0.76
	GFP	21.54 ± 0.50	22.09 ± 0.73
G178C	CFP	20.26 ± 0.23	21.05 ± 0.34
	GFP	20.60 ± 0.19	20.58 ± 0.29

Table 5.1. Real-Time PCR analysis of RNA levels for LcrF variants.

For each variant of the LcrF 5' UTR, C(T) values at 25°C and 37°C differed by less than one cycle, implying that RNA levels differ by less than 2-fold across temperatures. In light of the invariance of RNA levels, the large change in protein fluorescence levels from 25°C to 37°C implies post-transcriptional regulation by the LcrF 5' UTR.

5.4 CONCLUSIONS

Structural analysis reveals a stem-loop structure that was expected around the Shine-Dalgarno sequence, and protein fluorescence assays show that mutations to the stem-loop structure yield the expected results. In addition, it appears that the internal

bubble directly following the Shine-Dalgarno sequence is extremely important for the function of the thermosensor, as deletion of the bubble or mutation to eliminate the bubble very effectively quench protein expression at higher temperatures. In conjunction with the lack of change of the RNA levels at 25°C and 37°C, these results imply that the 5' UTR of LcrF acts as an RNA thermosensor to post-transcriptionally regulate protein levels with varying temperatures.

5.5 REFERENCES

Bacot, A.W., Martin, C.J. 1914. Observations on the mechanism of the transmission of plague by fleas. *J. Hyg. Plague Suppl.* **4:** 423-439.

Caron, J., Coffield, L.M., and Scott, J.R. 1989. A plasmid-encoded regulatory gene, rns, required for expression of the CS1 and CS2 adhesins of enterotoxigenic Escherichia coli. *Proc Natl Acad Sci U S A* **86:** 963-967.

Cornelis, G.R., Boland, A., Boyd, A.P., Geuijen, C., Iriarte, M., Neyt, C., Sory, M.P., and Stainier, I. 1998. The virulence plasmid of Yersinia, an antihost genome. *Microbiol Mol Biol Rev* **62:** 1315-1352.

Duplaix, N. 1988. Fleas--the lethal leapers. *Natl. Geogr.* **173:** 672-694.

Guzman, L.M., Belin, D., Carson, M.J., and Beckwith, J. 1995. Tight regulation, modulation, and high-level expression by vectors containing the arabinose PBAD promoter. *J Bacteriol* **177:** 4121-4130.

Hoe, N.P., and Goguen, J.D. 1993. Temperature sensing in Yersinia pestis: translation of the LcrF activator protein is thermally regulated. *J Bacteriol* **175:** 7901-7909.

Hoe, N.P., Minion, F.C., and Goguen, J.D. 1992. Temperature sensing in Yersinia pestis: regulation of yopE transcription by lcrF. *J Bacteriol* **174:** 4275-4286.

Hu, P., Elliott, J., McCready, P., Skowronski, E., Garnes, J., Kobayashi, A., Brubaker, R.R., and Garcia, E. 1998. Structural organization of virulence-associated plasmids of Yersinia pestis. *J Bacteriol* **180:** 5192-5202.

Johansson, J., Mandin, P., Renzoni, A., Chiaruttini, C., Springer, M., and Cossart, P. 2002. An RNA thermosensor controls expression of virulence genes in Listeria monocytogenes. *Cell* **110:** 551-561.

Kawarasaki, Y., Griswold, K.E., Stevenson, J.D., Selzer, T., Benkovic, S.J., Iverson, B.L., and Georgiou, G. 2003. Enhanced crossover SCRATCHY: construction and high-throughput screening of a combinatorial library containing multiple non-homologous crossovers. *Nucleic Acids Res* **31:** e126.

Konkel, M.E., and Tilly, K. 2000. Temperature-regulated expression of bacterial virulence genes. *Microbes Infect* **2:** 157-166.

Morita, M., Kanemori, M., Yanagi, H., and Yura, T. 1999a. Heat-induced synthesis of sigma32 in Escherichia coli: structural and functional dissection of rpoH mRNA secondary structure. *J Bacteriol* **181:** 401-410.

Morita, M.T., Tanaka, Y., Kodama, T.S., Kyogoku, Y., Yanagi, H., and Yura, T. 1999b. Translational induction of heat shock transcription factor sigma32: evidence for a built-in RNA thermosensor. *Genes Dev* **13:** 655-665.

Nocker, A., Hausherr, T., Balsiger, S., Krstulovic, N.P., Hennecke, H., and Narberhaus, F. 2001. A mRNA-based thermosensor controls expression of rhizobial heat shock genes. *Nucleic Acids Res* **29:** 4800-4807.

Perry, R.D., and Fetherston, J.D. 1997. Yersinia pestis--etiologic agent of plague. *Clin Microbiol Rev* **10:** 35-66.

Perry, R.D., Straley, S.C., Fetherston, J.D., Rose, D.J., Gregor, J., and Blattner, F.R. 1998. DNA sequencing and analysis of the low-Ca2+-response plasmid pCD1 of Yersinia pestis KIM5. *Infect Immun* **66:** 4611-4623.

Prosseda, G., Falconi, M., Giangrossi, M., Gualerzi, C.O., Micheli, G., and Colonna, B. 2004. The virF promoter in Shigella: more than just a curved DNA stretch. *Mol Microbiol* **51:** 523-537.

Rohde, J.R., Luan, X.S., Rohde, H., Fox, J.M., and Minnich, S.A. 1999. The Yersinia enterocolitica pYV virulence plasmid contains multiple intrinsic DNA bends which melt at 37 degrees C. *J Bacteriol* **181:** 4198-4204.

Sandhu, G.S., Aleff, R.A., and Kline, B.C. 1992. Dual asymmetric PCR: one-step construction of synthetic genes. *Biotechniques* **12:** 14-16.

Soukup, G.A., and Breaker, R.R. 1999. Relationship between internucleotide linkage geometry and the stability of RNA. *Rna* **5:** 1308-1325.

Sudarsan, N., Wickiser, J.K., Nakamura, S., Ebert, M.S., and Breaker, R.R. 2003. An mRNA structure in bacteria that controls gene expression by binding lysine. *Genes Dev* **17:** 2688-2697.

Tabor, J.J., Bayer, T.S., Simpson, Z.B., Levy, M., and Ellington, A.D. 2008. Engineering stochasticity in gene expression. *Mol Biosyst* **4:** 754-761.

Tanaka, K., Muramatsu, S., Yamada, H., and Mizuno, T. 1991. Systematic characterization of curved DNA segments randomly cloned from Escherichia coli and their functional significance. *Mol Gen Genet* **226:** 367-376.

Waldminghaus, T., Heidrich, N., Brantl, S., and Narberhaus, F. 2007. FourU: a novel type of RNA thermometer in Salmonella. *Mol Microbiol* **65:** 413-424.

Winkler, W.C., Cohen-Chalamish, S., and Breaker, R.R. 2002. An mRNA structure that controls gene expression by binding FMN. *Proc Natl Acad Sci U S A* **99:** 15908-15913.

Bibliography

Albrecht, M.T., Li, H., Williamson, E.D., LeButt, C.S., Flick-Smith, H.C., Quinn, C.P., Westra, H., Galloway, D., Mateczun, A., Goldman, S.*, et al.* 2007. Human monoclonal antibodies against anthrax lethal factor and protective antigen act independently to protect against Bacillus anthracis infection and enhance endogenous immunity to anthrax. *Infect Immun* **75:** 5425-5433.

Amit, A.G., Mariuzza, R.A., Phillips, S.E., and Poljak, R.J. 1986. Three-dimensional structure of an antigen-antibody complex at 2.8 A resolution. *Science* **233:** 747-753.

Arkin, A.P., and Youvan, D.C. 1992. Optimizing nucleotide mixtures to encode specific subsets of amino acids for semi-random mutagenesis. *Biotechnology (N Y)* **10:** 297-300.

Bacot, A.W., Martin, C.J. 1914. Observations on the mechanism of the transmission of plague by fleas. *J. Hyg. Plague Suppl.* **4:** 423-439.

Barbas, C.F., 3rd, Kang, A.S., Lerner, R.A., and Benkovic, S.J. 1991. Assembly of combinatorial antibody libraries on phage surfaces: the gene III site. *Proc Natl Acad Sci U S A* **88:** 7978-7982.

Barderas, R., Desmet, J., Timmerman, P., Meloen, R., and Casal, J.I. 2008. Affinity maturation of antibodies assisted by in silico modeling. *Proc Natl Acad Sci U S A* **105:** 9029-9034.

Boder, E.T., Midelfort, K.S., and Wittrup, K.D. 2000. Directed evolution of antibody fragments with monovalent femtomolar antigen-binding affinity. *Proc Natl Acad Sci U S A* **97:** 10701-10705.

Bossart-Whitaker, P., Chang, C.Y., Novotny, J., Benjamin, D.C., and Sheriff, S. 1995. The crystal structure of the antibody N10-staphylococcal nuclease complex at 2.9 A resolution. *J Mol Biol* **253:** 559-575.

Braden, B.C., Fields, B.A., and Poljak, R.J. 1995. Conservation of water molecules in an antibody-antigen interaction. *J Mol Recognit* **8:** 317-325.

Braden, B.C., Souchon, H., Eisele, J.L., Bentley, G.A., Bhat, T.N., Navaza, J., and Poljak, R.J. 1994. Three-dimensional structures of the free and the antigen-complexed Fab from monoclonal anti-lysozyme antibody D44.1. *J Mol Biol* **243:** 767-781.

Bradley, K.A., Mogridge, J., Mourez, M., Collier, R.J., and Young, J.A. 2001. Identification of the cellular receptor for anthrax toxin. *Nature* **414:** 225-229.

Breithaupt, C., Schubart, A., Zander, H., Skerra, A., Huber, R., Linington, C., and Jacob, U. 2003. Structural insights into the antigenicity of myelin oligodendrocyte glycoprotein. *Proc Natl Acad Sci U S A* **100:** 9446-9451.

Brossier, F., Levy, M., Landier, A., Lafaye, P., and Mock, M. 2004. Functional analysis of Bacillus anthracis protective antigen by using neutralizing monoclonal antibodies. *Infect Immun* **72:** 6313-6317.

Brunger, A.T. 1993. Assessment of phase accuracy by cross validation: the free R value. Methods and applications. *Acta Crystallogr D Biol Crystallogr* **49:** 24-36.

Brunger, A.T., Adams, P.D., Clore, G.M., DeLano, W.L., Gros, P., Grosse-Kunstleve, R.W., Jiang, J.S., Kuszewski, J., Nilges, M., Pannu, N.S., *et al.* 1998. Crystallography & NMR system: A new software suite for macromolecular structure determination. *Acta Crystallogr D Biol Crystallogr* **54 (Pt 5):** 905-921.

Cadwell, R.C., and Joyce, G.F. 1992. Randomization of genes by PCR mutagenesis. *PCR Methods Appl* **2:** 28-33.

Cadwell, R.C., and Joyce, G.F. 1994. Mutagenic PCR. *PCR Methods Appl* **3:** S136-140.

Cardinale, A., and Biocca, S. 2008. Combating protein misfolding and aggregation by intracellular antibodies. *Curr Mol Med* **8:** 2-11.

Caron, J., Coffield, L.M., and Scott, J.R. 1989. A plasmid-encoded regulatory gene, rns, required for expression of the CS1 and CS2 adhesins of enterotoxigenic Escherichia coli. *Proc Natl Acad Sci U S A* **86:** 963-967.

Carter, C.W., Jr., and Carter, C.W. 1979. Protein crystallization using incomplete factorial experiments. *J Biol Chem* **254:** 12219-12223.

Chen, G., Hayhurst, A., Thomas, J.G., Harvey, B.R., Iverson, B.L., and Georgiou, G. 2001. Isolation of high-affinity ligand-binding proteins by periplasmic expression with cytometric screening (PECS). *Nat Biotechnol* **19:** 537-542.

Chen, W., and Georgiou, G. 2002. Cell-Surface display of heterologous proteins: From high-throughput screening to environmental applications. *Biotechnol Bioeng* **79:** 496-503.

Chen, Z., Moayeri, M., Zhou, Y.H., Leppla, S., Emerson, S., Sebrell, A., Yu, F., Svitel, J., Schuck, P., St Claire, M.*, et al.* 2006. Efficient neutralization of anthrax toxin by chimpanzee monoclonal antibodies against protective antigen. *J Infect Dis* **193:** 625-633.

Cho, H.S., Mason, K., Ramyar, K.X., Stanley, A.M., Gabelli, S.B., Denney, D.W., Jr., and Leahy, D.J. 2003. Structure of the extracellular region of HER2 alone and in complex with the Herceptin Fab. *Nature* **421:** 756-760.

Cirino, N.M., Sblattero, D., Allen, D., Peterson, S.R., Marks, J.D., Jackson, P.J., Bradbury, A., and Lehnert, B.E. 1999. Disruption of anthrax toxin binding with the use of human antibodies and competitive inhibitors. *Infect Immun* **67:** 2957-2963.

Cohen, G.H., Sheriff, S., and Davies, D.R. 1996. Refined structure of the monoclonal antibody HyHEL-5 with its antigen hen egg-white lysozyme. *Acta Crystallogr D Biol Crystallogr* **52:** 315-326.

Colman, P.M., Laver, W.G., Varghese, J.N., Baker, A.T., Tulloch, P.A., Air, G.M., and Webster, R.G. 1987. Three-dimensional structure of a complex of antibody with influenza virus neuraminidase. *Nature* **326:** 358-363.

Cornelis, G.R., Boland, A., Boyd, A.P., Geuijen, C., Iriarte, M., Neyt, C., Sory, M.P., and Stainier, I. 1998. The virulence plasmid of Yersinia, an antihost genome. *Microbiol Mol Biol Rev* **62:** 1315-1352.

Corper, A.L., Sohi, M.K., Bonagura, V.R., Steinitz, M., Jefferis, R., Feinstein, A., Beale, D., Taussig, M.J., and Sutton, B.J. 1997. Structure of human IgM rheumatoid factor Fab bound to its autoantigen IgG Fc reveals a novel topology of antibody-antigen interaction. *Nat Struct Biol* **4:** 374-381.

Cote, C.K., Rossi, C.A., Kang, A.S., Morrow, P.R., Lee, J.S., and Welkos, S.L. 2005. The detection of protective antigen (PA) associated with spores of Bacillus anthracis and the effects of anti-PA antibodies on spore germination and macrophage interactions. *Microb Pathog* **38:** 209-225.

Cui, X., Li, Y., Moayeri, M., Choi, G.H., Subramanian, G.M., Li, X., Haley, M., Fitz, Y., Feng, J., Banks, S.M., *et al.* 2005. Late treatment with a protective antigen-directed monoclonal antibody improves hemodynamic function and survival in a lethal toxin-infused rat model of anthrax sepsis. *J Infect Dis* **191:** 422-434.

D'Arcy, A., Mac Sweeney, A., Stihle, M., and Haber, A. 2003. The advantages of using a modified microbatch method for rapid screening of protein crystallization conditions. *Acta Crystallogr D Biol Crystallogr* **59:** 396-399.

D'Arcy, A., Sweeney, A.M., and Haber, A. 2004. Practical aspects of using the microbatch method in screening conditions for protein crystallization. *Methods* **34:** 323-328.

Daugherty, P.S., Chen, G., Olsen, M.J., Iverson, B.L., and Georgiou, G. 1998. Antibody affinity maturation using bacterial surface display. *Protein Eng* **11:** 825-832.

Davies, D.R., and Cohen, G.H. 1996. Interactions of protein antigens with antibodies. *Proc Natl Acad Sci U S A* **93:** 7-12.

De Lorenzo, C., Palmer, D.B., Piccoli, R., Ritter, M.A., and D'Alessio, G. 2002. A new human antitumor immunoreagent specific for ErbB2. *Clin Cancer Res* **8:** 1710-1719.

de Lorimier, R.M., Smith, J.J., Dwyer, M.A., Looger, L.L., Sali, K.M., Paavola, C.D., Rizk, S.S., Sadigov, S., Conrad, D.W., Loew, L., *et al.* 2002. Construction of a fluorescent biosensor family. *Protein Sci* **11:** 2655-2675.

Duplaix, N. 1988. Fleas--the lethal leapers. *Natl. Geogr.* **173:** 672-694.

Evans, E.J., Esnouf, R.M., Manso-Sancho, R., Gilbert, R.J., James, J.R., Yu, C., Fennelly, J.A., Vowles, C., Hanke, T., Walse, B.*, et al.* 2005. Crystal structure of a soluble CD28-Fab complex. *Nat Immunol* **6:** 271-279.

Farady, C.J., Egea, P.F., Schneider, E.L., Darragh, M.R., and Craik, C.S. 2008. Structure of an Fab-protease complex reveals a highly specific non-canonical mechanism of inhibition. *J Mol Biol* **380:** 351-360.

Fields, B.A., Goldbaum, F.A., Ysern, X., Poljak, R.J., and Mariuzza, R.A. 1995. Molecular basis of antigen mimicry by an anti-idiotope. *Nature* **374:** 739-742.

Fischmann, T.O., Bentley, G.A., Bhat, T.N., Boulot, G., Mariuzza, R.A., Phillips, S.E., Tello, D., and Poljak, R.J. 1991. Crystallographic refinement of the three-dimensional structure of the FabD1.3-lysozyme complex at 2.5-A resolution. *J Biol Chem* **266:** 12915-12920.

Francisco, J.A., Campbell, R., Iverson, B.L., and Georgiou, G. 1993. Production and fluorescence-activated cell sorting of Escherichia coli expressing a functional antibody fragment on the external surface. *Proc Natl Acad Sci U S A* **90:** 10444-10448.

Francisco, J.A., Earhart, C.F., and Georgiou, G. 1992. Transport and anchoring of beta-lactamase to the external surface of Escherichia coli. *Proc Natl Acad Sci U S A* **89:** 2713-2717.

Fromant, M., Blanquet, S., and Plateau, P. 1995. Direct random mutagenesis of gene-sized DNA fragments using polymerase chain reaction. *Anal Biochem* **224:** 347-353.

Gai, S.A., and Wittrup, K.D. 2007. Yeast surface display for protein engineering and characterization. *Curr Opin Struct Biol* **17:** 467-473.

Gao, C., Mao, S., Kaufmann, G., Wirsching, P., Lerner, R.A., and Janda, K.D. 2002. A method for the generation of combinatorial antibody libraries using pIX phage display. *Proc Natl Acad Sci U S A* **99:** 12612-12616.

Gao, C., Mao, S., Lo, C.H., Wirsching, P., Lerner, R.A., and Janda, K.D. 1999. Making artificial antibodies: a format for phage display of combinatorial heterodimeric arrays. *Proc Natl Acad Sci U S A* **96:** 6025-6030.

Gubbins, M.J., Berry, J.D., Corbett, C.R., Mogridge, J., Yuan, X.Y., Schmidt, L., Nicolas, B., Kabani, A., and Tsang, R.S. 2006. Production and characterization of neutralizing monoclonal antibodies that recognize an epitope in domain 2 of Bacillus anthracis protective antigen. *FEMS Immunol Med Microbiol* **47:** 436-443.

Gunneriusson, E., Samuelson, P., Uhlen, M., Nygren, P.A., and Stahl, S. 1996. Surface display of a functional single-chain Fv antibody on staphylococci. *J Bacteriol* **178:** 1341-1346.

Guzman, L.M., Belin, D., Carson, M.J., and Beckwith, J. 1995. Tight regulation, modulation, and high-level expression by vectors containing the arabinose PBAD promoter. *J Bacteriol* **177:** 4121-4130.

Harvey, B.R., Georgiou, G., Hayhurst, A., Jeong, K.J., Iverson, B.L., and Rogers, G.K. 2004. Anchored periplasmic expression, a versatile technology for the isolation of high-affinity antibodies from Escherichia coli-expressed libraries. *Proceedings of the National Academy of Sciences* **101:** 9193-9198.

Hayhurst, A. 2000. Improved expression characteristics of single-chain Fv fragments when fused downstream of the Escherichia coli maltose-binding protein or upstream of a single immunoglobulin-constant domain. *Protein Expr Purif* **18:** 1-10.

Hayhurst, A., Happe, S., Mabry, R., Koch, Z., Iverson, B.L., and Georgiou, G. 2003. Isolation and expression of recombinant antibody fragments to the biological warfare pathogen Brucella melitensis. *J Immunol Methods* **276:** 185-196.

Hoe, N.P., and Goguen, J.D. 1993. Temperature sensing in Yersinia pestis: translation of the LcrF activator protein is thermally regulated. *J Bacteriol* **175:** 7901-7909.

Hoe, N.P., Minion, F.C., and Goguen, J.D. 1992. Temperature sensing in Yersinia pestis: regulation of yopE transcription by lcrF. *J Bacteriol* **174:** 4275-4286.

Hoogenboom, H.R. 2002. Overview of antibody phage-display technology and its applications. *Methods Mol Biol* **178:** 1-37.

Hu, P., Elliott, J., McCready, P., Skowronski, E., Garnes, J., Kobayashi, A., Brubaker, R.R., and Garcia, E. 1998. Structural organization of virulence-associated plasmids of Yersinia pestis. *J Bacteriol* **180:** 5192-5202.

Huang, M., Syed, R., Stura, E.A., Stone, M.J., Stefanko, R.S., Ruf, W., Edgington, T.S., and Wilson, I.A. 1998. The mechanism of an inhibitory antibody on TF-initiated blood coagulation revealed by the crystal structures of human tissue factor, Fab 5G9 and TF.G9 complex. *J Mol Biol* **275:** 873-894.

Huber, M., Vor Dem Esche, U., Grunow, R., and Bessler, W.G. 2005. Generation of mouse polyclonal and human monoclonal antibodies against Bacillus anthracis toxin. *Drugs Exp Clin Res* **31:** 35-43.

Hull, A.K., Criscuolo, C.J., Mett, V., Groen, H., Steeman, W., Westra, H., Chapman, G., Legutki, B., Baillie, L., and Yusibov, V. 2005. Human-derived, plant-produced monoclonal antibody for the treatment of anthrax. *Vaccine* **23:** 2082-2086.

Igonet, S., Vulliez-Le Normand, B., Faure, G., Riottot, M.M., Kocken, C.H., Thomas, A.W., and Bentley, G.A. 2007. Cross-reactivity studies of an anti-Plasmodium vivax apical membrane antigen 1 monoclonal antibody: binding and structural characterisation. *J Mol Biol* **366:** 1523-1537.

Jancarik, J., and Kim, S.H. 1991. Sparse matrix sampling: a screening method for crystallization of proteins. *Journal of Applied Crystallography* **24:** 409-411.

Jeong, K.J., and Lee, S.Y. 1999. High-level production of human leptin by fed-batch cultivation of recombinant Escherichia coli and its purification. *Appl Environ Microbiol* **65:** 3027-3032.

Jeong, K.J., Seo, M.J., Iverson, B.L., and Georgiou, G. 2007. APEx 2-hybrid, a quantitative protein-protein interaction assay for antibody discovery and engineering. *Proceedings of the National Academy of Sciences* **104:** 8247-8252.

Jiang, L., Althoff, E.A., Clemente, F.R., Doyle, L., Rothlisberger, D., Zanghellini, A., Gallaher, J.L., Betker, J.L., Tanaka, F., Barbas, C.F., 3rd*, et al.* 2008. De novo computational design of retro-aldol enzymes. *Science* **319:** 1387-1391.

Jiao, G.S., Cregar, L., Wang, J., Millis, S.Z., Tang, C., O'Malley, S., Johnson, A.T., Sareth, S., Larson, J., and Thomas, G. 2006. Synthetic small molecule furin inhibitors derived from 2,5-dideoxystreptamine. *Proc Natl Acad Sci U S A* **103:** 19707-19712.

Johansson, J., Mandin, P., Renzoni, A., Chiaruttini, C., Springer, M., and Cossart, P. 2002. An RNA thermosensor controls expression of virulence genes in Listeria monocytogenes. *Cell* **110:** 551-561.

Johnson, K. 2008. Monoclonal therapeutics and companion diagnostic products, pp. 133. BCC Research, Wellesley, MA.

Jones, T.A., Zou, J.Y., Cowan, S.W., and Kjeldgaard, M. 1991. Improved methods for building protein models in electron density maps and the location of errors in these models. *Acta Crystallogr A* **47 (Pt 2):** 110-119.

Karginov, V.A., Robinson, T.M., Riemenschneider, J., Golding, B., Kennedy, M., Shiloach, J., and Alibek, K. 2004. Treatment of anthrax infection with combination of ciprofloxacin and antibodies to protective antigen of Bacillus anthracis. *FEMS Immunol Med Microbiol* **40:** 71-74.

Kawarasaki, Y., Griswold, K.E., Stevenson, J.D., Selzer, T., Benkovic, S.J., Iverson, B.L., and Georgiou, G. 2003. Enhanced crossover SCRATCHY: construction and high-throughput screening of a combinatorial library containing multiple non-homologous crossovers. *Nucleic Acids Res* **31:** e126.

Kelly, C.D., O'Loughlin, C., Gelder, F.B., Peterson, J.W., Sower, L.E., and Cirino, N.M. 2007. Rapid generation of an anthrax immunotherapeutic from goats using a novel non-toxic muramyl dipeptide adjuvant. *J Immune Based Ther Vaccines* **5:** 11.

Kissinger, C.R., Gehlhaar, D.K., Smith, B.A., and Bouzida, D. 2001. Molecular replacement by evolutionary search. *Acta Crystallogr D Biol Crystallogr* **57:** 1474-1479.

Kjer-Nielsen, L., Dunstone, M.A., Kostenko, L., Ely, L.K., Beddoe, T., Mifsud, N.A., Purcell, A.W., Brooks, A.G., McCluskey, J., and Rossjohn, J. 2004. Crystal structure of the human T cell receptor CD3 epsilon gamma heterodimer complexed to the therapeutic mAb OKT3. *Proc Natl Acad Sci U S A* **101:** 7675-7680.

Kobiler, D., Gozes, Y., Rosenberg, H., Marcus, D., Reuveny, S., and Altboum, Z. 2002. Efficiency of protection of guinea pigs against infection with Bacillus anthracis spores by passive immunization. *Infect Immun* **70:** 544-560.

Konkel, M.E., and Tilly, K. 2000. Temperature-regulated expression of bacterial virulence genes. *Microbes Infect* **2:** 157-166.

Kronqvist, N., Lofblom, J., Jonsson, A., Wernerus, H., and Stahl, S. 2008. A novel affinity protein selection system based on staphylococcal cell surface display and flow cytometry. *Protein Eng Des Sel* **21:** 247-255.

Kundrot, C.E. 2004. Which strategy for a protein crystallization project? *Cell Mol Life Sci* **61:** 525-536.

Laffly, E., Danjou, L., Condemine, F., Vidal, D., Drouet, E., Lefranc, M.P., Bottex, C., and Thullier, P. 2005. Selection of a macaque Fab with framework regions like those in humans, high affinity, and ability to neutralize the protective antigen (PA) of Bacillus anthracis by binding to the segment of PA between residues 686 and 694. *Antimicrob Agents Chemother* **49:** 3414-3420.

Lee, J.E., Fusco, M.L., Hessell, A.J., Oswald, W.B., Burton, D.R., and Saphire, E.O. 2008. Structure of the Ebola virus glycoprotein bound to an antibody from a human survivor. *Nature* **454:** 177-182.

Li, H., Dunn, J.J., Luft, B.J., and Lawson, C.L. 1997. Crystal structure of Lyme disease antigen outer surface protein A complexed with an Fab. *Proc Natl Acad Sci U S A* **94:** 3584-3589.

Li, M., Gustchina, A., Alexandratos, J., Wlodawer, A., Wunschmann, S., Kepley, C.L., Chapman, M.D., and Pomes, A. 2008. Crystal structure of a dimerized cockroach allergen Bla g 2 complexed with a monoclonal antibody. *J Biol Chem* **283:** 22806-22814.

Li, S., Schmitz, K.R., Jeffrey, P.D., Wiltzius, J.J., Kussie, P., and Ferguson, K.M. 2005. Structural basis for inhibition of the epidermal growth factor receptor by cetuximab. *Cancer Cell* **7:** 301-311.

Li, Y., Li, H., Smith-Gill, S.J., and Mariuzza, R.A. 2000. Three-dimensional structures of the free and antigen-bound Fab from monoclonal antilysozyme antibody HyHEL-63. *Biochemistry* **39:** 6296-6309.

Li, Y., Li, H., Yang, F., Smith-Gill, S.J., and Mariuzza, R.A. 2003. X-ray snapshots of the maturation of an antibody response to a protein antigen. *Nat Struct Biol* **10:** 482-488.

Li, Z., Woo, C.J., Iglesias-Ussel, M.D., Ronai, D., and Scharff, M.D. 2004. The generation of antibody diversity through somatic hypermutation and class switch recombination. *Genes Dev* **18:** 1-11.

Little, S.F., Ivins, B.E., Fellows, P.F., and Friedlander, A.M. 1997. Passive protection by polyclonal antibodies against Bacillus anthracis infection in guinea pigs. *Infect Immun* **65:** 5171-5175.

Little, S.F., Leppla, S.H., and Cora, E. 1988. Production and characterization of monoclonal antibodies to the protective antigen component of Bacillus anthracis toxin. *Infect Immun* **56:** 1807-1813.

Liu, H., Smith, T.J., Lee, W.M., Mosser, A.G., Rueckert, R.R., Olson, N.H., Cheng, R.H., and Baker, T.S. 1994. Structure determination of an Fab fragment that neutralizes human rhinovirus 14 and analysis of the Fab-virus complex. *J Mol Biol* **240:** 127-137.

Lo, A.S., Zhu, Q., and Marasco, W.A. 2008. Intracellular antibodies (intrabodies) and their therapeutic potential. *Handb Exp Pharmacol***:** 343-373.

Lok, S.M., Kostyuchenko, V., Nybakken, G.E., Holdaway, H.A., Battisti, A.J., Sukupolvi-Petty, S., Sedlak, D., Fremont, D.H., Chipman, P.R., Roehrig, J.T.*, et al.* 2008. Binding of a neutralizing antibody to dengue virus alters the arrangement of surface glycoproteins. *Nat Struct Mol Biol* **15:** 312-317.

Luft, J.R., Collins, R.J., Fehrman, N.A., Lauricella, A.M., Veatch, C.K., and DeTitta, G.T. 2003. A deliberate approach to screening for initial crystallization conditions of biological macromolecules. *J Struct Biol* **142:** 170-179.

Mabry, R., Rani, M., Geiger, R., Hubbard, G.B., Carrion, R., Jr., Brasky, K., Patterson, J.L., Georgiou, G., and Iverson, B.L. 2005. Passive protection against anthrax by using a high-affinity antitoxin antibody fragment lacking an Fc region. *Infect Immun* **73:** 8362-8368.

Market, E., and Papavasiliou, F.N. 2003. V(D)J recombination and the evolution of the adaptive immune system. *PLoS Biol* **1:** E16.

Maynard, J.A., Maassen, C.B., Leppla, S.H., Brasky, K., Patterson, J.L., Iverson, B.L., and Georgiou, G. 2002. Protection against anthrax toxin by recombinant antibody fragments correlates with antigen affinity. *Nat Biotechnol* **20:** 597-601.

Mazor, Y., Blarcom, T.V., Mabry, R., Iverson, B.L., and Georgiou, G. 2007. Isolation of engineered, full-length antibodies from libraries expressed in Escherichia coli. *Nat Biotech* **25:** 563.

McCoy, A.J. 2007. Solving structures of protein complexes by molecular replacement with Phaser. *Acta Crystallogr D Biol Crystallogr* **63:** 32-41.

McPherson, A. 1989. *Preparation and analysis of protein crystals*. Krieger Publishing Company, Malabar, FL, pp. 384.

McPherson, A. 1999. *Crystallization of biological macromolecules*, 1st ed. Cold Spring Harbor Laboratory Press, Woodbury, NY, pp. 586.

Menez, R., Michel, S., Muller, B.H., Bossus, M., Ducancel, F., Jolivet-Reynaud, C., and Stura, E.A. 2008. Crystal structure of a ternary complex between human prostate-specific antigen, its substrate acyl intermediate and an activating antibody. *J Mol Biol* **376:** 1021-1033.

Meselson, M., Guillemin, J., Hugh-Jones, M., Langmuir, A., Popova, I., Shelokov, A., and Yampolskaya, O. 1994. The Sverdlovsk anthrax outbreak of 1979. *Science* **266:** 1202-1208.

Messer, A., and McLear, J. 2006. The therapeutic potential of intrabodies in neurologic disorders: focus on Huntington and Parkinson diseases. *BioDrugs* **20:** 327-333.

Miyazaki, H., and Kataoka, K. 1996. Preparation of polyacrylamide derivatives showing thermo-reversible coacervate formation and their potential application to two-phase separation processes. *Polymer* **37:** 681-685.

Moayeri, M., and Leppla, S.H. 2004. The roles of anthrax toxin in pathogenesis. *Curr Opin Microbiol* **7:** 19-24.

Mogridge, J., Mourez, M., and Collier, R.J. 2001. Involvement of domain 3 in oligomerization by the protective antigen moiety of anthrax toxin. *J Bacteriol* **183:** 2111-2116.

Mohamed, N., Clagett, M., Li, J., Jones, S., Pincus, S., D'Alia, G., Nardone, L., Babin, M., Spitalny, G., and Casey, L. 2005. A high-affinity monoclonal antibody to anthrax protective antigen passively protects rabbits before and after aerosolized Bacillus anthracis spore challenge. *Infect Immun* **73:** 795-802.

Morita, M., Kanemori, M., Yanagi, H., and Yura, T. 1999a. Heat-induced synthesis of sigma32 in Escherichia coli: structural and functional dissection of rpoH mRNA secondary structure. *J Bacteriol* **181:** 401-410.

Morita, M.T., Tanaka, Y., Kodama, T.S., Kyogoku, Y., Yanagi, H., and Yura, T. 1999b. Translational induction of heat shock transcription factor sigma32: evidence for a built-in RNA thermosensor. *Genes Dev* **13:** 655-665.

Muller, Y.A., Chen, Y., Christinger, H.W., Li, B., Cunningham, B.C., Lowman, H.B., and de Vos, A.M. 1998. VEGF and the Fab fragment of a humanized neutralizing antibody: crystal structure of the complex at 2.4 A resolution and mutational analysis of the interface. *Structure* **6:** 1153-1167.

Mylvaganam, S.E., Paterson, Y., and Getzoff, E.D. 1998. Structural basis for the binding of an anti-cytochrome c antibody to its antigen: crystal structures of FabE8-cytochrome c complex to 1.8 A resolution and FabE8 to 2.26 A resolution. *J Mol Biol* **281:** 301-322.

Niemi, M., Jylha, S., Laukkanen, M.L., Soderlund, H., Makinen-Kiljunen, S., Kallio, J.M., Hakulinen, N., Haahtela, T., Takkinen, K., and Rouvinen, J. 2007. Molecular interactions between a recombinant IgE antibody and the beta-lactoglobulin allergen. *Structure* **15:** 1413-1421.

Nilsson, B., Moks, T., Jansson, B., Abrahmsen, L., Elmblad, A., Holmgren, E., Henrichson, C., Jones, T.A., and Uhlen, M. 1987. A synthetic IgG-binding domain based on staphylococcal protein A. *Protein Eng* **1:** 107-113.

Nocker, A., Hausherr, T., Balsiger, S., Krstulovic, N.P., Hennecke, H., and Narberhaus, F. 2001. A mRNA-based thermosensor controls expression of rhizobial heat shock genes. *Nucleic Acids Res* **29:** 4800-4807.

Otwinowski, Z., and Minor, W. 1997. Processing of X-ray diffraction data collected in oscillation mode. *Methods Enzymol* **27:** 307-326.

Owenius, R., Osterlund, M., Lindgren, M., Svensson, M., Olsen, O.H., Persson, E., Freskgard, P.O., and Carlsson, U. 1999. Properties of spin and fluorescent labels at a receptor-ligand interface. *Biophys J* **77:** 2237-2250.

Paddle, B.M., Wong, V.K., and Muller, B.D. 2006. The cytotoxic effect of anthrax lethal toxin on human lung cells in vitro and the protective action of bovine antibodies to PA and LF. *J Appl Toxicol* **26:** 162-168.

Padlan, E.A., Silverton, E.W., Sheriff, S., Cohen, G.H., Smith-Gill, S.J., and Davies, D.R. 1989. Structure of an antibody-antigen complex: crystal structure of the HyHEL-10 Fab-lysozyme complex. *Proc Natl Acad Sci U S A* **86:** 5938-5942.

Pannifer, A.D., Wong, T.Y., Schwarzenbacher, R., Renatus, M., Petosa, C., Bienkowska, J., Lacy, D.B., Collier, R.J., Park, S., Leppla, S.H.*, et al.* 2001. Crystal structure of the anthrax lethal factor. *Nature* **414:** 229-233.

Pavlou, A.K., and Belsey, M.J. 2005. The therapeutic antibodies market to 2008. *Eur J Pharm Biopharm* **59:** 389-396.

Pelat, T., Hust, M., Laffly, E., Condemine, F., Bottex, C., Vidal, D., Lefranc, M.P., Dubel, S., and Thullier, P. 2007. High-affinity, human antibody-like antibody fragment (single-chain variable fragment) neutralizing the lethal factor (LF) of Bacillus anthracis by inhibiting protective antigen-LF complex formation. *Antimicrob Agents Chemother* **51:** 2758-2764.

Perrakis, A., Sixma, T.K., Wilson, K.S., and Lamzin, V.S. 1997. wARP: improvement and extension of crystallographic phases by weighted averaging of multiple-refined dummy atomic models. *Acta Crystallogr D Biol Crystallogr* **53:** 448-455.

Perry, R.D., and Fetherston, J.D. 1997. Yersinia pestis--etiologic agent of plague. *Clin Microbiol Rev* **10:** 35-66.

Perry, R.D., Straley, S.C., Fetherston, J.D., Rose, D.J., Gregor, J., and Blattner, F.R. 1998. DNA sequencing and analysis of the low-Ca2+-response plasmid pCD1 of Yersinia pestis KIM5. *Infect Immun* **66:** 4611-4623.

Peterson, J.W., Comer, J.E., Noffsinger, D.M., Wenglikowski, A., Walberg, K.G., Chatuev, B.M., Chopra, A.K., Stanberry, L.R., Kang, A.S., Scholz, W.W.*, et al.* 2006. Human monoclonal anti-protective antigen antibody completely protects rabbits and is synergistic with ciprofloxacin in protecting mice and guinea pigs against inhalation anthrax. *Infect Immun* **74:** 1016-1024.

Petosa, C., Collier, R.J., Klimpel, K.R., Leppla, S.H., and Liddington, R.C. 1997. Crystal structure of the anthrax toxin protective antigen. *Nature* **385:** 833-838.

Prabakaran, P., Gan, J., Feng, Y., Zhu, Z., Choudhry, V., Xiao, X., Ji, X., and Dimitrov, D.S. 2006. Structure of severe acute respiratory syndrome coronavirus receptor-binding domain complexed with neutralizing antibody. *J Biol Chem* **281:** 15829-15836.

Prasad, L., Waygood, E.B., Lee, J.S., and Delbaere, L.T. 1998. The 2.5 A resolution structure of the jel42 Fab fragment/HPr complex. *J Mol Biol* **280:** 829-845.

Proba, K., Worn, A., Honegger, A., and Pluckthun, A. 1998. Antibody scFv fragments without disulfide bonds made by molecular evolution. *J Mol Biol* **275:** 245-253.

Prosseda, G., Falconi, M., Giangrossi, M., Gualerzi, C.O., Micheli, G., and Colonna, B. 2004. The virF promoter in Shigella: more than just a curved DNA stretch. *Mol Microbiol* **51:** 523-537.

Read, R.J. 1986. Improved Fourier coefficients for maps using phases from partial structures with errors. *Acta Crystallog. sect. A* **42:** 140-149.

Reetz, M.T., Kahakeaw, D., and Lohmer, R. 2008. Addressing the numbers problem in directed evolution. *Chembiochem* **9:** 1797-1804.

Renard, M., Belkadi, L., and Bedouelle, H. 2003. Deriving topological constraints from functional data for the design of reagentless fluorescent immunosensors. *J Mol Biol* **326:** 167-175.

Rivera, J., Nakouzi, A., Abboud, N., Revskaya, E., Goldman, D., Collier, R.J., Dadachova, E., and Casadevall, A. 2006. A monoclonal antibody to Bacillus anthracis protective antigen defines a neutralizing epitope in domain 1. *Infect Immun* **74:** 4149-4156.

Rohde, J.R., Luan, X.S., Rohde, H., Fox, J.M., and Minnich, S.A. 1999. The Yersinia enterocolitica pYV virulence plasmid contains multiple intrinsic DNA bends which melt at 37 degrees C. *J Bacteriol* **181:** 4198-4204.

Rosovitz, M.J., Schuck, P., Varughese, M., Chopra, A.P., Mehra, V., Singh, Y., McGinnis, L.M., and Leppla, S.H. 2003. Alanine-scanning mutations in domain 4 of anthrax toxin protective antigen reveal residues important for binding to the cellular receptor and to a neutralizing monoclonal antibody. *J Biol Chem* **278:** 30936-30944.

Rothlisberger, D., Khersonsky, O., Wollacott, A.M., Jiang, L., DeChancie, J., Betker, J., Gallaher, J.L., Althoff, E.A., Zanghellini, A., Dym, O., *et al.* 2008. Kemp elimination catalysts by computational enzyme design. *Nature* **453:** 190-195.

Russell, P.K. 2007. Project BioShield: what it is, why it is needed, and its accomplishments so far. *Clin Infect Dis* **45 Suppl 1:** S68-72.

Sakata, T., Yan, Y., and Marriott, G. 2005a. Family of site-selective molecular optical switches. *J Org Chem* **70:** 2009-2013.

Sakata, T., Yan, Y., and Marriott, G. 2005b. Optical switching of dipolar interactions on proteins. *Proc Natl Acad Sci U S A* **102:** 4759-4764.

Sandhu, G.S., Aleff, R.A., and Kline, B.C. 1992. Dual asymmetric PCR: one-step construction of synthetic genes. *Biotechniques* **12:** 14-16.

Santelli, E., Bankston, L.A., Leppla, S.H., and Liddington, R.C. 2004. Crystal structure of a complex between anthrax toxin and its host cell receptor. *Nature* **430:** 905-908.

Sawada-Hirai, R., Jiang, I., Wang, F., Sun, S.M., Nedellec, R., Ruther, P., Alvarez, A., Millis, D., Morrow, P.R., and Kang, A.S. 2004. Human anti-anthrax protective antigen neutralizing monoclonal antibodies derived from donors vaccinated with anthrax vaccine adsorbed. *J Immune Based Ther Vaccines* **2:** 5.

Scobie, H.M., and Young, J.A. 2005. Interactions between anthrax toxin receptors and protective antigen. *Curr Opin Microbiol* **8:** 106-112.

Scobie, H.M., Rainey, G.J., Bradley, K.A., and Young, J.A. 2003. Human capillary morphogenesis protein 2 functions as an anthrax toxin receptor. *Proc Natl Acad Sci U S A* **100:** 5170-5174.

Segelke, B.W. 2001. Efficiency analysis of sampling protocols used in protein crystallization screening. *Journal of Crystal Growth* **232:** 553-362.

Self, C.H., and Thompson, S. 1996. Light activatable antibodies: models for remotely activatable proteins. *Nat Med* **2:** 817-820.

Sellman, B.R., Mourez, M., and Collier, R.J. 2001. Dominant-negative mutants of a toxin subunit: an approach to therapy of anthrax. *Science* **292:** 695-697.

Sheriff, S., Silverton, E.W., Padlan, E.A., Cohen, G.H., Smith-Gill, S.J., Finzel, B.C., and Davies, D.R. 1987. Three-dimensional structure of an antibody-antigen complex. *Proc Natl Acad Sci U S A* **84:** 8075-8079.

Shieh, H.S., Stallings, W.C., Stevens, A.M., and Stegeman, R.A. 1995. Using sampling techniques in protein crystallization. *Acta Crystallogr D Biol Crystallogr* **51:** 305-310.

Shimoboji, T., Ding, Z., Stayton, P.S., and Hoffman, A.S. 2001. Mechanistic investigation of smart polymer-protein conjugates. *Bioconjug Chem* **12:** 314-319.

Shimoboji, T., Ding, Z.L., Stayton, P.S., and Hoffman, A.S. 2002a. Photoswitching of ligand association with a photoresponsive polymer-protein conjugate. *Bioconjug Chem* **13:** 915-919.

Shimoboji, T., Larenas, E., Fowler, T., Hoffman, A.S., and Stayton, P.S. 2003. Temperature-induced switching of enzyme activity with smart polymer-enzyme conjugates. *Bioconjug Chem* **14:** 517-525.

Shimoboji, T., Larenas, E., Fowler, T., Kulkarni, S., Hoffman, A.S., and Stayton, P.S. 2002b. Photoresponsive polymer-enzyme switches. *Proc Natl Acad Sci U S A* **99:** 16592-16596.

Shoop, W.L., Xiong, Y., Wiltsie, J., Woods, A., Guo, J., Pivnichny, J.V., Felcetto, T., Michael, B.F., Bansal, A., Cummings, R.T.*, et al.* 2005. Anthrax lethal factor inhibition. *Proc Natl Acad Sci U S A* **102:** 7958-7963.

Shusta, E.V., Raines, R.T., Pluckthun, A., and Wittrup, K.D. 1998. Increasing the secretory capacity of Saccharomyces cerevisiae for production of single-chain antibody fragments. *Nat Biotechnol* **16:** 773-777.

Singh, Y., Klimpel, K.R., Quinn, C.P., Chaudhary, V.K., and Leppla, S.H. 1991. The carboxyl-terminal end of protective antigen is required for receptor binding and anthrax toxin activity. *J Biol Chem* **266:** 15493-15497.

Sivasubramanian, A., Maynard, J.A., and Gray, J.J. 2008. Modeling the structure of mAb 14B7 bound to the anthrax protective antigen. *Proteins* **70:** 218-230.

Soukup, G.A., and Breaker, R.R. 1999. Relationship between internucleotide linkage geometry and the stability of RNA. *Rna* **5:** 1308-1325.

Staats, H.F., Alam, S.M., Scearce, R.M., Kirwan, S.M., Zhang, J.X., Gwinn, W.M., and Haynes, B.F. 2007. In vitro and in vivo characterization of anthrax anti-protective antigen and anti-lethal factor monoclonal antibodies after passive transfer in a mouse lethal toxin challenge model to define correlates of immunity. *Infect Immun* **75:** 5443-5452.

Stavnezer, J., and Amemiya, C.T. 2004. Evolution of isotype switching. *Semin Immunol* **16:** 257-275.

Steiniger, S.C., Altobell, L.J., 3rd, Zhou, B., and Janda, K.D. 2007. Selection of human antibodies against cell surface-associated oligomeric anthrax protective antigen. *Mol Immunol* **44:** 2749-2755.

Stura, E.A., Nemerow, G.R., and Wilson, I.A. 1992. Strategies in the crystallization of glycoproteins and protein complexes. *Journal of Crystal Growth* **122:** 273-285.

Su, H.P., Golden, J.W., Gittis, A.G., Hooper, J.W., and Garboczi, D.N. 2007. Structural basis for the binding of the neutralizing antibody, 7D11, to the poxvirus L1 protein. *Virology* **368:** 331-341.

Subramanian, G.M., Cronin, P.W., Poley, G., Weinstein, A., Stoughton, S.M., Zhong, J., Ou, Y., Zmuda, J.F., Osborn, B.L., and Freimuth, W.W. 2005. A phase 1 study of PAmAb, a fully human monoclonal antibody against Bacillus anthracis protective antigen, in healthy volunteers. *Clin Infect Dis* **41:** 12-20.

Sudarsan, N., Wickiser, J.K., Nakamura, S., Ebert, M.S., and Breaker, R.R. 2003. An mRNA structure in bacteria that controls gene expression by binding lysine. *Genes Dev* **17:** 2688-2697.

Tabor, J.J., Bayer, T.S., Simpson, Z.B., Levy, M., and Ellington, A.D. 2008. Engineering stochasticity in gene expression. *Mol Biosyst* **4:** 754-761.

Tanaka, K., Muramatsu, S., Yamada, H., and Mizuno, T. 1991. Systematic characterization of curved DNA segments randomly cloned from Escherichia coli and their functional significance. *Mol Gen Genet* **226:** 367-376.

Thomas, K.J., Sherman, D.B., Amiss, T.J., Andaluz, S.A., and Pitner, J.B. 2006. A long-wavelength fluorescent glucose biosensor based on bioconjugates of galactose/glucose binding protein and Nile Red derivatives. *Diabetes Technol Ther* **8:** 261-268.

Thomas, R., Patenaude, S.I., MacKenzie, C.R., To, R., Hirama, T., Young, N.M., and Evans, S.V. 2002. Structure of an anti-blood group A Fv and improvement of its binding affinity without loss of specificity. *J Biol Chem* **277:** 2059-2064.

Thompson, S., Dessi, J., and Self, C.H. 2008. The construction and in vitro testing of photo-activatable cancer targeting folated anti-CD3 conjugates. *Biochem Biophys Res Commun* **366:** 526-531.

Tulip, W.R., Varghese, J.N., Laver, W.G., Webster, R.G., and Colman, P.M. 1992. Refined crystal structure of the influenza virus N9 neuraminidase-NC41 Fab complex. *J Mol Biol* **227:** 122-148.

Turk, B.E., Wong, T.Y., Schwarzenbacher, R., Jarrell, E.T., Leppla, S.H., Collier, R.J., Liddington, R.C., and Cantley, L.C. 2004. The structural basis for substrate and inhibitor selectivity of the anthrax lethal factor. *Nat Struct Mol Biol* **11:** 60-66.

Vagin, A., and Teplyakov, A. 1997. MOLREP: an automated program for molecular replacement. *J. Appl. Cryst.* **30:** 1022-1025.

Varadarajan, N., Rodriguez, S., Hwang, B.Y., Georgiou, G., and Iverson, B.L. 2008. Highly active and selective endopeptidases with programmed substrate specificities. *Nat Chem Biol* **4:** 290-294.

Vitale, L., Blanset, D., Lowy, I., O'Neill, T., Goldstein, J., Little, S.F., Andrews, G.P., Dorough, G., Taylor, R.K., and Keler, T. 2006. Prophylaxis and therapy of

inhalational anthrax by a novel monoclonal antibody to protective antigen that mimics vaccine-induced immunity. *Infect Immun* **74:** 5840-5847.

Waldminghaus, T., Heidrich, N., Brantl, S., and Narberhaus, F. 2007. FourU: a novel type of RNA thermometer in Salmonella. *Mol Microbiol* **65:** 413-424.

Walsh, J.J., Pesik, N., Quinn, C.P., Urdaneta, V., Dykewicz, C.A., Boyer, A.E., Guarner, J., Wilkins, P., Norville, K.J., Barr, J.R.*, et al.* 2007. A case of naturally acquired inhalation anthrax: clinical care and analyses of anti-protective antigen immunoglobulin G and lethal factor. *Clin Infect Dis* **44:** 968-971.

Wang, F., Ruther, P., Jiang, I., Sawada-Hirai, R., Sun, S.M., Nedellec, R., Morrow, P.R., and Kang, A.S. 2004. Human monoclonal antibodies that neutralize anthrax toxin by inhibiting heptamer assembly. *Hum Antibodies* **13:** 105-110.

Wedemayer, G.J., Patten, P.A., Wang, L.H., Schultz, P.G., and Stevens, R.C. 1997. Structural insights into the evolution of an antibody combining site. *Science* **276:** 1665-1669.

Wild, M.A., Xin, H., Maruyama, T., Nolan, M.J., Calveley, P.M., Malone, J.D., Wallace, M.R., and Bowdish, K.S. 2003. Human antibodies from immunized donors are protective against anthrax toxin in vivo. *Nat Biotechnol* **21:** 1305-1306.

Williams, B.R., and Zhu, Z. 2006. Intrabody-based approaches to cancer therapy: status and prospects. *Curr Med Chem* **13:** 1473-1480.

Winkler, W.C., Cohen-Chalamish, S., and Breaker, R.R. 2002. An mRNA structure that controls gene expression by binding FMN. *Proc Natl Acad Sci U S A* **99:** 15908-15913.

Wittrup, K.D. 2001. Protein engineering by cell-surface display. *Curr Opin Biotechnol* **12:** 395-399.

Young, J.A., and Collier, R.J. 2007. Anthrax toxin: receptor binding, internalization, pore formation, and translocation. *Annu Rev Biochem* **76:** 243-265.

Yu, X., Tsibane, T., McGraw, P.A., House, F.S., Keefer, C.J., Hicar, M.D., Tumpey, T.M., Pappas, C., Perrone, L.A., Martinez, O.*, et al.* 2008. Neutralizing antibodies derived from the B cells of 1918 influenza pandemic survivors. *Nature* **Advance online publication**.

Zhou, B., Carney, C., and Janda, K.D. 2008. Selection and characterization of human antibodies neutralizing Bacillus anthracis toxin. *Bioorg Med Chem* **16:** 1903-1913.

Zhou, T., Xu, L., Dey, B., Hessell, A.J., Van Ryk, D., Xiang, S.H., Yang, X., Zhang, M.Y., Zwick, M.B., Arthos, J.*, et al.* 2007. Structural definition of a conserved neutralization epitope on HIV-1 gp120. *Nature* **445:** 732-737.

Vita

Clinton Edward Leysath was born the oldest son of two children of Louis E. Leysath and Janice H. Leysath on December 2, 1975 in Houston, Texas. He graduated as salutatorian from Deer Park High School in 1994 and attended Texas A&M University in College Station beginning in the fall of that year. He began his research in chemistry in the summer of 1995 as an intern at Monsanto Co. in St. Louis, Missouri. He interned at Monsanto Co. during the summers of 1996 and 1997 as well, and received his Bachelor of Science in Chemistry in August of 1998, at which time he began working toward a second Bachelor of Science in Biochemistry. He completed that degree and graduated with honors in May of 1999 and moved to Houston, Texas to work in the laboratory of Dr. Michael Andreeff at the University of Texas MD Anderson Cancer Center. In February of 2001, he left MD Anderson to work in Research and Development at Ambion, Inc. in Austin, Texas. He continued research there until entering the Graduate School of the University of Texas at Austin in the fall of 2002.

Permanent address: 1606 William Trace, Baytown, TX 77523

This dissertation was typed by the author.